Human-Centered Control of the Indoor Thermal Environment

by

Ming Zhou

B.S., Applied Mechanics
Zhejiang University, China, 1987

M.S., Engineering Mechanics
Tsinghua University, China, 1989

Submitted to the Department of Mechanical Engineering in Partial Fulfillment of the Requirements for the Degree of

DOCTOR OF PHILOSOPHY

at the

MASSACHUSETTS INSTITUTE OF TECHNOLOGY

February 1998

Signature of Author _____
Department of Mechanical Engineering
December 1, 1997

Certified by _____
Haruhiko H. Asada, Professor of Mechanical Engineering
Thesis Supervisor

Certified by _____
Sheng Liu, Research Scientist of Mechanical Engineering
Thesis Co-supervisor

Accepted by _____
Ain A. Sonin
Chairman, Department Committee on Graduate Students

Human-Centered Control of the Indoor Thermal Environment

Ming Zhou

Submitted to the Department of Mechanical Engineering
on December 1, 1997 in Partial Fulfillment of the
Requirements for the Degree of Doctor of Philosophy in
Mechanical Engineering

ABSTRACT

One of the primary objectives of a heating, ventilating, and air-conditioning (HVAC) system is to provide a thermally comfortable indoor environment. Although there have been substantial advances in the design of HVAC systems in recent years, system performance with regard to thermal comfort has seen little progress. This can be attributed to the fact that the control paradigm for HVAC systems has remained relatively unchanged: regulating indoor environment variables such as air temperature without including human occupants in the feedback loop. This thesis presents a new methodology for HVAC control, which includes human occupants in a closed-loop control system. Instead of targeting the thermal comfort condition, which cannot be directly measured or effectively estimated, this research seeks to minimize the thermal load imposed by the thermal environment on the human thermoregulatory system to achieve a thermally neutralized physiological state. By doing so, the indoor environment is regulated based not on how one "feels", but how one responds physiologically.

From previous studies, it was identified that the body can effectively balance a thermal load by regulating the peripheral blood flow rate. It is proposed in this research to utilize the peripheral blood flow rate as the feedback signal to control a HVAC system. A wireless optical sensor embedded in a finger ring is used to measure the blood flow rate through a finger. For the purpose of analysis and systematic control design, a second-order, nonlinear model has been developed to describe the dynamic characteristics of the human thermoregulatory system, and has been verified by experiments on a group of human subjects.

Using the linearized thermoregulation model, a digital controller is designed using the pole placement technique. The nonlinear characteristic of the human thermoregulatory response is accounted for by adopting different linear models depending on the thermal state of the body. It is shown that the closed-loop system performs well during different thermal transients, and is robust enough to withstand substantial errors in several model parameters.

Thesis Supervisor: Haruhiko H. Asada
Title: Professor of Mechanical Engineering

Thesis Co-supervisor: Sheng Liu
Title: Research Scientist of Mechanical Engineering

TO MY FATHER
ZHOU ER-HUI

Acknowledgments

My thanks begin with my advisor, Professor Haruhiko H. Asada. I am very grateful not only for his guidance, insight, support, and financial assistance but also for the opportunity to work in the unique learning environment he created. the d'Arbeloff Laboratory for Information Systems and Technology at MIT.

I offer my sincere gratitude to my co-advisor, Dr. Sheng Liu, for his advice, support and encouragement. His expertise, inputs, and social skills have certainly made my life at MIT much easier than what it could have been.

I would also like to thank the other members of my thesis committee. Professor Anuradha M. Annaswamy and Professor Leon R. Glicksman, who contributed in their own ways. Their participation, comments, and suggestions greatly enhanced this thesis.

Thanks also to Professor Qingyan Chen and Professor Taiqing Qiu, who provided valuable inputs to my research work; Professor David Parks, for his financial support for my first year at MIT. Special thanks to Dr. Kuo-Wei Chang for providing the blood flow sensors and other helpful suggestions. I am also grateful to the following people who contributed to the completion of the HVAC test chamber in the d'Arbeloff Lab: Eric Epstein and Lakhan S. Verma from MIT physical plant, Michael Ramon and Rick Gacia from Andover Controls, Joe Fiedrich and his engineers from Stadler Corporation. I want to acknowledge Andover Controls (Andover, MA) and Stadler Corporation (Bedford, MA) for donating valuable equipment to the HVAC test chamber.

The first two years of my research work at the Intelligent Machine Laboratory at MIT was sponsored by Teco Electric & Machinery Co., Ltd., Taiwan. I would like to thank Mr. Hong Hsiang Lin, Mr. Williaw Hu, Mr. Wen-Tsong Liu, and Mr. Pei-Chih Wang from Teco for their support and valuable helps. Especially, I wish to thank Mr. Hwa-Wen Fann and Mr. Jer-Yiin Lee, for their efforts that made my 1995 trip to Teco such an enjoyable and memorable one.

Thanks to all my colleagues in the Intelligent Machine Laboratory for their help and friendship. Particularly I would like to thank Xiangdong He, Booho Yang, Sean Li, Mark West, Anton Pil, Sooyong Lee, Susan Ipri, Muralidhar Ravuri, Joe Spano, Brandon Gordon, Shrikant Savant, Steve Mascaro, Rolland Doubleday, Sokwoo Rhee, Bei Gu,

Bill Finger, Masayoshi Wada, Toshinori Mimura, Hyoseok Yang, and Yi Zhang. Special thanks to Joe Spano who made significant contributions to improve the English language of the this thesis. The list won't be complete if I fail to mention Kari Kulaszewicz, who provided countless assistance over the years.

I would like to mention some other people from the MIT community, who have shared some tough times with me at this institute: Hong Dai, Taofang Zeng, Jianjun Hu, Steve Tang, and Joseph Chen.

To my close friends, Shuling Hou, Yongcheng Shi, Jeanne He, Hui Wang, Honbin Luo, and many others, I want to thank you for much needed support, life advice, and caring.

I wish to thank my parents, in-laws, and other family members in China, for your love, understanding, support, patience, and encouragement over the years. I am also indebted to many other kind and generous people who made my journey to America possible.

Last, but not least, I wish to thank my beloved wife, Xiaowei Wang, for your love, support, companionship, and enriching my life in many special ways.

The last one and one half years of this work was supported by the Total Home Automation and Elderly/Health Care Research Consortium.

Contents

List of Figures

List of Tables

Chapter 1

Introduction

1.1 Background and Previous Work

Most buildings are equipped with specific heating, ventilating, and air-conditioning (HVAC) systems to provide healthy, comfortable indoor environments. In many cases, such as residential homes, thermal comfort is the primary reason for the installation of a HVAC system. Although in recent years, there have been substantial advances in the HVAC industry, system performance with regard to thermal comfort has seen little progress.

Traditional HVAC control has myopically focused on the temperature regulation problem. This temperature control paradigm often fails to achieve one of the primary objectives of HVAC systems – to make the occupants thermally comfortable; the main reason is that thermal comfort does not depend solely on air temperature. It has been known for years that the comfort of the occupants depends on several environmental variables, such as air velocity, air humidity and radiant temperature. Some human related variables, such as clothing insulation and activity level, can also influence the comfort condition. Obviously, a more comprehensive control objective is required in order to achieve a thermally comfortable condition.

To define an appropriate control objective, it is essential to clarify the concept of thermal comfort. As defined by ASHRAE[1][1], thermal comfort is *the condition of mind that expresses satisfaction with the thermal environment.* Because of the involvement of the condition of mind, effective control of thermal comfort is a highly non-trivial task.

Thermal comfort has been studied for years, and many thermal comfort indices have been developed. The value of a thermal comfort index indicates the comfort level of an occupant in the thermal environment. These comfort indices are functions of several

[1]The American Society of Heating, Refrigerating and Air-Conditioning Engineers.

environment variables and some human related variables. Two of the most well-known thermal comfort indices are the Effective Temperature (ET*) developed in [2], and the Predicted Mean Vote (PMV) developed in [3]. Although thermal comfort indices have been used for decades for the analysis of indoor climates and the design of HVAC systems, application to real time climate control has only achieved limited success.

There have been several attempts to apply thermal comfort indices to HVAC control [4, 5, 6, 7]; however, few practical results have been obtained. The reasons can be summarized as follows.

1. It is difficult to measure or predict the real time values of all the variables involved in the indices. For example, the local air velocity is difficult to measure because of the low speed and turbulence.

2. Thermal comfort indices are based on the statistical average of the traits of a certain population. As a result, they contain little or no user dependent information.

3. Because most thermal comfort indices are developed under uniform thermal environment conditions, additional constraints must be considered when they are applied to non-uniform thermal environments.

4. Current thermal comfort indices are developed for steady-state conditions of both the human body and the thermal environment. They cannot account for the different preferences of an occupant at different thermal states of the body. For example, a person will prefer a relatively cool indoor environment when he or she comes from a very hot outdoor environment. If a comfort index controller is used in this situation, the person will experience a long transient period with warm discomfort.

Advanced control methods have been proposed to overcome some of the above problems. For example, by modifying PMV and making the index adjustable to individual human occupant, Federspiel[8] developed a human supervised comfort control algorithm, which utilizes human sensational voting to tune the user-specific parameters in the index. This approach depends heavily on the direct human interaction with the machine. As a result, it faces the tough challenge of user acceptance.

1.2 Issues and Objectives

This thesis proposes and demonstrates a new approach to HVAC control to improve the comfort level of human occupants. Because the psychological states are difficult to monitor, let alone control, the thermal comfort definition by ASHRAE is not directly pursued. Instead, a physiological state of the body, which bridges the gap between the thermal sensation and the thermal environment, is controlled by HVAC systems. The objective is to regulate certain physiological state so that the minimum effort is required for the human thermoregulatory system to balance the body heat. As a result, a physiological neutral state can be reached.

The new control paradigm is illustrated in Figure 1.1. Unlike thermal comfort index control, which artificially integrates comfort related variables into a single index and regulates this index, the new control paradigm utilizes the human thermoregulatory system to integrate all related variables. Based on the physiological reaction of the body to the thermal environment, the HVAC system adjusts certain environment variables to minimize the effort of the human thermoregulatory system.

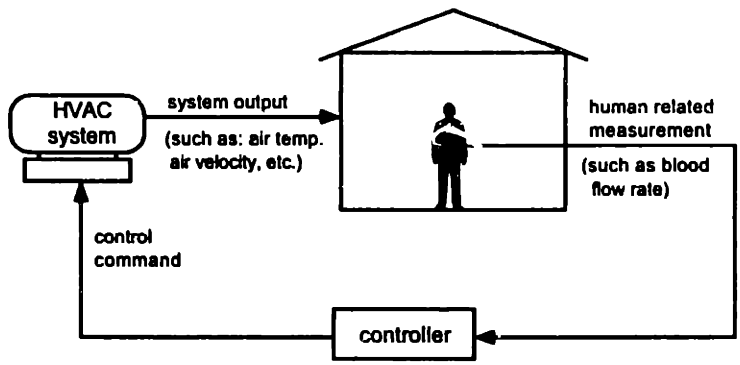

Figure 1.1: Human-centered control

One primary issue of this new approach is how to quantify and measure the effort of the thermoregulatory system. The effort is represented by the human thermal load, which is a function of the peripheral blood flow rate. Corresponding to the minimum effort is the preferred physiological state of the body. Chapter 2 provides a concise summary of the physiology of human thermoregulation.

With this new control objective, the basic concept of a new HVAC control system is outlined in Chapter 3. The feedback signal of this control system, the peripheral

blood flow rate, comes directly from the human body, thus human instrumentation is critical to make this approach practical. Sensors must be small, non-invasive, and can be placed at acceptable locations on human body. Effective measurement of peripheral blood flow rate and a prototype of a blood flow sensor are detailed in Chapter 3.

The new approach includes the human in a closed-loop algorithm. Since the human body has its own closed-loop control system, the stability of the overall control algorithm could be a potential problem. It has been shown by both analysis and experiments that the closed-loop system can become unstable if the controller is not designed properly. To provide a systematic way to design a robust and stable controller, certain knowledge of the plant dynamics is required. Chapter 4 and Chapter 5 provide models for the human thermoregulatory system and the indoor thermal environment respectively.

The human thermoregulatory system is a very complex physiological system. The model only provides a reasonable approximation of the real system, and certain modeling errors exist. The model-based control design should take the modeling errors into account to guarantee both stability and performance requirements. At the same time, there could be many uncertainties in the plant, such as local air velocity, clothing insulation, etc.. Disturbances may also appear in several forms, like outdoor environment changes or emotional changes of the occupant. The controller should be robust enough to deal with the uncertainties and reject different forms of disturbances. Essential control design issues are addressed in Chapter 6.

Chapter 2

Physiology of Human Thermoregulation

The fundamental issue of HVAC control is what should be regulated. There are many disadvantages in the traditional control approach, which regulates one or few environment variables. Ideally, the control objective is to achieve a desired mental state. Due to the technical difficulties in dealing with mental states, a realistic approach is to regulate the physiological states of the body. This chapter provides a review of the thermal states of the human body as well as the autonomic nervous control system which regulates the thermal states. Based on the understanding of the human thermoregulatory system, a desired physiological state of the body, termed as thermal neutrality, is defined. Thus the control objective is to achieve thermal neutrality.

2.1 Body Heat Balance

Like most mammals, human beings are homeothermic, which means they can maintain a relatively constant body temperature independent of the environment temperature. Under normal conditions, the human body temperature is about 37^oC or 98.6^oF. Although a circadian rhythm with a 24-hour period exists [9], it is still reasonable to assume a constant body temperature because of the small rhythm amplitude (about 1^oC).

In order to maintain a constant body temperature, a balance must exist between heat production and heat loss. In the following section, heat production and heat loss mechanisms will be summarized, followed by a review of the human thermoregulatory system.

2.1.1 Heat Production

The human body may accumulate heat in the following ways:

- Internal metabolism.
- External environment: such as solar radiation.
- Hot food that is ingested.

Among these heat sources, only the first one is generated by the human body, and is much more complicated than the others. Basal metabolic rate (BMR) can be used to compare metabolic rates between individuals. It is defined as the rate of energy production by the body during absolute rest determined under specific conditions by the rate of oxygen usage. BMR is expressed as the energy expenditure per unit surface area per hour. For a young adult, the BMR is about 35 $kcal/hr\ m^2$. BMR varies with age and gender. For example, BMR in a newborn infant is approximately twice that of an old person[10].

Different activities markedly affect metabolic rate. For certain activities, such as walking upstairs, the metabolic rate can be 20 times of BMR. The metabolic rate of a person in fever may be increased by as much as 100 per cent. The unit *met* is often used to measure the metabolic rate at different activity levels. One *met* is defined as 50 $kcal/hr\ m^2$, which equals the amount of energy produced by a resting man.

For a given activity level, metabolic rate also changes with ambient temperature. It has been shown that metabolic rate reaches its minimum when ambient temperature falls within the neutral range [11], and both downward and upward shifts of ambient temperature from this neutral range increase metabolic rate. Except for extreme cases, this change of metabolic rate is much smaller than the changes caused by increasing activity level.

In a cold environment, if the heat production rate is insufficient to maintain the body temperature, a further increase in metabolism is brought about by the involuntary contraction of the skeletal muscles, such as shivering. Shivering thermogenesis will be addressed in the section of human thermoregulatory system.

2.1.2 Heat Loss

Body heat is lost by conduction, convection, radiation, and evaporation of water.

Heat is lost by conduction through physical contact of the body with objects and substratum, whose temperature is lower than that of the body temperature. Under normal conditions, this amount of energy loss is much smaller than the loss through other modes, i.e. convection, radiation, and evaporation. For this reason, this portion of energy loss is neglected in the later analysis. This direct heat loss to the environment should not be confused with the heat that is conducted through the clothing and then released to the environment by convection and radiation. The latter is significant to the analysis and will be studied in more detail. From the part of the body surface covered by air, heat is transferred by convection, radiation and evaporation.

Convection heat loss is the energy transmitted to air whose temperature is lower than the skin temperature. It happens at exposed skin as well as the outer layer of clothing. This heat loss depends significantly on the local thermal environment, i.e., local air temperature, local air velocity, and turbulence level. Both external air flow and buoyancy-driven thermal plumes can cause dramatic changes in heat convection. Wind chill factor is a good example. As a matter of fact, convection is the dominant mechanism effected by most air conditioning systems to assist human occupants to balance their body heat.

Radiation is the loss of heat by infrared waves. At thermally comfortable conditions, this accounts for the highest percentage of the total heat loss. Unlike convection, radiation heat loss does not depends on local air properties. Instead, it is a function of environment radiant temperature, emissivity and temperature of the body surface, and the relative geometry of the body to its environment (shape factor).

The above three heat losses can become heat gains when the environment temperature is higher than body temperature. Under this extreme condition, the only way for the body to lose heat is by evaporation. Evaporation acts as a mechanism only to lose heat, not the other way around. There are three types of evaporation: 1, evaporation through respiration; 2, insensible perspiration (water diffusion); 3, thermal sweating (from eccrine glands). Among the three, sweating is the most effective mechanism to balance body heat in a hot environment.

Besides the above heat losses, there are some other minor heat losses associated with the body, such as the heat for the warming of food and air, liberation of CO_2, etc.

These heat losses only account for a very small amount of the total heat loss.

2.1.3 Body Temperatures

The heat produced within the body normally is lost to the environment by way of the body surface. In accordance with the physical laws of heat flow, the temperature near the body surface must be lower than that of the central parts. In the limbs there is a longitudinal temperature gradient, and there is also a radial temperature gradient. The result, owing to the irregular geometry of the body, is a complicated three dimensional temperature distribution. Because the fluctuations in body temperature caused by environmental temperature changes are distinctly greater near the body surface and at the ends of extremities, one can simplify the temperature distribution by dividing the body into a "poikilothermic" shell and a "homeothermic" core. The temperature of the shell varies under changing external conditions, while the core temperature remains at a constant value.

On closer examination we find that the temperature of the core itself is not constant in both space and time. Even under thermoneutral conditions, the core temperature difference is on the order of 0.2 ^oC - 1.2 ^oC[11]. The highest temperatures are found in the rectum, which is about 0.5 ^oC higher than the oral temperature. For practical purposes, it suffices to use the temperature at a specific site as a representative of the body core temperature, for one is usually interested in temporal changes in temperature. For instrumentation purpose, it is most important to select an easily accessible site with little spatial variation in temperature. Typical core temperature measurements are: esophageal temperature, oral temperature, and meatus temperature.

The shell temperature is usually characterized by the temperature of the skin, which is easily measurable. The temperature difference between two different points on the skin surface can be very large, measurement at a single point is quite inadequate. The temperatures at several places must be averaged to obtain a more meaningful value. It is common practice to obtain mean skin temperature from measurements at the forehead, chest, abdomen, upper arm, forearm, back of the hand, thigh, calf, and dorsum of the foot. The mean skin temperature is calculated by weighting these

temperature measurements in accordance with the body surface area they represent. Different weighting formulas can be found in [12].

2.2 The Regulation of Body Temperature

This section will review the overall structure of the human thermoregulatory system, the major effector mechanisms, as well as the associated neural control system, i.e. the autonomic nervous system.

2.2.1 Human Thermoregulatory System

It has been shown that the human body can gain or lose heat in many ways. The thermoregulatory system allows the human to balance the body heat within a wide range of thermal environment variables. This section will review the major components of the human thermoregulatory system.

Structure of the thermoregulatory system

Figure 2.1 shows the structure of the human thermoregulatory system. The major components of this system are: thermoreceptors (sensors), thermoregulation effectors (actuators), and the central nervous system (the controller).

Human thermal sensation is detected by internal and external sensors, and these signals are passed along to the central nervous system. The central nervous system activates appropriate effector mechanisms accordingly, so that the body temperature is kept within a certain range. The detailed principles for each of the components and the nervous and humoral control will be presented in the next subsection.

Effector mechanisms

The major effector mechanisms of the human thermoregulatory system are:

- vasoconstriction and vasodilatation,
- shivering,
- sweating.

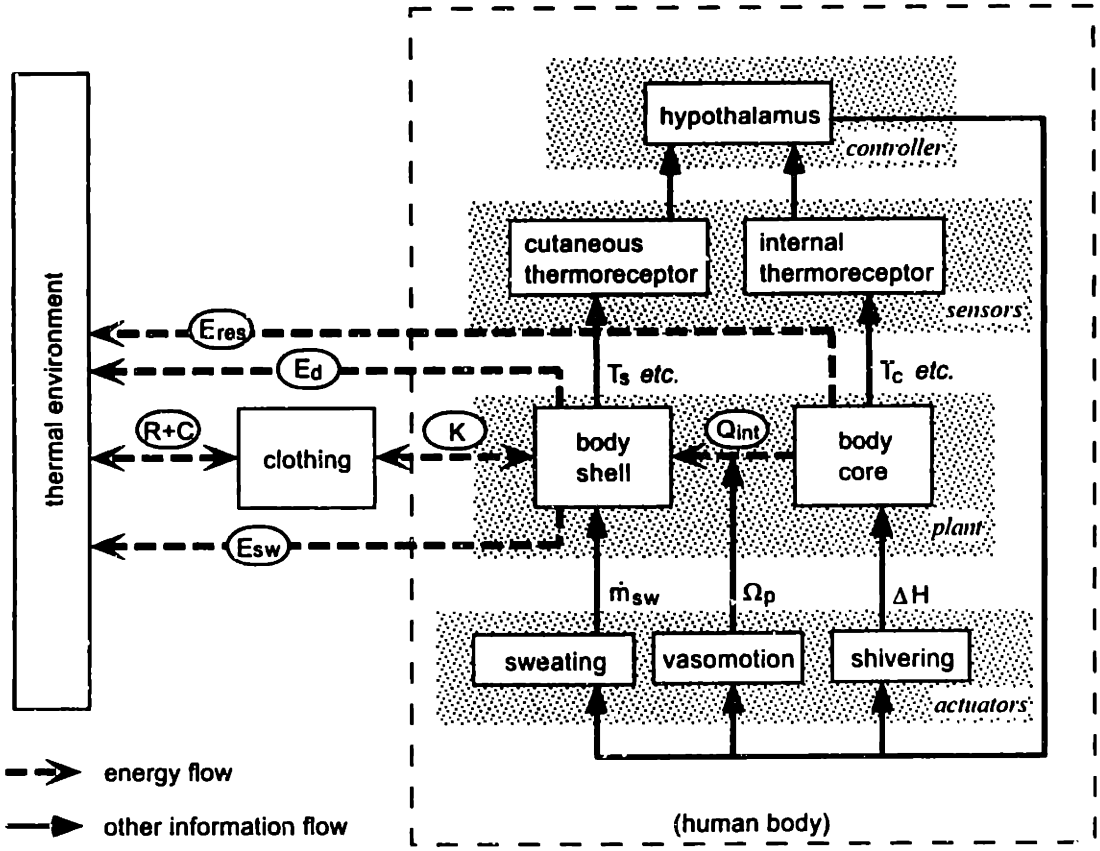

Figure 2.1: Human thermoregulatory control system

The most frequently used effector mechanism is the vasomotor control, i.e. the thermoregulatory control of peripheral blood flow. By changing the cutaneous blood flow, the human can control the amount of heat delivered from core to the outer surface of the body. Of the total heat produced within the body, less than half flows to the body surface by conduction through the tissues; most of it is transferred by convection in the blood stream. If the whole body is treated as a constant temperature core (the homeothermic core) plus a surrounding shell (a poikilothermic shell) which separates the core from the thermal environment, then the vasomotor control is the way the human body adjusts the equivalent thermal resistance (or conductance) of the shell, thus regulating the body heat loss. This regulation is effectively achieved by varying the blood flow rate from the core to the shell. For an adult, changes in the rate of blood flow can vary the thermal resistance of the body shell by a factor of 4 to 7, depending on the thickness of the body shell and subcutaneous fat [11].

In a cold environment, vasoconstriction takes place, in which case less blood is circulated to the outer layer of the body. As a result, less heat is transferred to the body surface by blood convection. In other words, we can say that the equivalent thermal conductivity of the shell is reduced, thus less heat is lost to the environment. On the other hand, in a hot environment, vasodilatation may double the body tissue conductivity so that body heat can be dissipated promptly as required.

Under certain or extremely cold conditions, when the normal metabolic rate can not balance the total heat loss to the environment, an increase in metabolism is brought about by the involuntary contraction of the skeletal muscles, such as shivering. Shivering is generally initiated first by a lowering of skin temperature without necessarily a fall in the core temperature. However, if in addition to skin cooling, the core temperature does fall, the shivering can become much more violent. Shivering increases to a maximum at a body temperature of around 34-35 ^oC. During shivering the changes that occur in overall heat production can be quite considerable and show an increase on the order of five to six times the resting metabolic rate. However, this increase rarely lasts for more than a few minutes; even the most violent shivering is characterized by periodic bursts of shaking interspersed with periods of almost complete rest. When averaged over a period of time, even with considerable body cooling, shivering does not increase the body heat production by more than 50-100 per cent. This level can be maintained over a period of an hour or more.

If the air temperature is higher than the body temperature, the only mechanism to lose body heat is through thermal sweating. Thermal sweating occurs from the eccrine glands in the skin. Eccrine glands are unevenly distributed over the entire skin, so sweating is not uniform over the body surface. Studies have shown that local sweat secretion depends on not only body and mean skin temperatures, but also local skin temperature. One result provided in [13] gives the local sweating rate as the following:

$$E_l = E_c \, e^{(T_{sl}-34)/10} \tag{2.1}$$

where E_c is the central drive dependent on core and average skin temperature in ^oC, and T_{sl} is the local skin temperature.

The whole body sweating response, which depends on a number of parameters such as skin wetness, state of acclimation, etc., is very difficult to model. Even though some attempts have been made, the results are still far from practically applicable.

2.2.2 Autonomic Control of Vasomotor

Since shivering and sweating only take place under extreme environment conditions, the discussion in this subsection will focus on the vasomotor control, the dominant effector mechanism when the environment condition is near neutral. Figure 2.2 provides an overview of the vasomotor control system, and the details of this control system are summarized as follows.

Autonomic nervous system

Temperature regulation in the body is controlled by the sympathetic nervous system, one of the two subdivisions of the autonomic nervous system. The autonomic nervous system is activated mainly by the Central Nervous System (CNS) located in the spinal cord, brain stem, and hypothalamus. It operates by means of visceral reflexes (Figure 2.3). Sensory signals enter the center of the spinal cord, brain stem, or hypothalamus, where in turn appropriate reflex responses are issued and transmitted back to the visceral organs to control their activities.

The autonomic nervous system has two subdivisions, sympathetic and parasympathetic systems. Each of the two subsystems has its own set of nerve fibers. The physiological anatomy of the two subsystem can be found in [14].

To understand how the body heat is regulated by the sympathetic nervous system, it is essential to know the basic aspect of information in nervous systems.

Information and signals

Physiological information is transmitted in the form of nerve impulses. A part of the body that is subjected to heat stress must first convert this information into nerve impulses, which are then transmitted to the CNS through afferent pathways. Specific areas of the brain convert abstract thoughts into nerve impulses that are then transmitted either elsewhere in the brain or into peripheral nerves to motor effectors throughout the

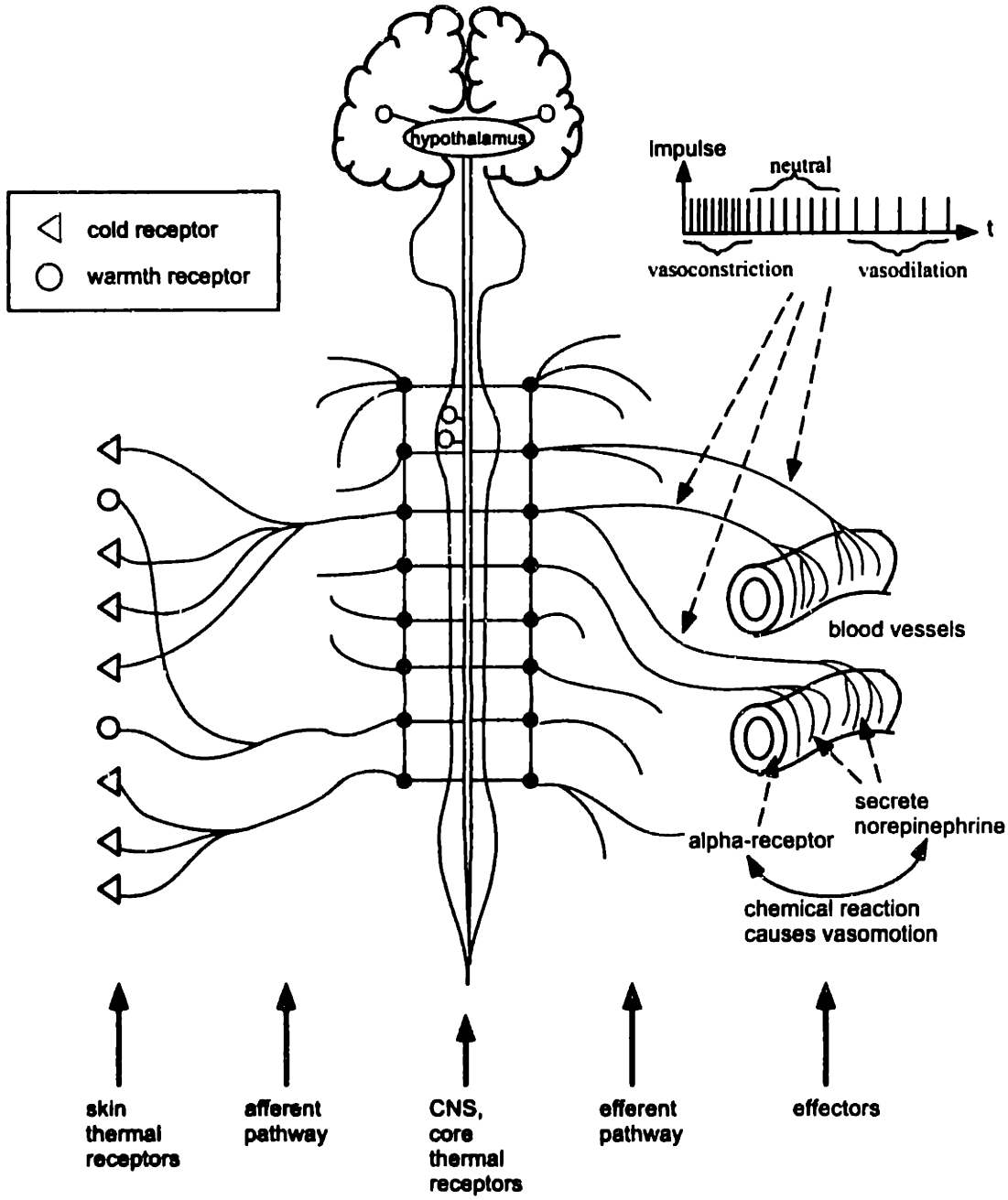

Figure 2.2: Reflex control of vasomotor

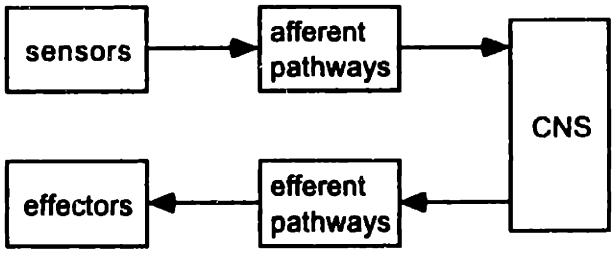

Figure 2.3: Reflex control of the autonomic nervous system

body. Each individual impulse has little meaning in terms of transmitted information. It is the overall pattern of the nerve impulses that carries the implied information. The pattern of nerve impulses includes the number of parallel nerve fibers activated (spatial summation), and the frequency of nerve impulses in each fiber (temporal summation).

Thermal receptors

The operation of the thermoregulatory system is mainly driven by human thermal sensation. The human being can perceive different gradation of cold and heat through two types of sensory receptors: the cold receptor, and the warmth receptor.

The cold and warmth receptors are located immediately under the skin at discrete but separated points, each having a stimulatory diameter of about 1 mm. In most areas of the body there are 3 to 4 times as many cold receptors as warmth receptors. The density of the receptors is far from uniform, it ranges from 15 - 25 cold points per square centimeter in lips, to less than 1 cold point per square centimeter in some broad surface areas of the body. Because there are far more cold receptors than warmth receptors in the skin, the detection of temperature in the skin mainly concerns cool and cold instead of warm temperatures.

Signals from cold receptors are transmitted via delta nerve fibers at velocities up to 20 m/s. It is believed that warmth signals are transmitted over type C nerve fibers at transmission velocities of only 0.4 to 2 m/s[14].

Internal thermal receptors have also been discovered by experiments. Heat-sensitive neurons have been identified in the preoptic area of the hypothalamus, which function as temperature sensors for controlling the core temperature. A few cold-sensitive neurons have also been found in other parts of the hypothalamus. However, the number of these

are few, and they play a negligible role in regulating body temperature. More about central nervous thermoreception can be found in [13].

The thermal receptors are stimulated by the change in their metabolic rates, due to the fact that temperature variation can alter the rate of intracellular chemical reactions about two-fold for every 10 ^{o}C change. In other words, thermal detection results from chemical stimulation of the endings of nerve fibers, rather than from direct physical stimulation.

Sympathetic vasomotor system

The most important part of the CNS involved in thermoregulation is the hypothalamus. The signals from the body peripheral and internal thermal receptors are integrated and processed in the posterior hypothalamus area to control body temperature. Efferent signals are discharged from this area to appropriate effectors through sympathetic nerves.

Efferent nerves in which increased impulse frequency raises the active tension of the vessel musculature are called *vasoconstrictor nerves*. Similarly, vasodilator nerves can be defined. The sympathetic nerves carry both vasoconstrictor and vasodilator nerve fibers, but by far the most important of these are the sympathetic vasoconstrictor fibers. Sympathetic vasoconstrictor fibers are distributed to essentially all segments of the circulation; however, this distribution is not uniform. It is less potent in regulating the blood flows in muscles and in the brain, while it is very powerful in regulating the peripheral blood flow rate.

The vasoconstrictor system is tonically active. That is, it has an inherent tendency to transmit nerve impulses all the time. The resting tone of the vessels is maintained by the continual (tonic) discharge of one and a half to two impulses per second. These impulses maintain a partial state of contraction in blood vessels, a state called *vasomotor tone*. Because of this vasomotor tone, the neurally controlled state of contraction of the vascular muscles of blood vessels can be varied in both directions to produce both vasoconstriction and - without the need for special fibers - vasodilatation. The vasomotor control in skin is solely controlled through this vasoconstrictor system. Maximal vasoconstrictor effects are elicited with a frequency of 10 impulses per second[11].

In addition to vasoconstrictor fibers, the sympathetic nerves to the skeletal muscles also carry sympathetic vasodilator fibers. However, the sympathetic vasodilator system plays a very small role in the thermoregulation of the body, and therefore details will not be discussed here.

Humoral regulation

Once the impulse signals from the CNS arrive at an effector organ, such as blood vessels, the effector organ takes appropriate actions. The actions are the result of certain chemical reactions induced by the sympathetic signals.

The sympathetic nerve endings secrete one of the two hormones: acetylcholine and norepinephrine. These hormones, which are called *sympathetic mediators*, act on the different organs to cause the respective sympathetic effects. The sympathetic mediators stimulate the effector organs by first reacting with receptor substances in the effector cells. The receptor, in most instances, is in the cell membrane and is a protein molecule. The mechanism for function of the receptor is that the hormone first binds with the receptor and this causes a basic change in the molecular structure of the receptor compound. Because the receptor is in integral part of the cell membrane, this structure change often alters the permeability of the cell membrane to various ions. The ionic changes then usually alter the membrane potential to produce the responses.

There are two types of receptors, namely alpha receptor and beta receptor. The sympathetic mediators excite the alpha and beta receptors differently. The sympathetic reactions with alpha receptors govern vasoconstriction, while the reactions with beta receptors control vasodilatation.

2.3 Thermal Neutrality and Human Thermal Load

The structure, components, and mechanisms of the human thermoregulatory system have been presented. In this section, the desired thermal state of the body, thermal neutrality, is defined. A deviation from this desired state is measured by means of human thermal load, which is also defined in this section.

2.3.1 Thermal Neutral Conditions

The thermally neutral state is defined as the steady-state of the body at which neither the mechanisms for heat dissipation nor those for protection against cold are active. This state is also referred to as *thermal neutrality.*

More specifically, thermal neutrality is an integrated state of the body at which:

1. the body is under a steady-state condition;

2. vasomotor is controlled by the thermoregulatory system only; and

3. none of the vasomotor control modes is activated.

The first condition is clear and simple. The second condition implies that cutaneous blood flow is determined by thermal effects only. Since body exercises can cause significant changes in cutaneous blood flow, the second condition requires the body to be at rest. Under the last two conditions, it is guaranteed that neither sweating nor shivering will take place. This is because sweating always comes with strong vasodilatation. and shivering takes place at the highest level of vasoconstriction.

The third condition can be elaborated in different ways. It can be expressed in terms of neural control properties, humoral control properties, or some net results of these controls, such as blood flow rate through cutaneous vessels.

In terms of neural control, thermal neutrality is a state of the body when the impulse frequency of the vasoconstrictor efferent signals (f_c) is equal to the frequency of the vasomotor tone (f_{tone}):

$$f_c = f_{tone} \tag{2.2}$$

Since the effectors are activated as a result of the chemical reactions between the hormones and the receptors, it is also possible to quantify condition 3 by using the amounts of specific hormones in the cutaneous tissue. Since there could be more than one hormone involved in the thermoregulation at the same time, more detailed studies are needed to define thermal neutrality in terms of hormones or other chemicals.

The third way to quantify condition 3 is to use the net result of the thermoregulation actions. The vasomotor control causes changes in peripheral blood flow, and therefore

adjust the heat loss to the environment. So the third condition can be expressed in terms of peripheral blood flow rate Ω_p:

$$\Omega_p = \Omega_p^* \tag{2.3}$$

where Ω_p^* is the peripheral blood flow rate under conditions 1, 2 and equation 2.2.

Another important property of thermal neutrality is its connection with metabolic rate. The metabolic rate of a resting subject reaches its minimum value when the body state is at thermal neutrality[11]. When the body temperature drops, additional heat is required to maintain the core temperature. The more heat production, the higher the metabolic rate. On the other hand, if the body state is on the warm side, the activation of additional heat loss mechanisms will cause an increase in metabolic rate as well. As a result, the metabolic rate is minimal at thermal neutrality. This connection can also be used to define the state of thermal neutrality.

2.3.2 Human Thermal Load

Under different environment conditions, the thermal state of the body usually deviates from the desired state - thermal neutrality. Depending on the severity of the thermal environment, a subject may feel warm (cool) or hot (cold), and the amount of work demanded on the thermoregulatory system can be high or low. So one way to quantify the deviation from the neutrality is to use the amount of work imposed on the thermoregulatory system, which is defined as the *human thermal load*. In other words, human thermal load is the work load on the thermoregulatory system to maintain body temperature.

By definition, human thermal load is zero at thermal neutrality. A non-zero human thermal load can be represented by different variables. If equation (2.2) is used for the definition of thermal neutrality, then human thermal load can be written as:

$$L_f = f_c - f_{tone} \tag{2.4}$$

Human thermal load can also be defined as a function of peripheral blood flow rate:

$$L_\Omega = \Omega_p - \Omega_p^* \tag{2.5}$$

Of course, human thermal load can be defined in other forms in addition to (2.4) and (2.5). For example, it can be defined in terms of energy transfer of the body [15]. A practical criterion for selecting the form of the human thermal load is the accessibility of the physical or physiological variables that are involved. The frequency of an efferent signal is difficult to measure, so it is not convenient to use the definition (2.4) for practical purposes. On the other hand, as it will be shown later in the thesis. blood flow can be easily measured. So equation (2.5) will be used as the definition of human thermal load in the remainder of this thesis. In the following chapter. the human thermal load is utilized to develop a control algorithm with the objective of achieving thermal neutrality.

Chapter 3

Zero-Load Control of Indoor Thermal Environment

The review of the human physiology in Chapter 2 indicates that thermal neutrality is a preferred physiological state of the body. A new HVAC control system that achieves such a desired state is outlined in this chapter. The control objective is to minimize the human thermal load, and to achieve thermal neutrality. To obtain the human thermal load in real time, human instrumentation is required. Sensor design as well as the properties of the measured physiological signal are presented in this chapter. Experiments on human subjects illustrate the advantages of the new control system, as well as potential problems.

3.1 Zero-Load Control

The human body can balance body heat within a wide range of thermal environment conditions, but only a narrow interval in this wide range corresponds to comfort sensation. The definition of thermal comfort given in the previous chapter cannot be used to determine the comfort range because of the involvement of the condition of mind. The state of human mind is difficult to monitor, perhaps impossible to control. So from the control point of view, a more practical and tangible objective should be adopted in the control design. In this research, the control objective is defined as the physiological thermal neutrality.

As shown earlier, the thermal state of the human body is regulated by the human thermoregulatory system. At the same time, HVAC systems can also affect the thermal state of the body. Because both the human thermoregulatory system and HVAC system operate on the human body (Figure 3.1), we can define the role of the HVAC system as an assistant to the human thermoregulatory system, with the objective of maintaining a minimal load on the human autonomic regulatory system.

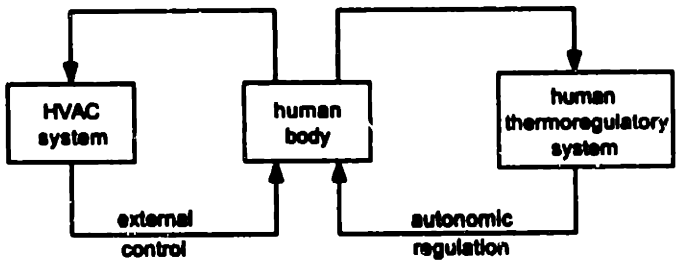

Figure 3.1: Two systems which change the thermal states of the body

The load on the human thermoregulatory system has been defined as:

$$L_\Omega = \Omega_p - \Omega_p^* \tag{3.1}$$

The control objective is to keep the value of L_Ω zero, hence the term *zero-load control* (ZLC). The achieved state of ZLC is thermal neutrality. Even though thermal neutrality is not equivalent to the thermal comfort as defined by ASHRAE, it is a state of the body when it's under the least stress. Experimental results have shown that at thermal neutrality, the thermal sensations of human subjects are very close to comfort. More about the correlation of thermal comfort and thermal neutrality will be addressed in Chapter 4.

The block diagram of a closed-loop zero-load control system is shown in Figure 3.2. With the human thermal load defined in Equation (3.1), peripheral blood flow rate Ω_p is used in the control system as the feedback signal. In this closed-loop control system, thermal neutrality can be reached by regulating one or more thermal environment variables, such as air temperature, air velocity, etc..

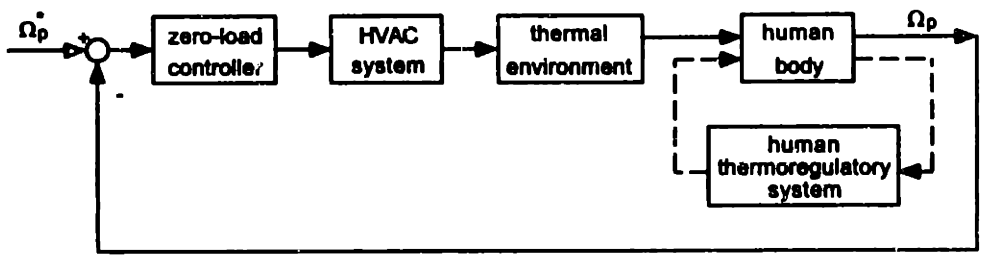

Figure 3.2: Block diagram for zero-load control of HVAC system

3.2 Peripheral Blood Flow

The proposed zero-load control requires the real time measurement of peripheral blood flow, i.e. the total blood flow rate from body core to body shell. In general, it is difficult to directly measure this total blood flow rate. On the other hand, blood flow through extremities, such as fingers, can be easily measured. Since peripheral blood flow is mainly controlled by the central nervous system (CNS) [11] for thermoregulation. measurements of blood flow through extremities can be utilized for monitoring the human thermoregulatory system. In this research, the finger blood flow rate is selected as the blood flow signal.

There are many advantages to use finger blood flow rate as the feedback signal. They can be summarized as follows.

- Fingers are highly accessible. To make the proposed control algorithm practical. sensors must not be intrusive and should be located at acceptable locations. Since humans are used to wearing rings, a sensor embedded in a finger ring is most likely to be accepted by a human. A finger ring sensor as shown in Figure 3.3 is being developed in the d'Arbeloff Laboratory at MIT.

- Finger blood flow is most sensitive to thermal environment changes. An important function of the peripheral circulation is convective transfer of heat from body core to the skin surface. Physiological studies have shown that the cutaneous blood flow rate can be orders of magnitude higher than the rate required by the metabolism [16]. Since fingers mainly consist of skin and subcutaneous tissue. the thermoregulatory effect on the circulation system can be well observed by measuring the blood flow through a finger. Another reason that makes finger blood flow very sensitive to the thermal environment is the existence of a large number of arteriovenous anastomoses (AVA). AVA can cause significant changes in skin blood flow during thermoregulation, and its role in the thermoregulatory system has been clearly identified [17, 18, 19].

- It has been extensively studied. Since finger blood flow is easy to measure by many techniques, it has been extensively studied over the years. Correlation

between finger blood flow rate and other physiological parameters, such as skin temperature, core temperature, and activity level, have been established [20, 21].

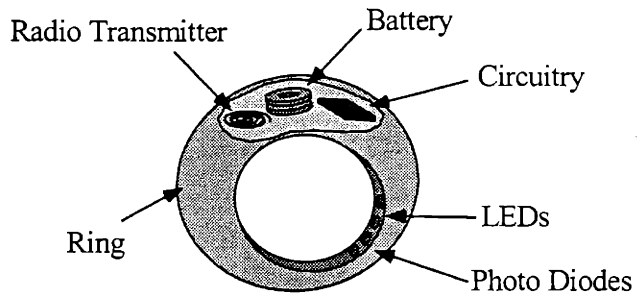

Figure 3.3: Finger ring sensor (*courtesy of Dr. Booho Yang*)

For the above reasons, finger blood flow rate is used as the representative of overall peripheral blood flow rate. We can redefine the human thermal load as:

$$L_\Omega = \Omega_f - \Omega_f^* \tag{3.2}$$

To use finger blood flow as the feedback signal, it is important to understand some basic properties of this physiological variable. Only those properties which are relevant to the feedback control problem will be addressed here.

It has been observed that there is a continuous oscillation between cutaneous vasoconstriction and vasodilatation under nearly neutral or warm environment. Figure 3.4 shows a sample of the finger blood flow data under a near neutral condition. The period of this oscillation is on the order of 1 minute, and the waves are synchronized over the whole body [13]. A filter shall be designed to eliminate the effect of such oscillation on the control system. More on filter design will be presented in the next section.

Information aggregation is another important property of finger blood flow rate. Because peripheral blood flow is controlled by the CNS, any thermal stimuli on any part of the body will be reflected to some degree in the finger blood flow. This has been confirmed by many physiological experiments. Such a property is very beneficial to thermal environment control because it can be used to tackle local discomfort problems such as draft. Figure 3.5 shows the change of finger blood flow when a draft situation is created. At the 2-minute time mark, a mini-fan (3 in. diameter) was turned on and blew

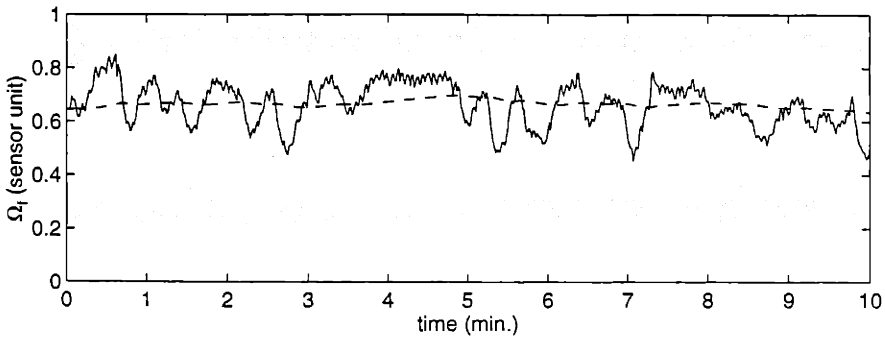

Figure 3.4: A sample of finger blood flow measurement: solid line shows recorded data (sampling period = 1 sec.), dash line is the filtered result.

air towards the neck of the subject who was resting at a near neutral condition. Finger blood flow quickly dropped when the draft condition was imposed. By combining finger blood flow and some other signals, such as local skin temperature, one can detect the existence of air draft or other forms of local discomfort.

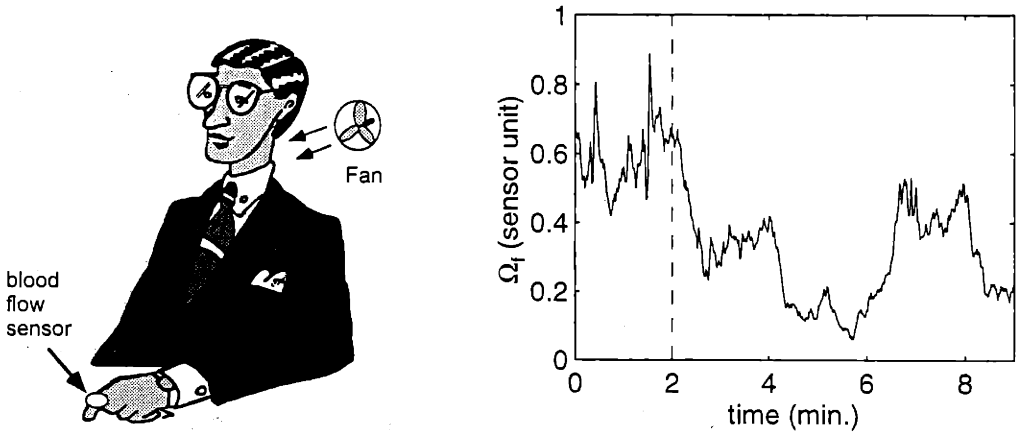

(a) draft situation

(b) blood flow change

Figure 3.5: The change of finger blood flow under a draft condition (the fan was turned on at the dash line)

Of course, not every aspect of finger blood flow plays a positive role in our control problem. The human body is a complicated system, and many non-thermal factors may also cause changes in peripheral blood flow. For example, emotion, posture, exercise, and many abnormal conditions such as fainting can induce significant changes in the

finger blood flow [16]. However, many non-thermal effects can be detected and treated using various methods. For example, physical exercise can be detected from additional physiological signals, so their effects can be compensated with the knowledge of corresponding physiological models. The effects of emotion and posture usually exist for some short time period. Using proper signal processing techniques and special consideration in controller design, the influence of emotion and posture on the control system can be minimized.

3.3 Instrumentation Issues of ZLC

3.3.1 Blood Flow Measurement

There are many ways to measure blood flow rate. Some commonly used methods include venous occlusion plethysmography, photoelectric plethysmography, thermal conductance or conductivity methods, to name a few. The details of these methods can be found in [22]. Among these methods, venous occlusion plethysmography is the most commonly used in the physiological study of blood flow in extremities because of its simplicity and quantitative reliability over a wide range of temperature. However, because of the bulky apparatus, it is not a good candidate for real time applications. Instead, photoelectric plethysmography is selected for this research, since the sensor device can be made relatively compact and easy to carry. Another advantage of this method over the venous occlusion method is its ability to make continuous measurements.

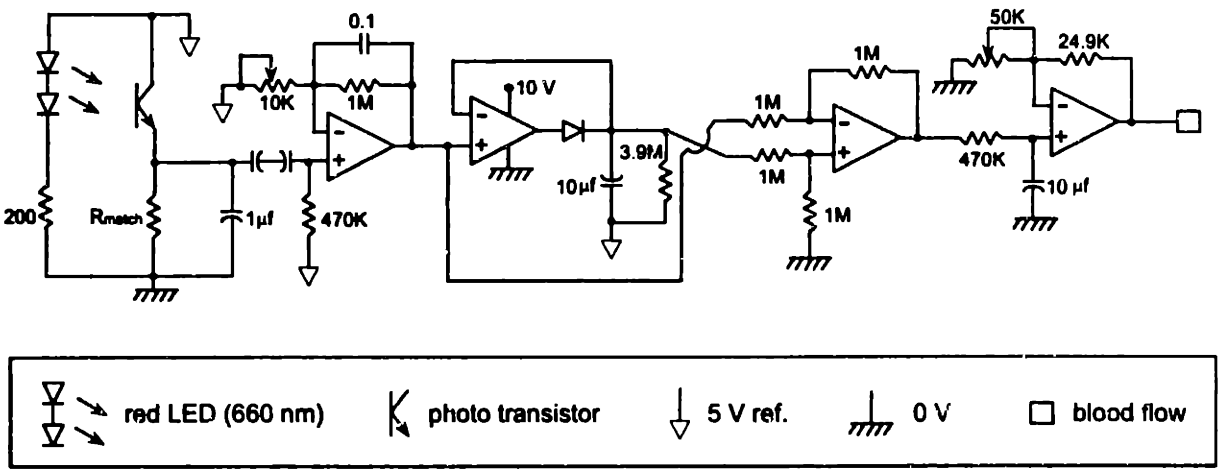

Figure 3.6: Electronic circuit of the blood flow sensor

Figure 3.6 shows the electronic circuit of the photoelectric sensor used in current research work. The principle of photoelectric plethysmography is as follows. The absorptivity of body tissue varies according to the amount of blood flow through it. By detecting the reflection from the skin for a given light source, the change of the absorptivity of the tissue can be measured, which can be related to the amount of blood flow through the tissue. Therefore, it is an indirect method and does not provide an absolute value of the blood flow rate. The signal directly measured from the sensor is the blood flow rate in some sensor unit. Calibration is needed to establish an accurate correlation between the sensor signal and the physical blood flow rate. Due to the differences in skin color and finger size, calibration should be done for every individual.

Another important issue regarding sensor design is the sensor interference in the blood flow dynamics. The possible sensor interference may come from two aspects: the mechanical aspect and the thermal aspect. The mechanical interference is very negligible because of the small pressure at the interface ($< 1\ mmHg$). To cause a change of the resistance in venule requires an pressure of 40 $mmHg$, while the resistance change in arteriole demands a pressure more than 100 $mmHg$.

The thermal interference may happen in two ways, through the vasomotor reflex and through local mechanisms. Because the sensor is so small, it does not cause any significant change in the overall heat transfer process, thus the reflex interference is minimal. However, the local effect of the sensor may not be as small. To find out the local effect, a simple test was performed. A blood flow sensor was first attached to a finger and the steady-state was reached. Then another identical sensor was put on the same finger right next to the first sensor with the purpose of disturbing the local condition. If any significant local effect would take place, the reading of the first sensor should indicate such a change. As shown in Figure 3.7, no noticeable change is observed.

3.3.2 Filter Design for the Blood Flow Sensor

As shown in Figure 3.4, the measured blood flow always fluctuates with a period of about 1 minute even under a steady-state condition. Some non-thermal disturbances,

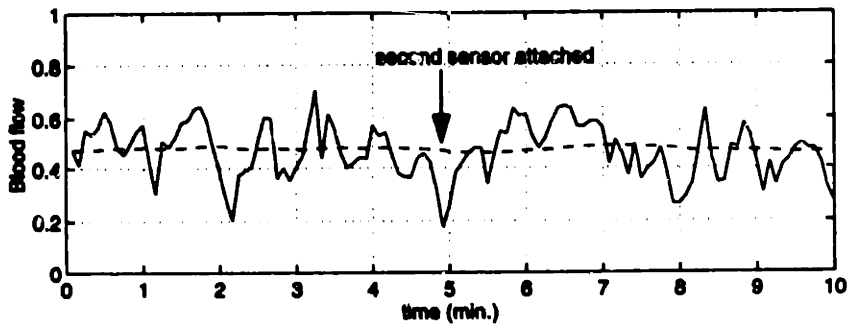

Figure 3.7: The test result for sensor interference with the natural blood flow. The solid line is the sensor measurement with a sampling time of 5 seconds. The dashed line is the filtered data.

such as changing the posture, may induce even larger fluctuations of blood flow within a short time period. To minimize these non-thermal effects on ZLC, a digital filter is used to preprocess the measured blood flow signal before it is used by the controller.

The frequencies of blood flow dynamics caused by changes of thermal environment are usually much lower than those caused by non-thermal disturbances. So a low-pass filter should be used in the blood flow sensor. A digital low-pass filter was designed and implemented in the software of the control system. The filter was a third order Butterworth filter, with a cutoff frequency of $3.3 \cdot 10^{-3}\ Hz$ (which corresponds to a time period of 5 minutes). For a sampling rate of 2 seconds, the transfer function of the digital filter is:

$$G_f(q^{-1}) = \frac{10^{-3} \cdot (0.0397 + 0.1191q^{-1} + 0.1191q^{-2} + 0.0397q^{-3})}{1.0 - 2.8604q^{-1} + 2.7304q^{-2} - 0.8697q^{-3}} \tag{3.3}$$

In continuous time system, it corresponds to the following transfer function:

$$G_f(s) = \frac{10^{-4} \cdot (0.3971s^3 + 0.5574s^2 + 0.4159s + 0.4258)}{s^3 + 0.06983s^2 + 0.002438s + 0.00004258} \tag{3.4}$$

Figure 3.8 shows a sample of the real time sensor measurement, and its filtered result. Because of the filter dynamics, there is a phase lag between the real time data and the filtered data. The dashed line shown in Figure 3.8 is the filtered data with the phase lag removed. For real time applications, this phase lag should be compensated for in the control design if stability and certain system performances are to be guaranteed.

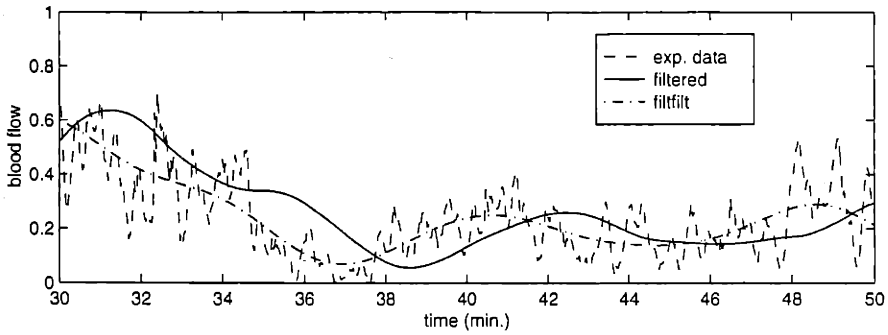

Figure 3.8: A sample of the original blood flow measurement (dashed line), the filtered signal (solid line), and the zero-phase filtered signal generated by Matlab function *filtfilt* (dashdot line).

3.3.3 Sensor Calibration and Thermal Load Evaluation

To implement the ZLC algorithm, one or both of the following values must be determined for each human subject. These values are:

1. The reference value Ω_f^*, which corresponds to the value of Ω_f at thermal neutrality. This value must be identified in order to evaluate the human thermal load, no matter what controller is used.

2. The ratio, r_Ω, between Ω_f in sensor units (the voltage output from the sensor) and $\bar{\Omega}_p$ in physical units (for example: $liter/m^2hr$). This value may or may not be required depending on which method of control design is selected. For a model-free controller, such as the PI controller to be shown in the next section, this value is not necessary. However, for a model-based controller, this ratio is important, and must be provided in order to obtain a reliable controller.

Two methods to obtain the value of Ω_f^* are presented in this thesis. Both methods are based on experimental data. The first method determines the Ω_f^* using human voting. The human subject is exposed to many different thermal environmental conditions, and the finger blood flow in the sensor unit as well as the thermal sensation of the subject are recorded. The value of finger blood flow corresponding to the comfortable voting can be used as a good approximation of Ω_f^*. The results of this method give only approximations to Ω_f^* due to the involvement of human voting, i.e. the involvement of

the mind. The value of Ω_f^* is a function of only physiological states by definition, not of the condition of mind. Human thermal sensation is a very complex phenomenon, particularly during a thermal transient. To obtain a reliable value of Ω_f^* using this method, the voting under steady-state condition shall be used. As a result, the overall procedure is very time-consuming.

The other method uses the model of the human thermoregulatory system, and will be presented in Section 4.3. Compared to the first method, this approach requires much less experimental effort.

The ratio r_Ω can also be determined in two different ways. The first method is to directly measure both $\bar{\Omega}_p$ and Ω_f, the ratio of the two variables can be obtained immediately. The accuracy of this method depends on how accurate $\bar{\Omega}_p$ can be measured. By definition, $\bar{\Omega}_p$ is the average peripheral blood flow per unit skin area, which is difficult to measure even in a laboratory environment. Usually, this value is approximated from the blood flow rate through a limb.

The second method is based on the human thermoregulatory model, and will be presented in Section 4.3. If the model of the human thermoregulatory system is available, both Ω_f^* and r_Ω can be evaluated easily.

3.4 Preliminary Experimental Results of ZLC

To give a proof-of-concept demonstration of the ZLC method, experiments on human subjects were carried out in the HVAC test chamber in the d'Arbeloff Laboratory at MIT. The design of the test chamber as well as its device control system are provided in Appendix A.

There are three air supplies and one air return in the test chamber. Two of the air supplies are wall diffusers, and the other is a ceiling diffuser. For the following experiments, all these diffusers are fully open, and supply air temperatures are controlled at the same reference value. The supply air temperature was used to regulate the occupant's finger blood flow rate. Human subjects were seated at certain locations in the chamber and relaxed. The clothing insulation is 0.6 clo[1], corresponding to a short-

[1] 1 clo = 0.155 Km^2/W. More about the clothing insulation will be presented in Section 4.2.3.

sleeve T-shirt, long trousers, belt, calf-length athletic socks, and soft-soled athletic shoes.

The test procedure is described as follows. The subject was pre-heated or pre-cooled in the chamber for a period of time, so the thermal state of the subject was set away from thermal neutrality. The controller was then turned on, and room air temperature was changed according to the real time value of finger blood flow rate.

The zero-load controller used in the experiments was a simple proportional - integral (PI) controller:

$$T_0 = T_0^r + K_P(\Omega_f^* - \Omega_f) + K_I \int_t (\Omega_f^* - \Omega_f)dt \tag{3.5}$$

where T_0^r is a reference supply temperature, K_P is the proportional gain, and K_I is the integral gain. The integral term is used to eliminate the steady-state error of the closed-loop system. The control gains were manually tuned when the subject was seated at location I (Figure 3.12). In designing the PI controller, the only knowledge required about the plant (including the human subject and the thermal environment) is the directional information, i.e., an increase of supply air temperature will increase the blood flow rate, and *vice versa*.

Figure 3.9 shows the results of a cooling test. The subject was pre-warmed in the chamber for an hour at air temperature 31 ^oC. The controller was then turned on to regulate the blood flow rate of the subject by changing supply air temperature. The plots do not include the pre-warming phase, and control starts at time 0.

From Figure 3.9, the dynamic effect of the thermal state of the body is quite obvious. The local air was cooled to about 23 ^oC when the subject first reached the neutral state, but the local air temperature kept rising to a certain value over time because of the dynamic transient of body states. This agrees well with human behavior control in a similar scenario. When a person enters an air conditioned room from a hot environment, he or she prefers a low air temperature. After some time, when his/her body is cooled down, he/she will set the temperature somewhat higher to prevent over-cooling. In our control approach, the controller can automatically compensate for this dynamic effect.

Figure 3.10 and 3.11 show the results of two similar tests on the same subject. The same PI gains were used for both cases. The only difference was the location of the

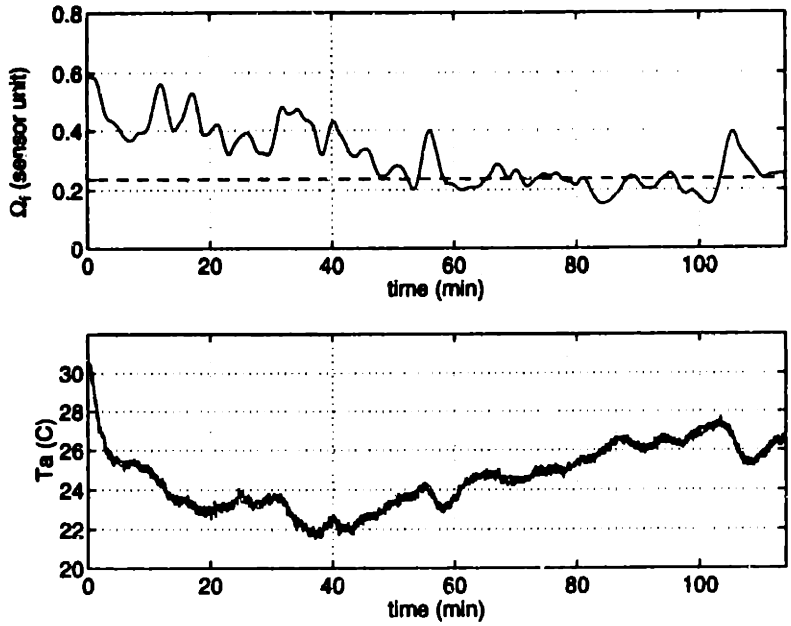

Figure 3.9: Zero-load control: starting from a warm state.

subject in the test chamber.

In the case of Figure 3.10, the subject was seated at location I (Figure 3.12), and the local air velocity was $0.15m/s$. The PI gains were tuned at this location. The same control gains were used in the case of Figure 3.11, when the subject was seated at location II. The local air velocity at location II was $0.3m/s$. Clearly, the closed-loop system became unstable at location II, which indicates that different control gains are required to keep the system stable at different locations.

The above experimental results indicate that a simple PI controller is not robust enough to guarantee the stability of the closed-loop system. To provide a systematic approach to designing a stable ZLC, certain knowledge of the plant is required. The next two chapters are dedicated to the modeling of the plant, which include the human occupant and the thermal environment. We will begin with the modeling of human thermoregulation.

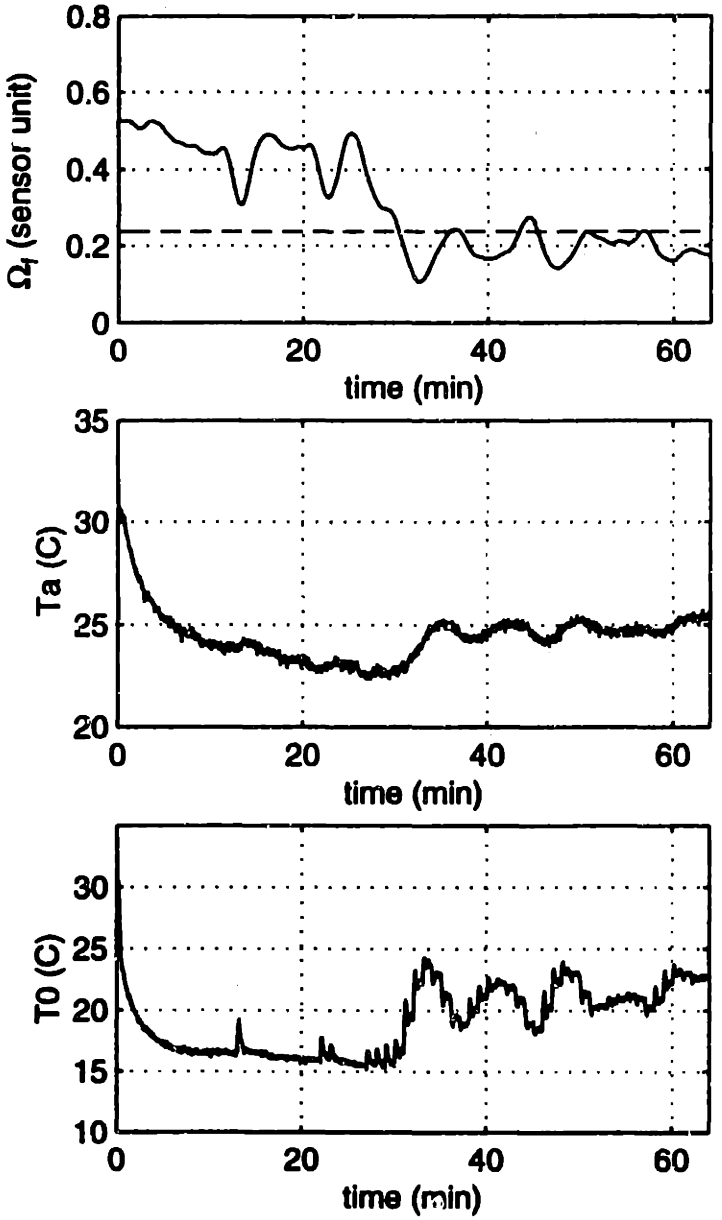

Figure 3.10: ZLC: PI controller, location I

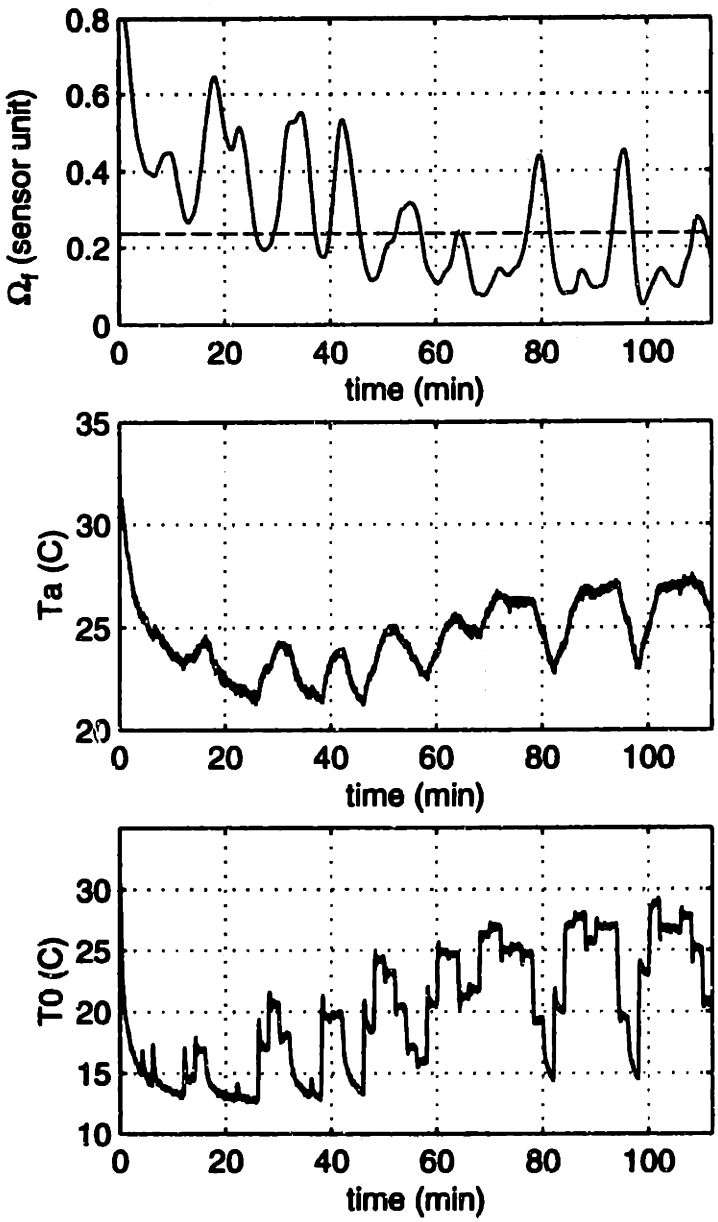

Figure 3.11: ZLC: PI controller, location II

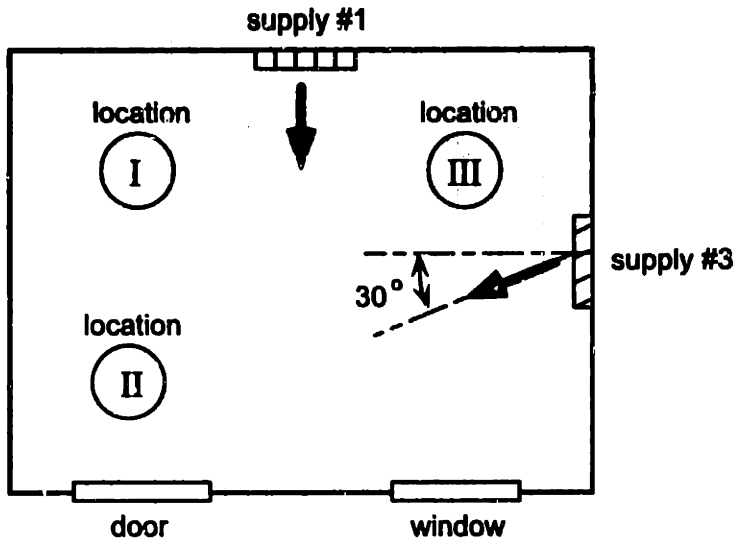

(a) subject locations (top view)

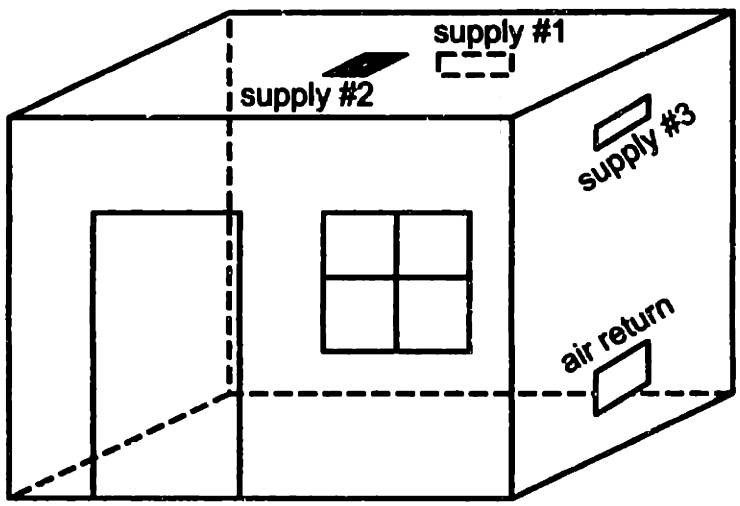

(b) diffuser locations

Figure 3.12: Subject locations and diffuser locations in the test chamber. All diffusers were fully open during the tests. More about the test chamber can be found in Appendix A.

Chapter 4

A Dynamic Model of Human Thermoregulation

To understand the dynamic behavior of peripheral blood flow and to design stable and robust zero-load controllers, a dynamic model of the human thermoregulatory system is needed. In this chapter, a low-order human thermoregulation model is presented. Based on the model, a sensor calibration method is developed, which provides values of r_Ω and Ω_f^*. Experiments on multiple human subjects were performed to verify the thermoregulation model. Comparisons between the model and experimental results provide estimations of the modeling errors, which will be used in model-based control design.

4.1 The Mathematical Model

The closed-loop control system, as shown in Figure 3.2, uses blood flow rate as the controlled variable. In this section, a dynamic model for the human thermoregulatory system is presented, which provides a mathematical description of how the blood flow changes in various thermal environments. This model, as shown in Figure 4.1, consists of two components: a passive system of the body, and an autonomic control system - the human thermoregulatory system.

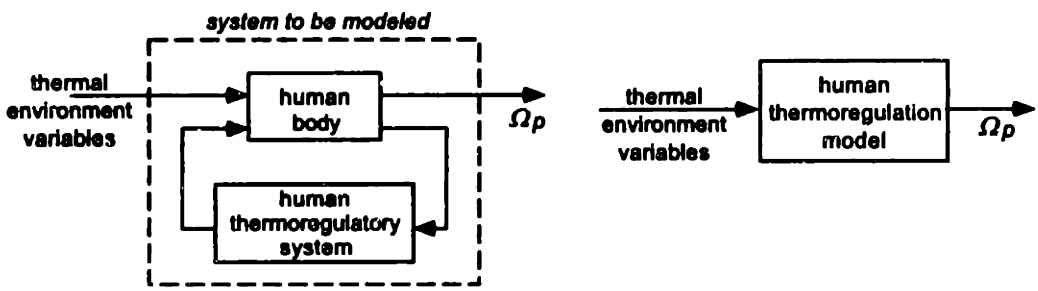

Figure 4.1: The model of the human thermoregulation

4.1.1 The Passive System

The modeling of heat and mass transfer inside the human body has been studied for many years, and many models have been developed. A review of these models can be found in [23, 24]. Models range from simple lumped parameter models to distributed parameter models such as finite element models. Since it is the dynamic behavior of related physiological variables that is most important to the control design, a low order model which can capture the dominant dynamics of blood flow is desired. For this reason, a two-node model developed by Gagge *et al.* [2] is adopted. The details of the model are as follows.

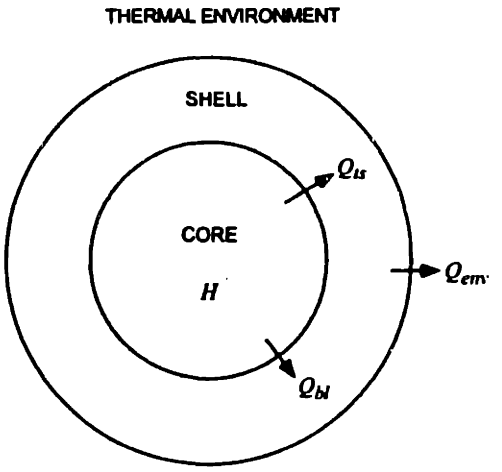

Figure 4.2: Two regions of the body: body core and body shell

The human body can be lumped into two thermal masses: the body core and the body shell (Figure 4.2). The thermal state of the human body is assumed to be uniquely determined by the core temperature T_c and the shell temperature T_s. By applying the first law of thermodynamics, the dynamics of the core and the shell can be written as:

$$C_c\dot{T}_c = H - Q_{ts} - Q_{bl} \tag{4.1}$$

$$C_s\dot{T}_s = Q_{ts} + Q_{bl} - Q_{env} \tag{4.2}$$

where:

$$H = M - E_{res} - W \tag{4.3}$$

$$Q_{ts} = h_K(T_c - T_s) \tag{4.4}$$

$$Q_{bl} = (\rho c_p)_{bl}\,\Omega_p(T_c - T_s) \tag{4.5}$$

$$Q_{env} = h_a(T_s - T_a) \tag{4.6}$$

The total amount of heat to be dissipated to the environment through skin surface is H. Part of the heat is transferred from the core to the surface by conduction through the tissue - Q_{ts}, while the rest of the heat is delivered to the surface by convection through blood flow - Q_{bl}. At a steady-state condition, the sum of Q_{ts} and Q_{bl} is equal to the amount of heat transferred to the thermal environment at the skin surface - Q_{env}.

Substituting equations (4.4-4.14) into the body dynamic model (4.1-4.2) and dividing both sides of the equations by the body area A_{Du}[1], we have:

$$\bar{C}_c\dot{T}_c = H/A_{Du} - \bar{h}_K(T_c - T_s) - (\rho c_p)_{bl}\bar{\Omega}_p(T_c - T_s) \tag{4.7}$$

$$\bar{C}_s\dot{T}_s = \bar{h}_K(T_c - T_s) + (\rho c_p)_{bl}\bar{\Omega}_p(T_c - T_s) - \bar{h}_a(T_s - T_a) \tag{4.8}$$

The physical properties of blood and tissue used in the model are listed in Table 4.1. Values of thermal conductivity for different body materials are also provided in the table.

properties	values	sources
$(c_p)_{bl}$	3899 J/kgK	[26]
$(c_p)_{ts}$	3135 J/kgK	[26]
$(\rho c_p)_{bl}$	$4.133 \cdot 10^6$ $J/(m^3K)$	[26]
$(\rho c_p)_{ts}$	$3.314 \cdot 10^6$ $J/(m^3K)$	[26]
K_{fat}	0.20 W/mK	[10]
K_{muscle}	0.39 W/mK	[10]
K_{ts}	0.3 W/mK	[27]

Table 4.1: Physical properties of human body materials

In the above human dynamic model, the following assumptions have been made:

[1]DuBois area[25], the surface area of the nude body in m^2, calculated from the weight (in kg) and the height (in cm) of the body: $A_{Du} = 0.00718 \cdot Weight^{0.425} \cdot Height^{0.725}$

- Neither sweating nor shivering takes place. The balance of body heat is achieved only through vasomotor control. So this model should be applied to conditions not too far away from thermal neutrality. In the original Gagge's model, the energy associated with sweating is also included.

- The energy transfer between thermal environment and skin surface is characterized by a single parameter h_a. This is a good approximation only when the clothing insulation is little ($I_{cl} < 1.0$). If there is significant clothing, the thermal capacitance of the clothing material as well as the air trapped in between layers of fabric can appreciably change the body dynamics. The dynamic effects induced by the thermal capacity of clothing can be found in other more sophisticated models, such as [28, 23, 24].

4.1.2 The Autonomic Control System

To complete the dynamic model given above, the autonomic control of peripheral blood flow must be modeled. This controller, which is part of the central nervous system, determines the amount of peripheral blood flow based on the signals transmitted from both skin and core thermal receptors.

It has been shown in Chapter 2 that there are two kinds of thermal signals, namely the warmth signal and the cold signal. For vasomotor control, the warmth signal (Σ_{warm}) is dominated by the core temperature, and the cold signal (Σ_{cold}) is determined by the skin temperature. That is:

$$\Sigma_{warm} = F_1(T_c) \tag{4.9}$$

$$\Sigma_{cold} = F_2(T_s) \tag{4.10}$$

and the peripheral blood flow rate is a function of Σ_{warm} and Σ_{cold}:

$$\Omega_p = F_3(\Sigma_{warm}, \Sigma_{cold}) \tag{4.11}$$

Based on the research work done at Yale Medical School[2, 29], the functions F_1,

F_2, and F_3 have the following form:

$$\Sigma_{warm} = \max(0, T_c - T_c^{\Sigma}) \tag{4.12}$$

$$\Sigma_{cold} = \min(0, T_s - T_s^{\Sigma}) \tag{4.13}$$

and the peripheral blood flow per unit skin area is determined by the following equation:

$$\bar{\Omega}_p = \frac{6.3 + 75\Sigma_{warm}}{1 - 0.5\Sigma_{cold}} \quad (liter/hr\ m^2) \tag{4.14}$$

where

$$\bar{\Omega}_p = \Omega_p / A_{Du} \tag{4.15}$$

and the values of the reference states T_c^{Σ} and T_s^{Σ} are $36.6°C$ and $34.1°C$ respectively.

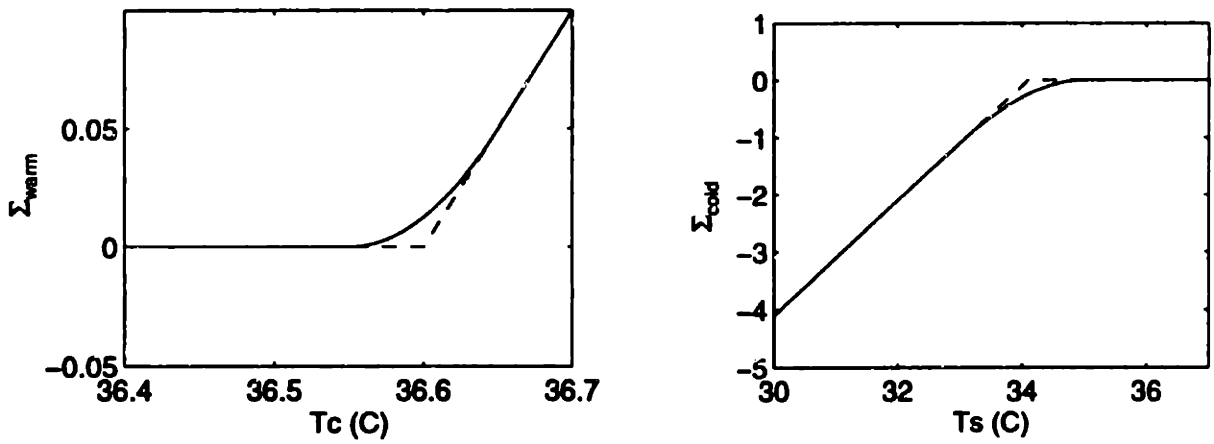

(a) Warmth signal

(b) Cold signal

Figure 4.3: Comparison of different models for thermal signals. The original thermal signals used by Gagge (dashed lines) and the C^1-continuous versions of the signals (solid line)

The warmth signal Σ_{warm} and cold signal Σ_{cold} as defined in equations (4.12. 4.13) have discontinuous derivatives at the neutral state (Figure 4.3). For both numerical and realistic reasons, smoother functions are preferred. The following functions which have continuous first order derivatives (C^1-continuous functions) will be used in the

thermoregulation model for control design.

$$\Sigma_{warm}(T_c) = \begin{cases} 0 & \text{if } T_c < 36.55\ ^oC, \\ a_3T_c^3 + a_2T_c^2 + a_1T_c + a_0 & \text{if } 36.55\ ^oC \leq T_c \leq 36.65\ ^oC, \\ T_c - T_c^{\Sigma} & \text{if } T_c > 36.65\ ^oC. \end{cases} \tag{4.16}$$

$$\Sigma_{cold}(T_s) = \begin{cases} T_s - T_s^{\Sigma} & \text{if } T_s < 33\ ^oC, \\ b_3T_s^3 + b_2T_s^2 + b_1T_s + b_0 & \text{if } 33\ ^oC \leq T_s \leq 35\ ^oC, \\ 0 & \text{if } T_s > 35\ ^oC. \end{cases} \tag{4.17}$$

where: $a_3 = 6.0837 \cdot 10^{-10}$, $a_2 = 5.0000$, $a_1 = -365.50$, $a_0 = 6679.5$, $b_3 = -0.025000$, $b_2 = 2.3000$, $b_1 = -69.125$, and $b_0 = 673.75$. The two C^1-continuous functions and their original counterparts are shown in Figure 4.3.

4.2 Model Parameters and Variables

There are many parameters and variables involved in the human thermoregulation model (4.7), (4.8), and (4.14). These parameters and variables can be classified into the following three groups: user-specific parameters, state-dependent variables, and human-environment variables. In the current model, the human-environment interaction is characterized by a single heat transfer coefficient h_a.

4.2.1 User-Specific Parameters

There are many parameters in the thermoregulation model that are user dependent. For example, body weight, which determines the thermal mass of the body and affects the body surface A_{Du}, can vary significantly from one user to another. It is not difficult to show that the thermoregulation dynamics of a 100 lb person are noticeably different from those of a 200 lb person. To predict the dynamics accurately using the model, such user-dependent parameters must be properly identified. Table 4.2 lists some basic human factors which have an impact on the thermoregulation dynamics.

The height and weight of an occupant can be provided either through direct measurement, user input, or database lookup. The information of fatness can be obtained through certain sensors. As it will be shown later in the thesis, the effect of fatness is

Table 4.2: Basic human factors which can change the thermoregulation dynamics

parameter	impact on the model
weight	thermal masses, A_{Du}
height	A_{Du}
fatness	body conductance h_K

not as significant as other user-specific parameters, and an average value is good enough for the majority of people.

Another important parameter related to human occupants is the clothing insulation. Clothing brings in additional thermal resistance and thermal capacitance to the system. The resistance of clothing causes change in the heat transfer coefficient h_a, while the capacitance of clothing introduces high order dynamics. In the case of light clothing ($I_{cl} < 1.0$), the capacitance of clothing is much smaller than that of the body, so its effect on the dynamics of human thermoregulatory system can be neglected. The quantitative study of influence of clothing insulation on h_a will be presented in Section 4.2.3.

In addition to the basic human factors mentioned above, some instrumentation related parameters should also be identified. One important parameter is the blood flow rate at thermal neutrality. The determination of this value as well as other sensor calibration issues are addressed in other sections of this thesis.

4.2.2 State-Dependent Variables

In our model, the body tissue conductance h_K and thermal masses C_s and C_c are considered to be non-constant and state-dependent variables. Figure 4.4 shows the differences of body regions at different thermal states. Because of the significant difference between hot and cold states, it is essential to incorporate these non-constant variables into the dynamic model. The original lumped parameter model, which assumes constant h_K, C_s, and C_c, does a poor job predicting transient behavior (Figure 4.11-4.12). To simplify the problem, it is assumed that all the state-dependent variables are functions of only skin temperature.

No systematic study of these body variables as a function of thermal states is per-

Figure 4.4: Sizes of the core (dark region) and the shell (light region) at different thermal states

formed in current research. In the following derivation, only basic human factors and heuristics are used. The results have not been directly verified by any experiments.

The variables to be studied can be normalized using corresponding reference values. After normalization, these variables can be expressed in a non-dimensional function form. So each variable is characterized by one reference value and a non-dimensional function. All variables evaluated at thermal neutrality are considered as the reference values.

Assuming the shell thermal mass at thermal neutrality is C_s^*, then

$$\frac{C_s}{C_s^*} = g(T_s) \tag{4.18}$$

where the value of C_s^* and the function $g(T_s)$ are determined as follows. Thermal mass C_s is proportional to the mass of the corresponding region:

$$C_s = (c_p)_{ts}\, m_s \tag{4.19}$$

Since $c_{ts} = 3492 J/kg \cdot K$ and $m_s^* = 4\% m_b$ [2], we have:

$$C_s^* = (c_p)_{ts} m_s^* = 140\ m_b \qquad (J/K) \tag{4.20}$$

By definition, we have:

$$g(T_s^{\Sigma}) = 1 \tag{4.21}$$

Using equation (4.19), the function $g(T_s)$ can be written as:

$$g(T_s) = \frac{m_s(T_s)}{m_s^*} \tag{4.22}$$

At $T_s = 20\ ^oC$, the body is at a very cold state, and the shell consists of hands, arms, feet, legs, and part of the trunk. These body parts account for 60% of the body mass [30], i.e. $m_s(20) = 60\%\ m_b$, hence

$$g(20) = \frac{m_s(20)}{m_s^*} = \frac{60\%\ m_b}{4\%\ m_b} = 15 \tag{4.23}$$

The function $g(T_s)$ is assumed to have the following form:

$$g(T_s) = \begin{cases} \beta_1 + \beta_2(T_s - 36)^2 & \text{if } T_s < 36\ ^oC, \\ \beta_1 & \text{if } T_s \geq 36\ ^oC. \end{cases} \tag{4.24}$$

Using equations (4.21) and (4.23), the coefficients β_1 and β_2 can be determined as 0.8 and 0.0554, respectively.

Once the thermal mass of the shell is evaluated, the thermal mass of the core can be calculated by subtracting the shell thermal mass from the total thermal mass of the body:

$$C_c = C_b - C_s = (c_p)_{ts} \cdot m_b - C_s \tag{4.25}$$

Similarly, a non-dimensional function for tissue conductance is used. That is:

$$\frac{h_K}{h_K^*} = f(T_s) \tag{4.26}$$

where h_K^* is the body conductance at thermal neutrality. By definition, we have:

$$f(T_s^\Sigma) = 1 \tag{4.27}$$

Body conductance h_K can be approximated as:

$$h_K = \frac{K_{ts} \cdot A_{cond}}{\delta_{cond}} \tag{4.28}$$

where tissue conductivity $K_{ts} \approx 0.3 W/m \cdot K$ [27, 10], conduction length δ_{cond} is approximately the average thickness of the shell, and the conduction area A_{cond} equals the

surface area of the core region. Figure 4.4 clearly shows the changes of δ_{cond} and A_{cond} at different thermal states of the body.

At thermal neutrality, $A_{cond}(T_s^{\Sigma}) \approx A_{Du}$ and $\delta_{cond}(T_s^{\Sigma}) = 2\ cm$[29], substituting these values into equation (4.28) gives:

$$h_K^* = h_K(T_s^{\Sigma}) \approx \frac{0.3\ A_{Du}}{0.02} = 15 A_{Du} \qquad (W/K) \tag{4.29}$$

The above formula can be generalized to take into account the difference in fat level. A user-adaptable parameter κ can be introduced as:

$$h_K^* = \kappa A_{Du} \tag{4.30}$$

Special effort is required to identify the value of κ for each user. As it will be shown later, equation (4.29) provides reasonably accurate results for most people. In the future chapters, equation (4.29) will be used for analysis and design.

To determine function $f(T_s)$, let's consider some special cases. At a cold state of $T_s = 20\ ^oC$, the core region reduces to its minimum size which consists of the major part of the trunk and head. So it is reasonable to use the area of the trunk and head to represent the conduction area which is about 40% of the total body area [10], i.e. $A_{cond}(20) = area(head + trunk) = 40\%\ A_{Du}$. At this cold condition, the value of δ_{cond} doubles the value at thermal neutrality: $\delta_{cond}(20)/\delta_{cond}(T_s^{\Sigma}) \approx 2$. Using these results, function f can be evaluated at 20 ^oC:

$$f(20) = \frac{\delta_{cond}(T_s^{\Sigma})}{\delta_{cond}(20)} \cdot \frac{A_{cond}(20)}{A_{cond}(T_s^{\Sigma})} \approx \frac{1}{2} \cdot 0.4 = 0.2 \tag{4.31}$$

The value of f can also be estimated at a hot state. At $T_s = 36\ ^oC$, the conduction area extends to the entire body surface: $A_{cond}(36) = A_{Du}$, and conduction length reduces to half of its value at the neutral condition: $\delta_{cond}(36)/\delta_{cond}(T_s^{\Sigma}) \approx 1/2$. So the value of function f at 36 ^oC is:

$$f(36) = \frac{\delta_{cond}(T_s^{\Sigma})}{\delta_{cond}(36)} \cdot \frac{A_{cond}(36)}{A_{cond}(T_s^{\Sigma})} \approx 2 \cdot 1 = 2 \tag{4.32}$$

The function f can be represented by polynomial functions as:

$$f(T_s) = \begin{cases} a_1 T_s^3 + a_2 T_s^2 + a_3 T_s + a_4 & \text{if } 20\ ^oC < T_s \le T_s^{\Sigma}, \\ b_1 T_s^3 + b_2 T_s^2 + b_3 T_s + b_4 & \text{if } T_s^{\Sigma} \le T_s \le 36\ ^oC \\ 2 & \text{if } T_s > 36\ ^oC \end{cases} \tag{4.33}$$

with continuous first order derivatives at boundary points. The coefficients a's and b's can be determined using the specific values of f estimated above and the continuity conditions. These conditions are:

$$f^+(20) = 0.2$$
$$f^-(T_s^\Sigma) = 1.0$$
$$f^+(T_s^\Sigma) = 1.0$$
$$f^-(36) = 2.0$$
$$df^+/dT_s(20) = 0$$
$$df^-/dT_s(36) = 0$$
$$df^-/dT_s = df^+/dT_s$$
$$d^2f^+/dT_s^2(20) = 0$$

The resulting value for the coefficients are:

$$\begin{aligned} a_1 &= 0.00028538598990 \\ a_2 &= -0.01712315939403 \\ a_3 &= 0.34246318788386 \\ a_4 &= -2.08308791921930 \\ b_1 &= -0.2444373443 \\ b_2 &= 25.6577939220 \\ b_3 &= -896.9887676710 \\ b_4 &= 10445.5634498068 \end{aligned}$$

Third order polynomials are chosen for function f to provide a continuous first order derivative of the function. By doing so, there will be no singularity when the model is linearized at any reference point.

4.2.3 Heat Transfer Coefficient $\bar{h}_a$

The heat transfer between the surface of the human body and its surrounding air is characterized by a single heat transfer coefficient $\bar{h}_a$. The value of $\bar{h}_a$ depends on

may factors, such as local air velocity, clothing insulation, etc.. To determine the real time value of $\bar{h}_a$, it is important to know the heat transfer process between the skin surface and the air. For a clothed body, as shown in Figure 4.5, the body heat is first transferred to the clothing surface by conduction (Q_{cond}). The heat is then dissipated to the environment in two different modes: convection (Q_{conv}) and radiation (Q_{rad}). If the thermal capacity of clothing is neglected, then we have:

$$Q_{cond} = Q_{conv} + Q_{rad} \equiv Q_{env} \tag{4.34}$$

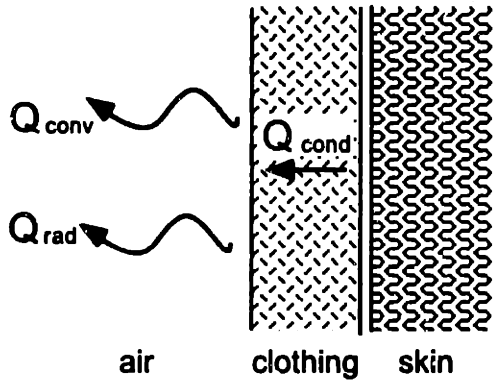

Figure 4.5: Heat transfer modes at the skin surface

The conductive heat Q_{cond} highly depends on the clothing insulation, which is represented by I_{cl}. The unit of I_{cl} is *clo*, and 1 *clo* is equal to 0.155 Km^2/W. The values of I_{cl} can be found from the database created by the Institute for Environmental Research, Kansas State University[31]. The database provides the *clo*-values for a large number of typical clothing ensembles. The conductive heat per unit skin area can be determined as:

$$\bar{Q}_{cond} = \bar{h}_{cond}(T_s - T_{cl}) = \frac{1}{0.155\, I_{cl}}(T_s - T_{cl}) \tag{4.35}$$

where:

$$\bar{h}_{cond} = \frac{1}{0.155\, I_{cl}} \tag{4.36}$$

Similarly, the convective heat flux can be written as:

$$\bar{Q}_{conv} = \bar{h}_{conv}(T_{cl} - T_a) \tag{4.37}$$

The convective heat transfer coefficient $\bar{h}_{conv}$ at the body surface has been studied by many researchers, and many results have been published over the years[10, 3, 32]. In this research work, the formula developed by Colin and Houdas[32] is used. According to Colin and Houdas, the convective heat transfer coefficient at the body surface consists of two parts: one corresponds to the natural convection and the other to the forced convection. The total convective heat transfer coefficient is:

$$\bar{h}_{conv} = \kappa_0 + \kappa_1 v_a^{2/3} \tag{4.38}$$

If all variables are in SI units, then the values for κ_0 and κ_1 are 2.67 and 8.72 respectively.

The radiation heat transfer at the clothing surface can be expressed as:

$$\bar{Q}_{rad} = \bar{h}_{rad}(T_{cl} - T_{mrt}) \tag{4.39}$$

where:

$$\bar{h}_{rad} = \epsilon\sigma[(T_{cl} + 273)^2 + (T_{mrt} + 273)^2][(T_{cl} + 273) + (T_{mrt} + 273)] \tag{4.40}$$

and ϵ is the emissivity of the outer surface of the clothed body (≈ 0.97[2]), and σ is the Stefan-Boltzmann constant: $5.67 \cdot 10^{-8}\ W/m^2K^4$. For the nominal condition of: $T_{cl} = 30°C$ and $T_{mrt} = 25°C$, the heat transfer coefficient $\bar{h}_{rad}$ is equal to 6.0 W/m^2K.

Under the assumption of $T_{mrt} = T_a$, the total heat loss to the environment can be written as:

$$\bar{Q}_{conv} + \bar{Q}_{rad} = (\bar{h}_{conv} + \bar{h}_{rad})(T_{cl} - T_a) \tag{4.41}$$

By using equations (4.6, 4.34, 4.35, 4.41), one can solve for the the total effective heat transfer coefficient ($\bar{h}_a$) between the skin surface and the air:

$$\bar{h}_a = \frac{\bar{h}_{cond}(\bar{h}_{conv} + \bar{h}_{rad})}{\bar{h}_{cond} + \bar{h}_{conv} + \bar{h}_{rad}} \tag{4.42}$$

where $\bar{h}_{cond}$, $\bar{h}_{conv}$ and $\bar{h}_{rad}$ are determined by equations (4.36),(4.38), and (4.40) respectively.

[2]The emissivity of human skin is close to 1.0 and most types of clothing have emissivity of about 0.95[3]. A mean value of 0.97 is commonly used.

4.3 An Application of the Model: Sensor Calibration

In Chapter 3, we have discussed that the values of Ω_f^* and r_Ω must be identified to implement the model-based ZLC. A few possible methods to determine these values were presented in chapter 3. Because those methods require either complicated instrumentation, a tedious test procedure, or the usage of human voting, they are not easy to perform outside the laboratory environment. This section provides a simple procedure to evaluate the ratio r_Ω based on a simple experiment and the human thermoregulation model. Using the obtained value of r_Ω and the vasomotor control model, the sensor reading at thermal neutrality, i.e Ω_f^*, can be calculated.

This procedure requires a simple test on the human subject. In the test, the body of the subject goes through a thermal transient process caused by a change of the thermal environment. One example of the environment change is a step change in local air temperature. During the transient period, the finger blood flow $\Omega_f(t)$ of the subject is measured and $\bar{\Omega}_p(t)$ is predicted by the thermoregulation model. Using the measured values of Ω_f and the computed values of $\bar{\Omega}_p$, the ratio r_Ω of the subject can be obtained by solving the following minimization problem:

$$r_\Omega = \arg\ \min[\int_t (\Omega_f(t) - r_\Omega \bar{\Omega}_p(t))^2 dt\ ] \tag{4.43}$$

In discrete time, it is equivalent to:

$$r_\Omega = \arg\ \min[\sum_{i=1}^{N} (\Omega_f(i) - r_\Omega \bar{\Omega}_p(i))^2\ ] \tag{4.44}$$

where N is the total number of sample points, and $\Omega_f(i)$ and $\bar{\Omega}_p(i)$ are values of Ω_f and $\bar{\Omega}_p$ at time i respectively. The above minimization problem can be solved explicitly, and the solution for r_Ω is:

$$r_\Omega = \frac{\sum_{i=1}^{N} \Omega_f(i) \cdot \bar{\Omega}_p(i)}{\sum_{i=1}^{N} \bar{\Omega}_p(i)^2} \tag{4.45}$$

The finger blood flow rate at thermal neutrality can be obtained from the model as well. When both the warmth signal Σ_{warm} and the cold signal Σ_{cold} are zero, the human thermoregulatory system does not do any work. By definition, it corresponds to a thermally neutral state. The average peripheral blood flow rate per unit skin area

$\bar{\Omega}_p$ under this condition is 6.3 $liter/m^2hr$ (Equation (4.14)). Therefore the finger blood flow rate under the neutral condition is:

$$\Omega_f^* = 6.3\, r_\Omega \qquad \text{(sensor unit)} \tag{4.46}$$

The results of the calibration process will be presented in the following section, together with experimental results of model validation.

4.4 Model Validation

4.4.1 Procedure and Experimental Setup

The model developed in this chapter predicts the dynamics of peripheral blood flow. The model consists of a passive system and an autonomic control system. We will not directly verify each system of the model. Instead, the model-predicted blood flow dynamics are compared with experimentally measured data. The comparison results can be used to evaluate the validity of the model.

All experiments were carried out in two adjacent rooms of similar geometry as shown in Figure 4.6. The air temperatures of the two rooms were controlled at different values by two identical air conditioner units. The temperature in one room is above conventional comfort temperature, and therefore is called the hot room. In the hot room, the average room temperature was controlled at a temperature between 29 ^oC and 31 ^oC, and the air velocity at the occupied location was about 0.12 m/s. Under these conditions, sweating was not observed on any human subject. The air temperature of the cold room was controlled at a value within the range of 13 ^oC to 18 ^oC, which is below the neutral range. The average air velocity of the cold room was about 0.15 m/s. No subject shivered in such a cold environment throughout the experiments. The room temperatures of each tests are listed in Table 4.4.

One of the model assumptions that have been made is that the mean radiant temperature is equal to the air temperature. For all the experiments, the air conditioners were left running for over night, so that the test environment reached a steady-state condition. The wall temperatures were then measured, and the mean radiant temperatures were calculated using these measurements. For the case when the air temperature

in the cold room was regulated at 14 ^oC and the hot room at 30 ^oC, the mean radiant temperatures were 15.1 ^oC in the cold room and 28.2 ^oC in the hot room. Since the skin temperatures of the subjects were in the range of 25 ^oC to 35 ^oC, the error caused by the assumption is very small for the cooling experiments, but may not be small in the case of heating. For the heating experiments, the assumption causes 10% average error in the total heat transfer coefficient h_a. Such discrepancy was not taken into account in the simulations of the experiments.

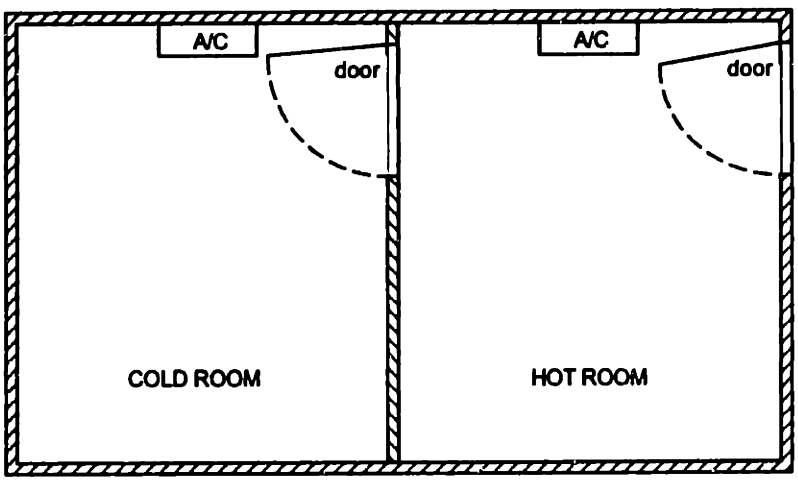

Figure 4.6: Experiment setup for verifying human model

Human subjects were kept in the hot room for half an hour before the start of testing. After the pre-warming period, human subjects quickly walked into the cold room and sat at a specified location. The subject was kept in the cold room for about one hour[3], and then walked back to the hot room and continued the tests for another hour. The subjects were instructed to sit in a chair throughout the tests except for the two room-changing periods. The subjects were encouraged to relax and remain awake, although they were allowed to do some reading. Under such condition, the internal heat H/A_{Du} equals 100 W/m^2[10]. Most experiments were performed during day time between 11:00AM and 5:00PM, except for two tests performed in the evenings. The first two tests (see Table 4.4) were performed in early April, and the rest of tests were carried out in early October.

[3]Some tests took less than one hour because the subjects felt too cold before the end of the hour.

Nine subjects were tested in the above experiments. They are all in their 20's or early 30's, and came from different part of the world. The subject information is tabulated in Table 4.3.

Table 4.3: Information of human subjects

subject	sex	height(m)	weight(kg)	$A_{Du}(m^2)$	clothing(clo)	origin
A	M	1.70	65	1.73	0.8	Southern China
B	M	1.80	75	1.91	0.5	California
C	F	1.74	65	1.75	0.9	Alaska
D	F	1.64	50	1.51	0.7	Northern China
E	M	1.62	55	1.56	0.6	Southern India
F	M	1.74	60	1.67	0.6	Eastern China
G	M	1.83	86	2.05	0.5	Alaska
H	M	1.83	79	1.97	0.5	New York
I	M	1.93	84	2.08	0.7	New York

4.4.2 Experimental Results

Experiments were performed on the nine human subjects, and there were ten test cases in total. Table 4.4 listed the conditions for the ten tests. Each of these tests includes a cooling period and a heating period.

In order to compared the experimental data to the model predictions, the ratio between the sensor unit and the physical unit, r_Ω, must be obtained first. Based on this ratio, the comparison between the experiments and the theory can be done both graphically and analytically. We will first present the results of r_Ω for all subjects. Using these values, both qualitative and quantitative analyses of the experimental results will be provided.

Calibration ratio r_Ω

The method to determine the r_Ω value has been discussed in Section 4.3. In each of the ten cases, the human subject went through a step change of the local air temperature, and the blood flow rate Ω_f was measured during the test period. Using the

Table 4.4: Test cases for model validation

test ID	subjects	T_{hot} (°C)	T_{cold} (°C)	plots
Test 1	D, F	29	16	4.15 - 4.16
Test 2	F	28	17	4.17
Test 3	D, F	30	14	4.18 - 4.19
Test 4	A	30	14	4.20
Test 5	G	31	14	4.21
Test 6	I	30	14	4.22
Test 7	E	31	14	4.23
Test 8	H	30	14	4.24
Test 9	B	31	14	4.25
Test 10	C	30	14	4.26

human thermoregulation model (4.7),(4.8), and (4.14), the blood flow rate in physical unit $\bar{\Omega}_p$ can be calculated for the same transient period. Substituting the Ω_f and $\bar{\Omega}_p$ values into equation (4.45), the value of r_Ω for each subject can be calculated. For instance, considering Test 1 and using the data of the heating phase, the r_Ω values for Subject D and Subject F are 0.0192 and 0.0333, respectively. Using these values and equation (4.46), the sensor reading at thermal neutrality of the two subjects are 0.12 (sensor unit) and 0.21 (sensor unit), respectively. Figure 4.7 and 4.8 show the results of this procedure when the heating phase data of Test 1 is used.

The values of r_Ω for all subjects were calculated based on the test data, and are listed in Table 4.5. These values range between 0.01 and 0.04, and the difference between two subjects can be significant. For example, the value of Subject F is nearly three times of that of Subject G.

Using the identified values of r_Ω and equation (4.46), the values of Ω_f^* for all subjects were calculated, as listed in Table 4.5. The Ω_f^* value for Subject F was also estimated using the method of thermal sensation voting (Section 3.3.3), and at $\Omega_f = 0.24$ sensor units, the thermal environment was voted near neutral. This value is very close to the one obtained by the model-based method.

The procedure described by equations (4.45) and (4.46) provides a simple way to evaluate Ω_f^*. To verify how reliable this method is, the procedure was repeated on the

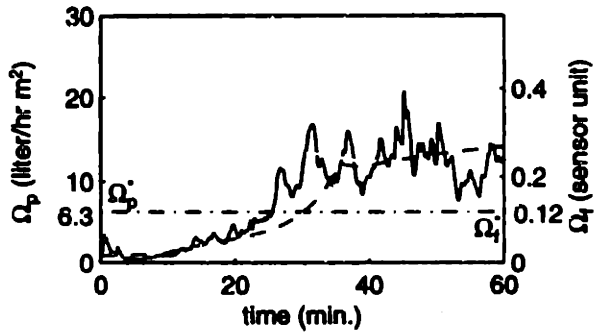

Figure 4.7: Sensor calibration for subject D. The measurement of Ω_f is plotted in solid line, while the model-predicted $\bar{\Omega}_p$ is plotted in dashed line

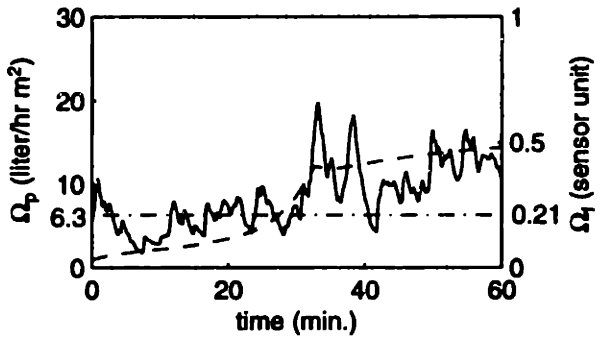

Figure 4.8: Sensor calibration for subject F. The measurement of Ω_f is plotted in solid line, while the model-predicted $\bar{\Omega}_p$ is plotted in dashed line

Table 4.5: The r_Ω and Ω_f^* values of the subjects calculated by using the model-based method

subject	r_Ω	Ω_f^* (sensor unit)
A	0.0310	0.20
B	0.0261	0.16
C	0.0294	0.19
D	0.0190	0.12
E	0.0262	0.17
F	0.0362	0.23
G	0.0131	0.08
H	0.0278	0.18
I	0.0196	0.12

same subject for several times, which included both heating and cooling experiments. The Ω_f^* value for each experiment was calculated. Figure 4.9 and Figure 4.10 show the Ω_f^* values obtained from different experiments for Subject D and Subject F. Six experiments were performed on Subject F and four experiments were performed on Subject D. The mean value of Ω_f^* for Subject F is 0.228, and the standard deviation is 0.023. For Subject D, the mean value is 0.116, and the standard deviation is 0.009. So the proposed calibration method is fairly reliable.

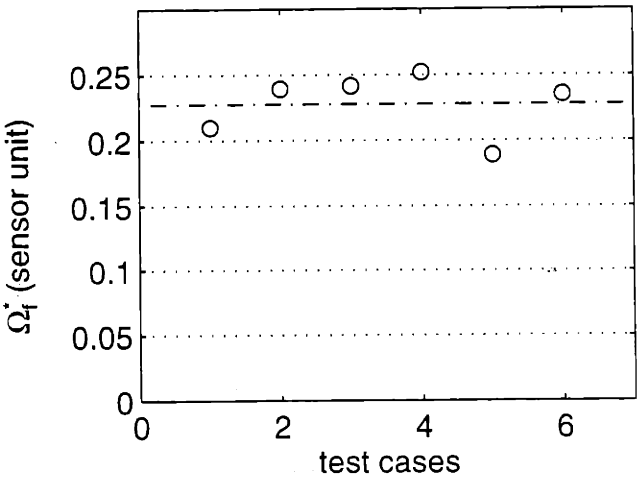

Figure 4.9: Blood flow rate of Subject F at neutral condition. Calculated by using the model-based approach

Using the r_Ω values provided in Table 4.5, the experimental data and model predictions of each test can be scaled properly, and plotted for comparison in the same figure. The plots for all tests are provided at the end of this chapter (Figures 4.15 - 4.26). Because the time scales of the blood flow dynamics are essential to model-based control design, the comparison between experiments and the model will focus on the time scales.

Time scales

The results of the ten tests on the nine subjects were shown in Figures 4.15 - 4.26. These figures show that the time scales of blood flow rate predicted by the thermoregulation model agrees well with those of the experimental data. For example, the experimental data shows a significant difference in time constant between the warm state of

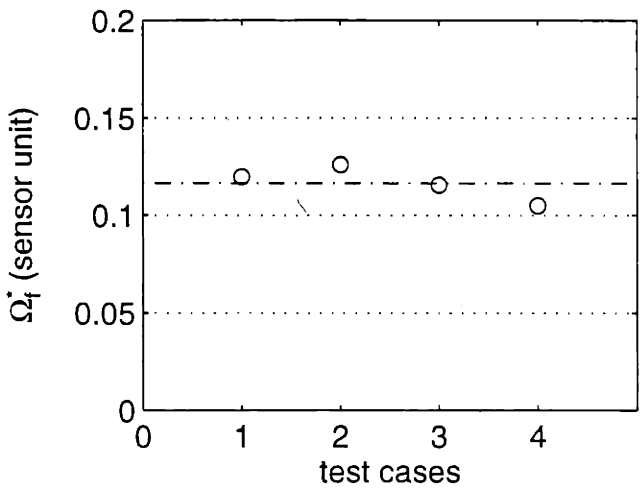

Figure 4.10: Blood flow rate of Subject D at neutral condition. Calculated by using the model-based approach

the body and the cold state of the body. The model predictions clearly indicate such a difference.

The quantitative analysis of the experimental results are performed in the following way. For the cooling test, the first order time constants are evaluated for both the experimental data (the solid line in the figures) and the model predictions (the dashed lines). A first order dynamic model is used to fit the experimental curve, and the resulting time constant is denoted by τ_{exp}. Similarly, the first order time constant for the model-predicted curve, τ_{model}, is obtained. The values of the two time constants for all subjects are tabulated in Table 4.6. These values were obtained from the cooling tests, and the data points between the initial state and the neutral state ($\bar{\Omega}_p = 6.3\ liter/m^2hr$) were used for the calculation of time constants.

As shown in Table 4.6, the relative difference between the two time constants ranges from 1% to 61%, with the majority less than 33%. Since the values of τ_{exp} are obtained from a single step responses with the presence of unpredictable internal disturbances (e.g. emotional changes), they are only approximations of the real first order time constants of the blood flow dynamics caused by a step change of the thermal environment.

The values of the time constant difference listed in Table 4.6 can be used as modeling errors for each subject. When a model-based controller is designed using the

Table 4.6: First order time constants for both experimental data and model predictions (obtained from the cooling tests, with a time window between the initial state and the neutral state)

test ID	subjects	τ_{exp} (sec.)	τ_{model} (sec.)	$e_\tau = \frac{\lvert\tau_{exp}-\tau_{model}\rvert}{\tau_{exp}}$
Test 1	D	164	190	15.8%
Test 1	F	679	365	46.2%
Test 2	F	772	299	61.2%
Test 3	D	370	295	20.2%
Test 3	F	435	334	23.2%
Test 4	A	671	517	23.0%
Test 5	G	273	182	33.3%
Test 6	I	401	406	1.2%
Test 7	E	176	116	34.0%
Test 8	H	320	185	42.2%
Test 9	B	113	133	17.7%
Test 10	C	503	353	29.8%

thermoregulation model, such modeling errors must be taken into account. As it will be shown later in Chapter 6, the stability of the closed-loop control system can still be guaranteed even though the modeling error can be as high as 61% in terms of time constant.

The results of the heating tests are more complicated than those of the cooling cases. At a cold state of the body, the blood flow dynamics are highly non-linear. The transient behavior of such dynamics cannot be fitted closely by first order dynamics. In other words, the time constant obtained from a first order fitting implies no essential information about the system. However, from these experiments, it is obvious that the blood flow dynamics is much slower in a cold state than that in a warm state. This property can be clearly demonstrated with the proposed model. To do so, the model is first linearized at the initial state of a test. The linearization of the model will be presented in Chapter 6. The dominant pole of the linear system is then calculated. the value of which implies the response speed of the system. The values of the dominant poles for all test cases are tabulated in Table 4.7. To provide some comparison, a second order model is used to fit the initial section of the experimental curve. and

the dominant pole of the resulting system (p_{exp}) is computed. Since the data used to obtain p_{exp} corresponds to a small fraction of a step response curve, the values listed in the table should only be used for order of magnitude analysis. Because the dynamics accelerates when the body gets warmer, the value $|p_{exp}|$ actually provide an upper bound for $|p_{model}|$. The first order time constants in Table 4.6 correspond to pole locations between $-1.3 \cdot 10^{-3}$ and $-8.8 \cdot 10^{-3}$, which are more than one order of magnitude different from the dominant poles of the cold states. This agrees quite well with the difference in response time between the warm state and the cold state.

Table 4.7: Dominant poles for both experimental data and model predictions (obtained from the heating tests with a time window of the initial 10 minutes)

test ID	subjects	p_{exp}	p_{model}
Test 1	D	$-1.1 \cdot 10^{-4}$	$-7.5 \cdot 10^{-5}$
Test 1	F	$-1.6 \cdot 10^{-4}$	$-7.6 \cdot 10^{-5}$
Test 2	F	$-1.8 \cdot 10^{-3}$	$-9.9 \cdot 10^{-5}$
Test 3	D	$-1.2 \cdot 10^{-4}$	$-7.2 \cdot 10^{-5}$
Test 3	F	$-8.5 \cdot 10^{-4}$	$-7.5 \cdot 10^{-5}$
Test 4	A	$-1.4 \cdot 10^{-4}$	$-8.0 \cdot 10^{-5}$
Test 5	G	$-2.8 \cdot 10^{-4}$	$-7.7 \cdot 10^{-5}$
Test 6	I	$-1.0 \cdot 10^{-4}$	$-7.3 \cdot 10^{-5}$
Test 7	E	$-9.1 \cdot 10^{-3}$	$-9.3 \cdot 10^{-5}$
Test 8	H	$-2.2 \cdot 10^{-4}$	$-6.4 \cdot 10^{-5}$
Test 9	B	$-3.1 \cdot 10^{-4}$	$-7.1 \cdot 10^{-5}$
Test 10	C	$-2.6 \cdot 10^{-4}$	$-8.5 \cdot 10^{-5}$

4.4.3 Effects of Non-Linear Model Parameters

To show the non-linear effect of model parameters, simulations using both constant parameters and non-linear parameters were performed for the case of Test 1, Subject D. Figures 4.11- 4.12 shows the results of these simulations as well as the experimental data. The dynamics predicted by the constant parameter model are significantly different from the measured data, while the results predicted by the non-linear model agree much better with the experimental data.

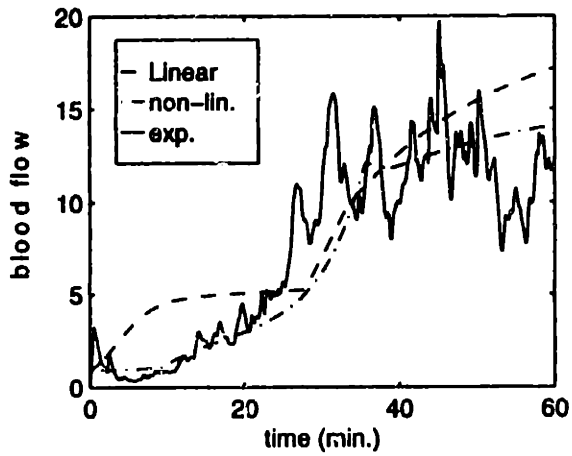

Figure 4.11: Comparison of different models and experimental data (Test 1, Subject D): blood flow

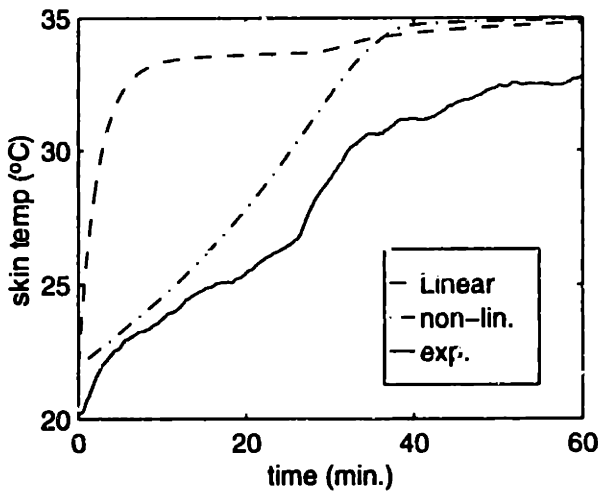

Figure 4.12: Comparison of different models and experimental data (Test 1, Subject D): skin temperature

4.5 Discussions

From the results of both the human model and experiments, the following characteristics of human dynamic behavior can be noticed.

- User dependency. The blood flow dynamics are different for different subjects. For example, even though the experiments on Subject D and Subject F in Test 1 and Test 3 were performed simultaneously under the same environment conditions,

the dynamics of human thermoregulation vary significantly (Figures 4.15, 4.16, 4.18, 4.19). Certain human factors, such as body weight and height, should be correctly identified to predict the dynamics accurately.

- Non-symmetric transient in heating and cooling. The time scale of blood flow dynamics varies significantly from one state to another. As shown in most of the test results, the response speed at a cold state of the body is much lower than that of a warm state. As a result, the cooling transient is much faster than that of the heating process in our two room experiments. The difference can be explained as follows. When a subject enters the cold room from the hot room, the skin temperature drops very fast. Such a change in skin temperature causes a rapid decrease in peripheral blood flow. At the end of the cooling test, both skin temperature and core temperature stay on the lower side of the normal ranges. When the subject comes back to the hot room in the second phase of the test, the blood flow cannot respond immediately because of the slow recovery of core temperature. This characteristic of the blood flow agrees well with the vasomotor control model (equation (4.14)).

  The above conclusion is true for most of the nine subjects. However, there is one exception, Subject E. As shown in Figure 4.23, the heating process of Subject E is almost as fast as the cooling process. It can be attributed to some fundamental difference in the thermoregulatory system of the subject from the others. This particular subject comes from south India, where the annual temperature range is between 70 ^oF and 110 ^oF. The vasomotor control system of this subject is believed to have a different form than equation (4.14). With exceptional cases like Subject E, it is concluded that the human thermoregulation model presented in this thesis at most applies to the majority of people, but not all.

- Correlation to thermal comfort. Many researchers have used skin temperature as one of the conditions for thermal comfort [3]. Using the results obtained so far, it is possible to compare skin temperature with blood flow to see which one correlates better to thermal sensation.

Let us take Test 1 as an example. During this test, Subject D and Subject F were cooled down first and then reheated. At the end of the experiments as shown in Figures 4.15 and 4.16, the skin temperatures of both subjects almost fully recovered the original values, while the blood flow rates regained only half of their original values. Before entering the cold room at the beginning of the tests, thermal sensation votings were in the range of warm to slightly warm based on the seven point psycho-physical ASHRAE scale[4]. The voting data as well as blood flow measurements are plotted in Figures 4.13 - 4.14. At the end of re-heating test, both subjects voted neutral. Such voting difference seems to agree with the blood flow difference observed in the plots. Therefore, skin temperature could be a good index for thermal comfort under steady-state conditions, while blood flow is a better choice for non-steady-state conditions. However, the dynamics of thermal sensation are much more complicated than the dynamics of any single physiological variable, such as the peripheral blood flow. We should not equate blood flow to thermal comfort. Again, our objective is to achieve physiological thermal neutrality.

This chapter presents a low-order dynamic model for the human thermoregulatory system. The model does in general agree with experimental data, although certain modeling errors exist. The modeling errors will be accounted for later in determining certain design parameters of a model-based ZLC. Before addressing the control design problem, we need to complete the plant model by developing a model for the indoor thermal environment.

[4]The seven-point scale uses 7 integers from -3 to +3 to represent the thermal comfort level. The value 0 corresponds to a thermally comfort condition. The positive numbers in ascending order represent slightly warm, warm, and hot respectively. The negative numbers in descending order represent slightly cool, cool, and cold respectively.

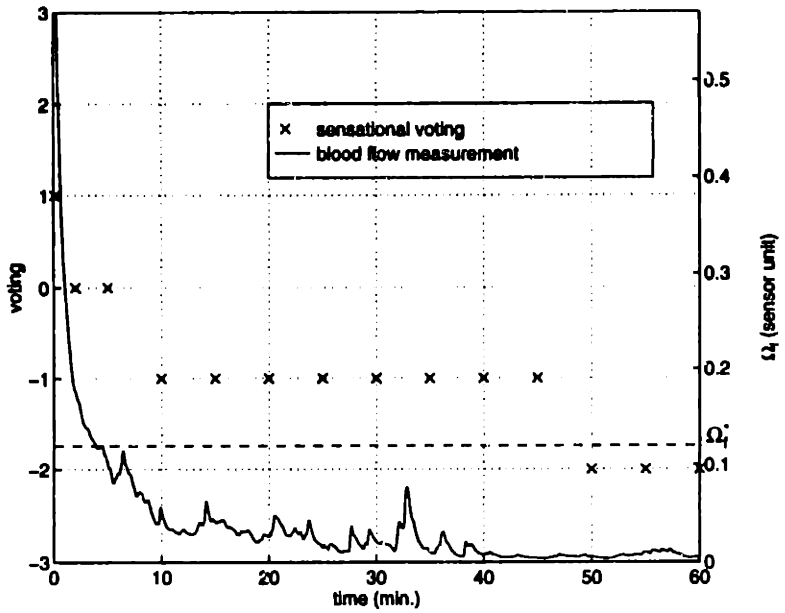

(a) cooling phase

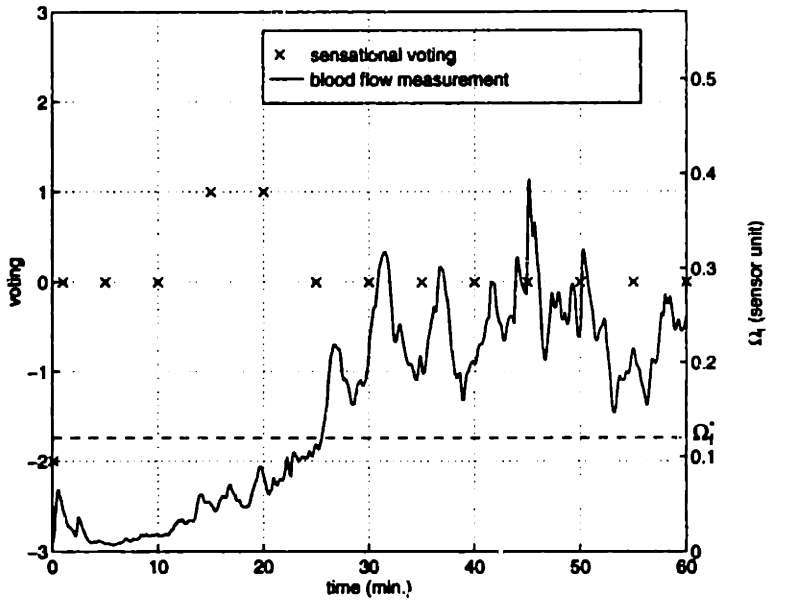

(b) heating phase

Figure 4.13: Thermal sensation and blood flow of Subject D, Test 1

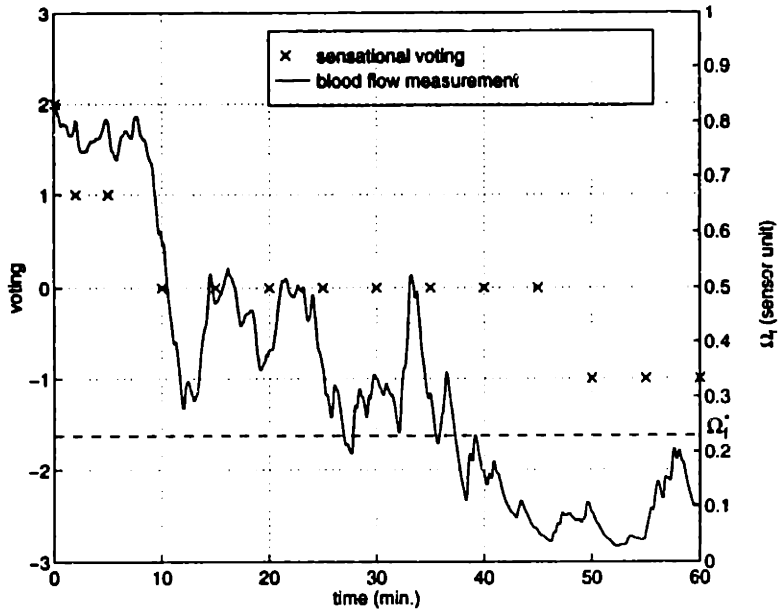

(a) cooling phase

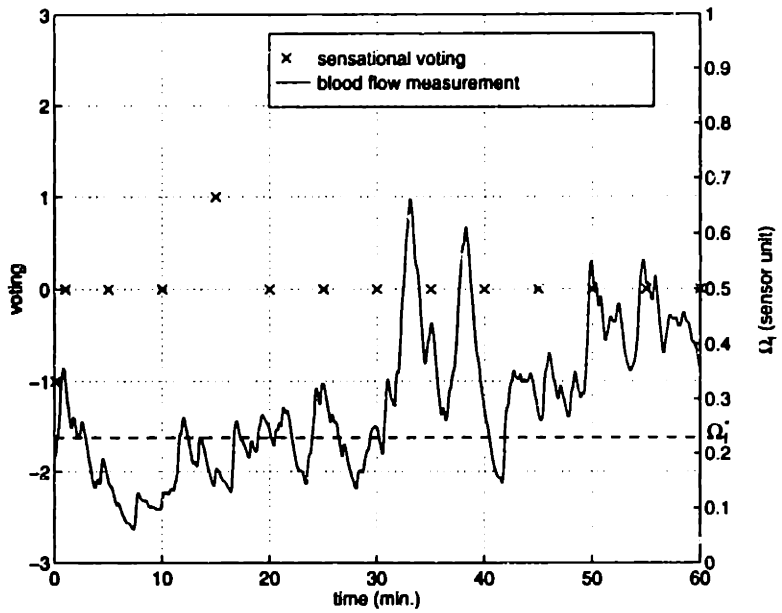

(b) heating phase

Figure 4.14: Thermal sensation and blood flow of Subject F, Test 1

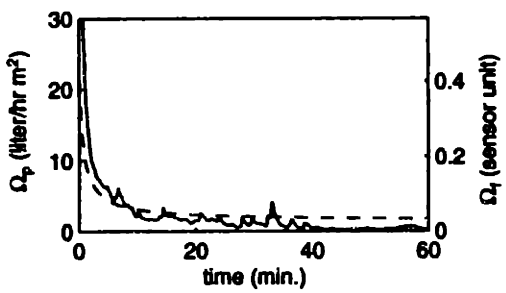

(a) Cooling: blood flow

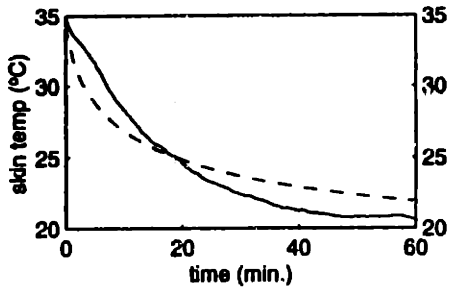

(b) Cooling: skin temperature

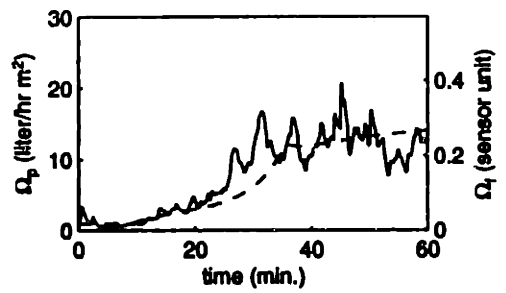

(c) Heating: blood flow

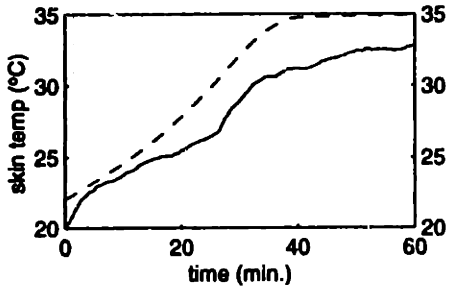

(d) Heating: skin temperature

Figure 4.15: Experimental results for Test 1, Subject D: solid line - sensor measurements; dashed line - model predictions.

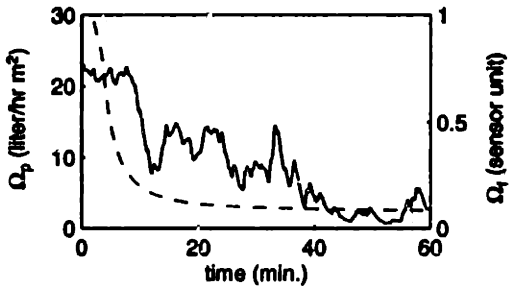

(a) Cooling: blood flow

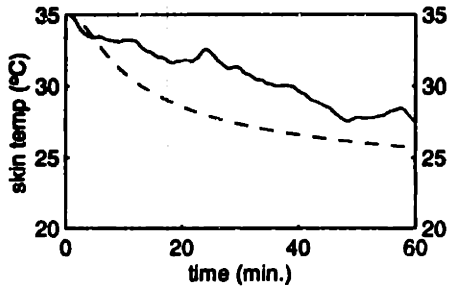

(b) Cooling: skin temperature

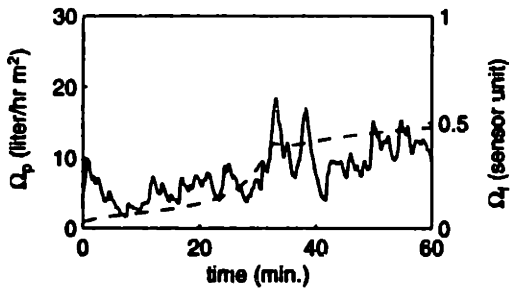

(c) Heating: blood flow

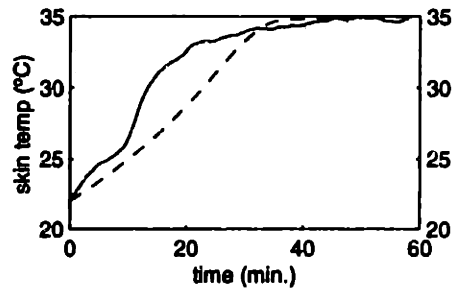

(d) Heating: skin temperature

Figure 4.16: Experimental results for Test 1, Subject F: solid line - sensor measurements; dashed line - model predictions.

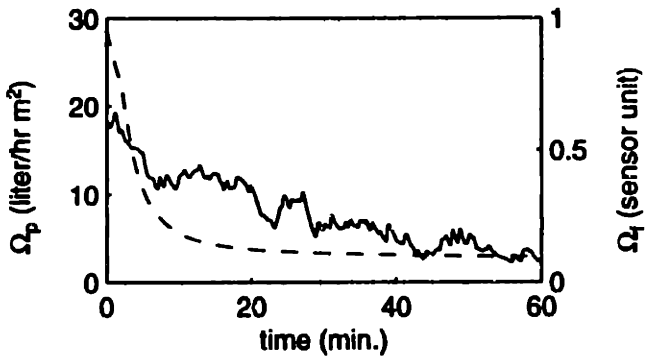

(a) cooling

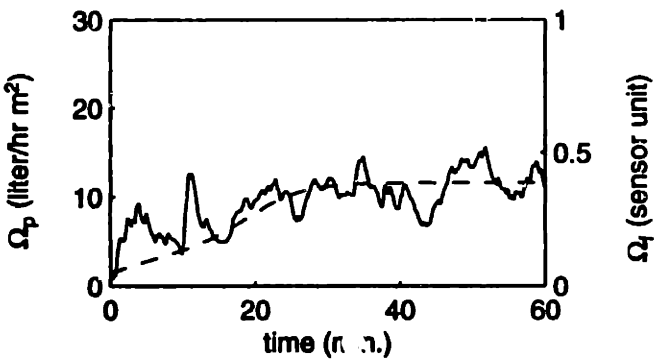

(b) heating

Figure 4.17: Experimental results for Test 2 (Subject F): solid line - sensor measurements; dashed line - model predictions.

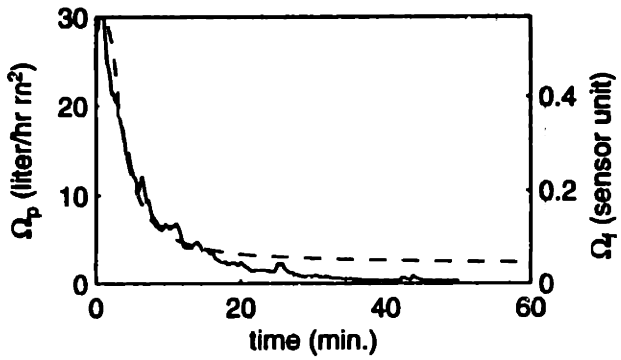

(a) cooling

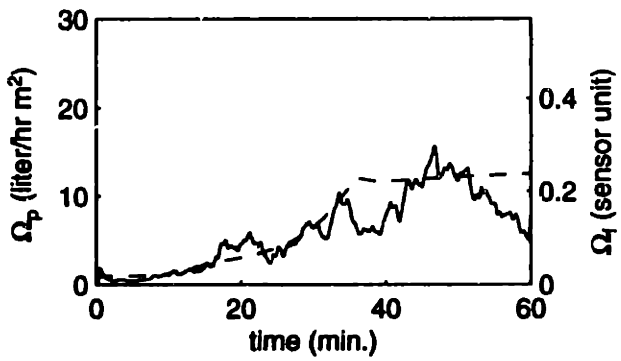

(b) heating

Figure 4.18: Experimental results for Test 3 (Subject D): solid line - sensor measurements; dashed line - model predictions.

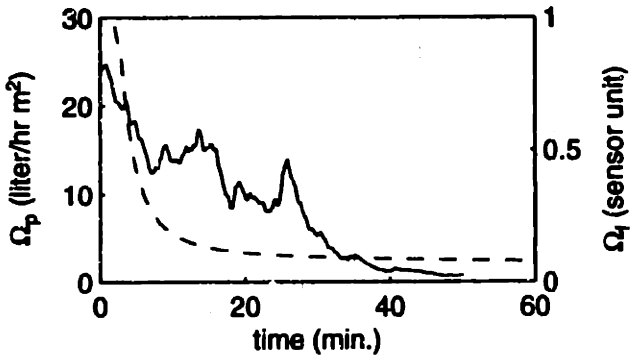

(a) cooling

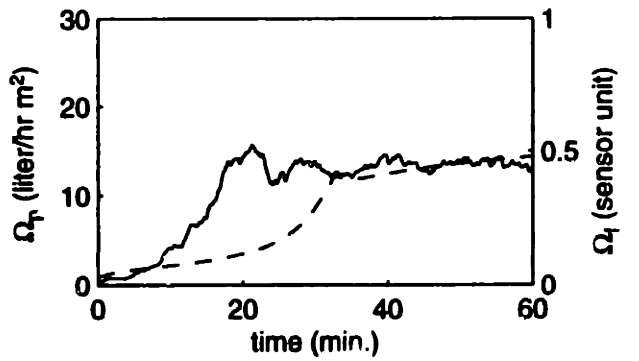

(b) heating

Figure 4.19: Experimental results for Test 3 (Subject F): solid line - sensor measurements; dashed line - model predictions.

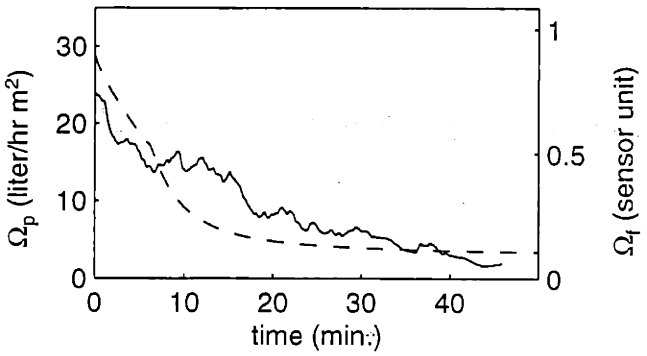

(a) cooling

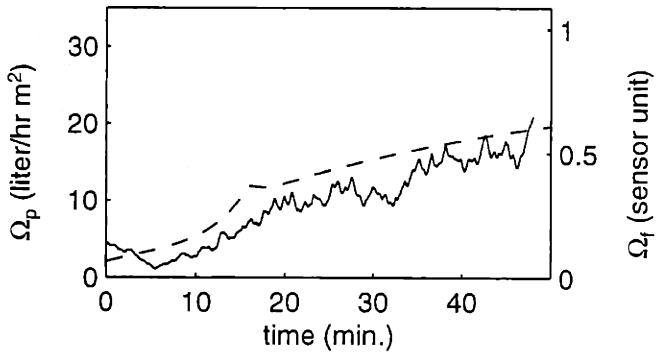

(b) heating

Figure 4.20: Experimental results for Test 4 (Subject A): solid line - sensor measurements; dashed line - model predictions.

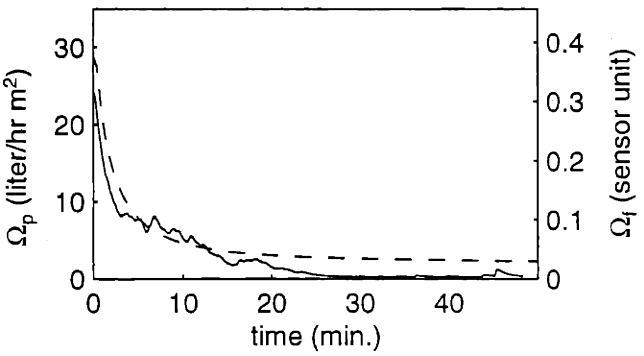

(a) cooling

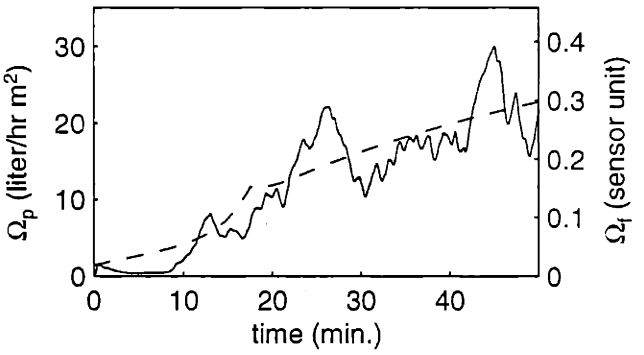

(b) heating

Figure 4.21: Experimental results for Test 5 (Subject G): solid line - sensor measurements; dashed line - model predictions.

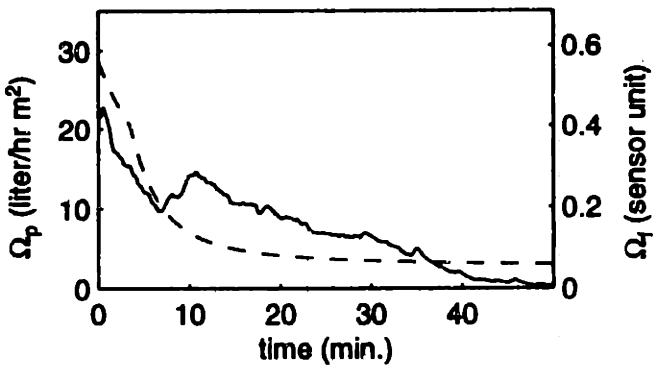

(a) cooling

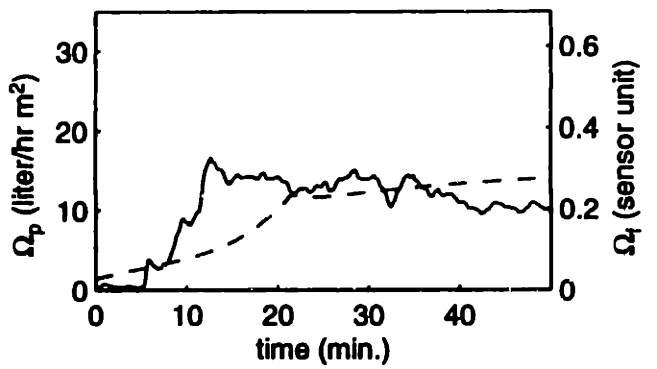

(b) heating

Figure 4.22: Experimental results for Test 6 (Subject I): solid line - sensor measurements; dashed line - model predictions.

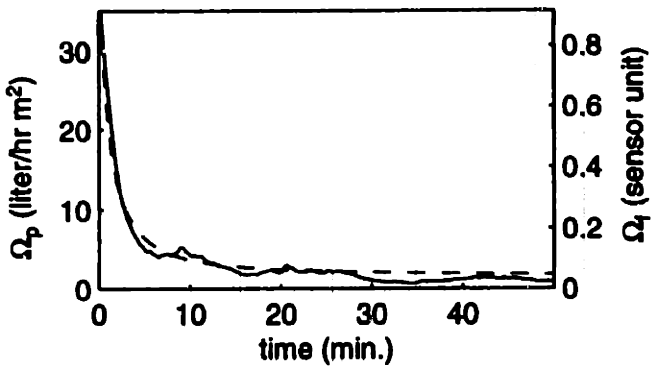

(a) cooling

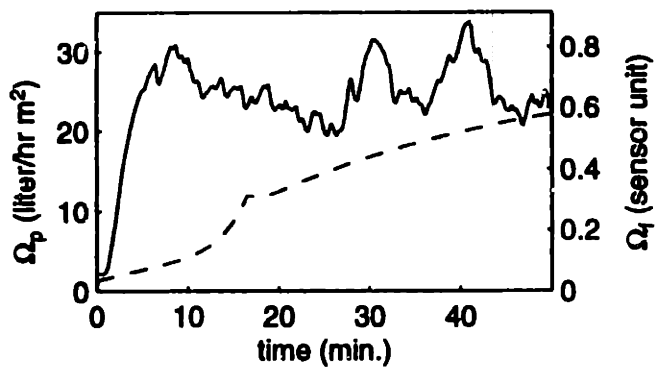

(b) heating

Figure 4.23: Experimental results for Test 7 (Subject E): solid line - sensor measurements; dashed line - model predictions.

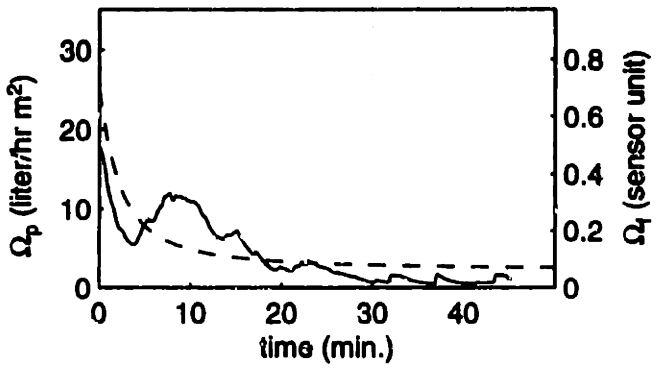

(a) cooling

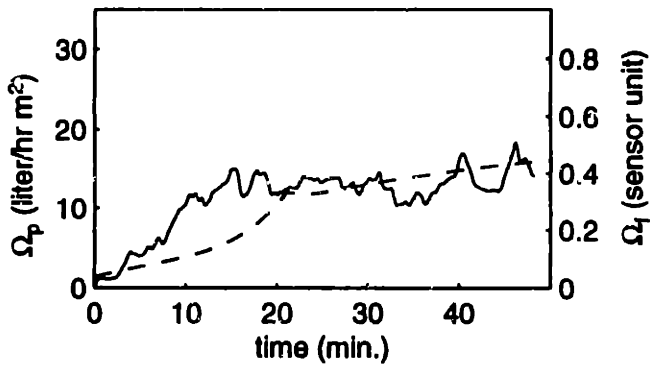

(b) heating

Figure 4.24: Experimental results for Test 8 (Subject H): solid line - sensor measurements; dashed line - model predictions.

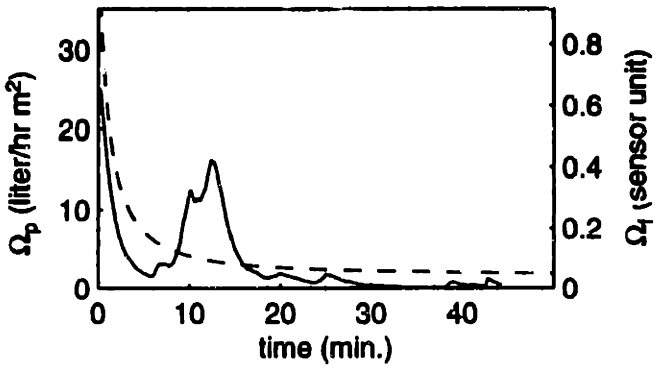

(a) cooling

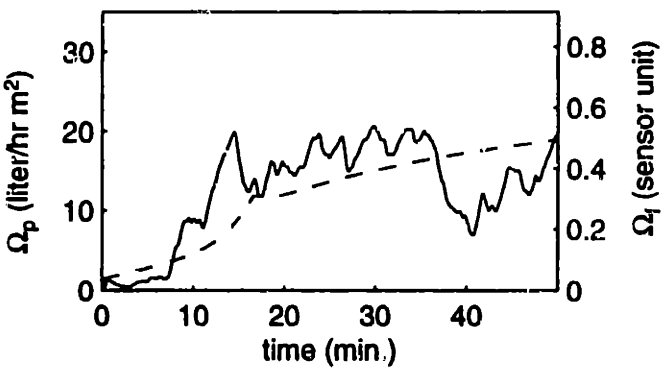

(b) heating

Figure 4.25: Experimental results for Test 9 (Subject B): solid line - sensor measurements; dashed line - model predictions.

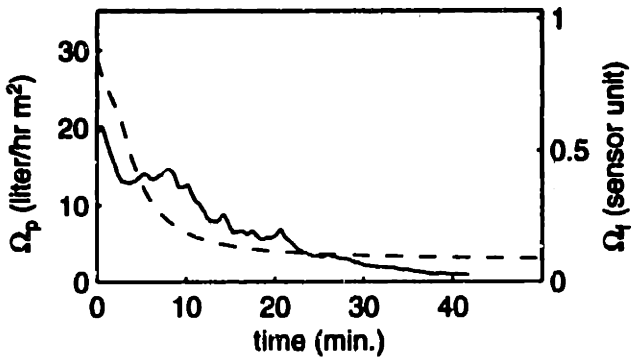

(a) cooling

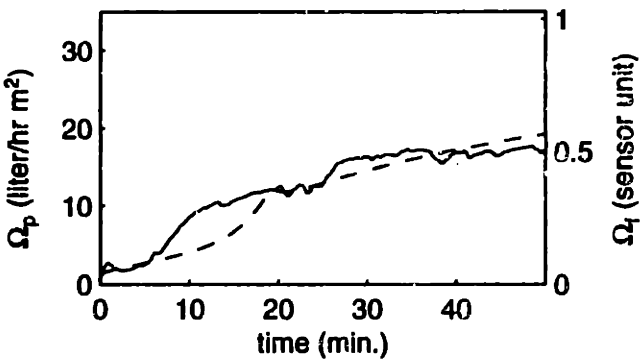

(b) heating

Figure 4.26: Experimental results for Test 10 (Subject C): solid line - sensor measurements; dashed line - model predictions.

Chapter 5

Thermal Environment Modeling

The thermal environment is an important component of the system in ZLC. ZLC is achieved by properly adjusting one or more thermal environment variables. A *thermal environment variable* is a physical attribute of the environment which can change the thermal state of the human body. Typical thermal environment variables are air temperature, air velocity, humidity, and radiant temperature. In the current phase of research, only air temperature is regulated by ZLC. Air humidity is assumed constant. and radiant temperature is assumed to be the same as air temperature. Models for air temperature and air velocity are provided in this chapter.

5.1 Model Assumptions

The dynamics of air temperature and air velocity in an enclosed space have been studied for decades. Models ranging from a single lumped-parameter model to highly sophisticated computational fluid dynamics (CFD) models have been developed over the years. However, not all models are suitable for the purpose of real time control. For example, although a CFD model can provide detailed information about any thermal environment, it can hardly be used for real time control because of the computational complexity as well as its dependency on accurate real time boundary conditions.

For the purpose of control, a low-order thermal environment model which can provide a good approximation of the dominant dynamics is preferred. Due to the large variety of HVAC systems as well as infinite possibilities of space geometry, it is very difficult, if not impossible, to develop a low-order model which applies to all possible scenarios. In this chapter, a low-order model is developed for certain thermal environments under the following assumptions.

- The air within the occupied zone is well-mixed, and the temperature gradient is

small in the region. The well-mixed region can be either the whole room space or a small region at the occupied location depending on the actual situation. The dynamics of air temperature in the well-mixed zone can be represented by a lumped parameter model.

- The air velocity dynamics are much faster than the air temperature dynamics, and the overall environment dynamics are dominated by the air temperature dynamics. Therefore, an algebraic air velocity model will suffice.

Under the above assumptions, air velocity at a location can be modeled as a time-varying parameter, rather than a state variable like air temperature. The following section provides one model for estimating this parameter in a special configuration.

5.2 Air Velocity Model

The air flow in a rectangular room, equipped with a single unit air conditioner, is studied in this section. The room space is divided into two regions, namely a jet zone, and a buffer zone. The jet zone is determined by the trajectory of the turbulent air jet. The space outside the jet zone and away from solid surfaces is defined as the buffer zone (Figure 5.3).

5.2.1 Turbulent Air Jets

The jet of a fluid has been extensively studied for its frequent occurrence in engineering systems, and several monographs [33, 34] have been published on jet theories. In this section, some relevant results are summarized. The derivations of these results can be found in the references.

In an air conditioned space, the air jet is usually a turbulent buoyant jet. The air velocity within the jet zone is determined by three features of the jet: velocity profile in the axial plane, the decay law of centerline velocity, and the trajectory of the jet. The first two features can be obtained from isothermal jet theory, while the last feature can be approximated by buoyant jet formulas.

An air jet can be divided into the following four zones (Figure 5.1), each of which corresponds to a different decay law of the centerline velocity:

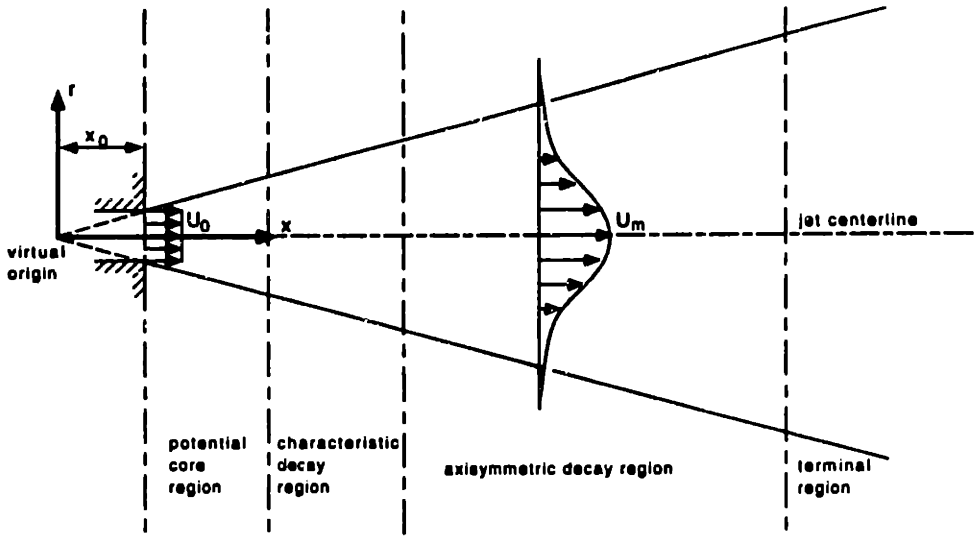

Figure 5.1: Four regions of a free jet

- Potential core region. This is the region immediately downstream of the jet opening where mixing of the jet air with the surrounding air is not complete. The centerline velocity is the same as the jet supply velocity: $U_m = U_0$. This region usually extends to 5 - 10 equivalent opening diameters.

- Characteristic decay region. After the consumption of the potential core by the free shear layer, the centerline velocity begins to gradually decrease so that $U_m/U_0 \propto 1/x^n$, where n has a value between 0.3 and 1.0. The extend of the region and the value of n depend on the shape of jet opening. For a plane air jet, this region becomes the predominant region and n equals to 0.5. For a free circular jet, this region is negligibly small. More details about the range of this zone and the n value can be found in [35, pages 106–108].

- Axisymmetric decay region. This region is usually referred to as the *fully developed region* for three-dimensional jet. For jets with low aspect ratio opening, this region is predominant and extends to about 100 equivalent diameters. The centerline velocity decreases inversely to the distance: $U_m/U_0 \propto 1/x$.

- Terminal region. This is a region of rapid diffusion, and the jet becomes indistinguishable from the surrounding air. The decay of the centerline velocity become

faster: $U_m/U_0 \propto 1/x^2$.

For the air jets generated by air conditioners, the axisymmetric decay region or the fully developed region predominates, and the formulas presented later in this section apply only to this region unless stated otherwise.

The velocity profile in the well-developed region can be represented by the following function:

$$U(x,r) = U_m(x)e^{-\frac{r^2}{b^2(x)}} \tag{5.1}$$

where the parameter b can be determined from the spreading hypothesis:

$$b = \beta x \tag{5.2}$$

Based on a large amount of test results, the spreading coefficient β was found to be:

$$\beta = 0.103 \tag{5.3}$$

Using the profile given in equation (5.1) and the momentum theory, the following decay law of the centerline velocity can be obtained:

$$\frac{U_m}{U_0} = \frac{1}{\beta}\sqrt{\frac{2}{\pi}}\left(\frac{x}{\sqrt{A_0}}\right)^{-1} \tag{5.4}$$

By integrating over the cross section, the jet flow rate F_J at a distance x from the jet origin is:

$$\frac{F_J(x)}{F_0} = \sqrt{2\pi}\beta\frac{x}{\sqrt{A_0}} \tag{5.5}$$

This equation indicates that air is entrained into the jet along its trajectory.

The trajectory of a buoyant jet deflects away from the original jet direction because of the buoyancy force. A non-dimensional parameter which indicates the relative strength of the buoyancy force to the inertia force is the *Archimedes number* (Ar):

$$Ar = \frac{g\alpha\sqrt{A_0}(T_a - T_0)}{U_0^2} \tag{5.6}$$

where T_a is the air temperature surrounding the jet which, in our special case, is the average buffer zone temperature. For ideal gas, the thermal expansion coefficient α is related to the absolute temperature $\mathbb{T}$ as:

$$\alpha = 1/\mathbb{T} \tag{5.7}$$

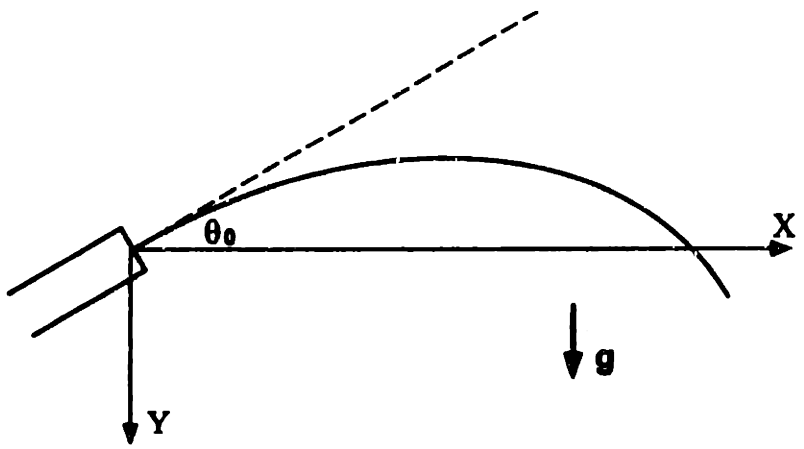

Figure 5.2: Inclined non-isothermal jet

Many formulas have been developed to predict the trajectory of a buoyant jet [36, 37, 38]. Among all these non-isothermal jet models, Frean's model [37] gives the best prediction of an air jet in a room. The trajectory of an inclined non-isothermal jet as shown in Figure 5.2 is given as:

$$\frac{y}{\sqrt{A_0}} = -\frac{x}{\sqrt{A_0}}\tan\theta_0 + 0.226Ar\left(\frac{x}{\cos\theta_0\sqrt{A_0}}\right)^{2.61} \tag{5.8}$$

The above model as well as most other trajectory formulas were developed for free air jets, i.e. the jets are in infinite free space and there is no interaction between the jets and solid surfaces. However, in an air conditioned space, the structure surfaces may cause significant change to the jet trajectory. For example, when the distance (D) between the jet centerline and a parallel wall surface is smaller than a critical value (D_c), the jet will attach to the surface and becomes a surface jet. This phenomena is known as *Coanda effect*. For a circular isothermal jet, the critical distance D_c is:

$$D_c = 6\sqrt{A_0} \tag{5.9}$$

More about wall surface jets and the interactions between jets and walls can be found in [34, 35].

5.2.2 Air Velocity in the Buffer Zone

Using the results of the jet model, air velocity in the buffer zone can be estimated by applying the mass conservation law. As shown in Figure 5.3, the cross section average

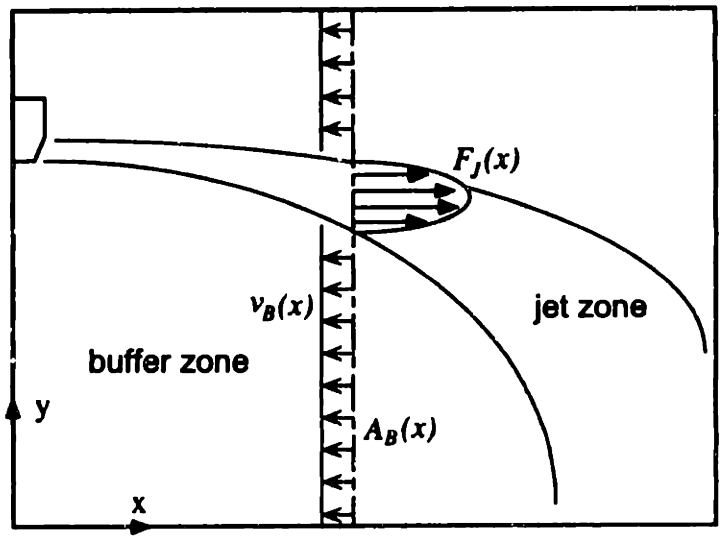

Figure 5.3: Buffer velocity model

velocity v_B at a distance x from the opening of the air conditioner should satisfy the following conservation equation:

$$v_B(x)\ A_B(x) = F_J(x) \tag{5.10}$$

where F_J is the volumetric air flow rate in the jet zone. By substituting equation (5.5) into this equations, we have:

$$\frac{v_B}{U_0} = \sqrt{2\pi}\beta\ \left(\frac{x}{\sqrt{A_0}}\right)\left(\frac{A_0}{A_{room} - A_J(x)}\right) \tag{5.11}$$

where the cross section area of jet $A_J(x)$ can be evaluated from jet profile as:

$$A_J(x) \approx 0.3x^2 \tag{5.12}$$

The velocity field in the buffer zone is by no means uniform. Its gradient is usually much larger than the temperature gradient in the same region. The magnitude of the velocity vector can change significantly in the buffer region, and the directional change may be even more dramatic. So the predicted buffer zone velocity should not be used as any local point air velocity. Instead, it is a good estimation of the average air velocity which is required for the evaluation of the total body heat transfer coefficient.

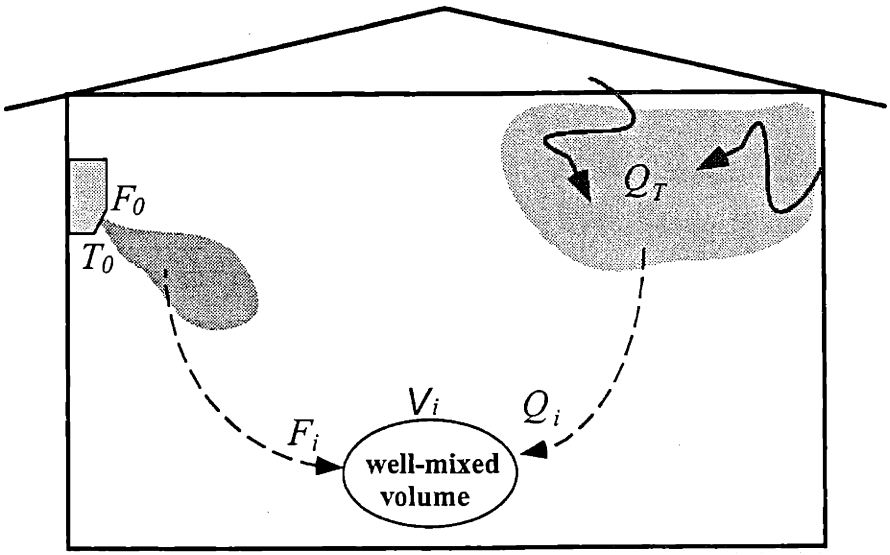

Figure 5.4: Modeling approach for a non-well-mixed environment

5.3 A Dynamic Model of Air Temperature

In case that the whole space is well-mixed, the dynamics of air temperature can be modeled using a single lumped-parameter model. Assuming the total thermal load to the air is Q_T, then the air temperature dynamics can be written as:

$$C_{env}\frac{dT_a}{dt} = (\rho c_p)_{air} F_0(T_0 - T_a) + Q_T \tag{5.13}$$

where C_{env} is the total thermal mass of the environment, F_0 is the supply air volume flow rate, and T_0 is the supply air temperature. The thermal mass C_{env} is generally larger than the thermal mass of the air because of the presence of other objects such as furniture. The value of C_{env} needs to be identified for each environment.

The above model can be generalized for non-well-mixed situations through the following treatment. At any location (i) within the thermal environment, there exists a locally well-mixed volume, within which the air temperature is nearly uniform (Figure 5.4). The exact size of this well-mixed volume (V_i) may vary from one location to another. If the total thermal load to the entire environment is Q_T, then only a fraction of this (Q_i) is applied to the locally well-mixed volume. By applying the first law to this volume, one has:

$$(\rho c_p)_{air} V_i \frac{dT_i}{dt} = (\rho c_p)_{air} F_i(T_0 - T_i) + Q_i \tag{5.14}$$

or:

$$\frac{dT_i}{dt} = a_i F_0(T_0 - T_i) + b_i Q_T \tag{5.15}$$

where a_i and b_i are parameters which shall be identified for each location.

Using the lumped-parameter model(5.13) or (5.15), the transfer function from supply air temperature T_0 to the environment air temperature T_a can be derived as:

$$G_e(s) = \frac{1}{1 + \tau_e s} \tag{5.16}$$

where the time constant τ_e is a function of the environmental thermal mass, and location in case of non well-mixed situations.

The above modeling approach simplifies the problem in many ways. For example, the transportation delay, which occurs in the air mixing process, is ignored. In case that the space is large or the air source is far away from the conditioned space as in some central air systems, the transportation time delay becomes significant, and the model must be adjusted accordingly. Another simplification made in the model is the interaction between the indoor air and the walls or outdoor conditions. The transfer function (5.16) is obtained by assuming the total thermal load to the environment, Q_T, is constant and independent of the indoor air temperature. Such an assumption yields a unit DC gain, which is not true in most cases.

One way to resolve the above problems is to increase the model order or complexity. This approach makes the application of real time control more difficult. Instead, our approach is to modify the transfer function (5.16), and make it more general without loosing the simplicity of the model. The modified transfer function is:

$$G_e(s) = \frac{K_e e^{-\tau_d^e s}}{1 + \tau_e s} \tag{5.17}$$

where τ_d^e is the pure time delay, and the DC gain K_e is less than one. As it will be shown in the following section, the transfer function (5.17) is a good approximation to the real air temperature dynamics.

5.4 Temperature Dynamics in the Test Chamber

To verify the air temperature model as shown in equation (5.17), transfer functions of air temperature at different locations in the test chamber were identified through

frequency identification procedures.

The test chamber was excited by input air temperature varying at different frequencies, and the air flow rate was fixed. The frequency responses at three different locations as shown in Figure 3.12 were recorded. The Bode plots of the results are shown in Figure 5.5, 5.6 and 5.7. The asymptotes of the magnitude plots at high frequency range have a slope of -20 db/dec, which, together with the phase plots, confirm the first order characteristic of air temperature dynamics. From these Bode plots, the transfer functions for each position are estimated as:

$$G_e^{(I)}(s) = \frac{0.53e^{-12s}}{1+123s} \tag{5.18}$$

$$G_e^{(II)}(s) = \frac{0.63e^{-6s}}{1+83s} \tag{5.19}$$

$$G_e^{(III)}(s) = \frac{0.5e^{-21s}}{1+126s} \tag{5.20}$$

These transfer functions show that:

- In the well-mixed thermal environment inside the test chamber, the time constants and steady state gains of air temperature dynamics are very close in the buffer region. A single lumped-parameter model can be used for different locations within the buffer region.
- The dynamics of air temperature in the path of air jet are noticeably different from that in the buffer zone. The time constant at location II (which is within the path of an air jet) is about 2/3 of the time constant of the buffer zone.
- The time delay varies from location to location, and the difference between two locations can be large.

This chapter provides a method to model the dynamics of indoor air temperature and air velocity for certain room configurations. The air temperature dynamics at three different locations in the test chamber were experimentally determined, and the results will be used in the next chapter for model-based ZLC design.

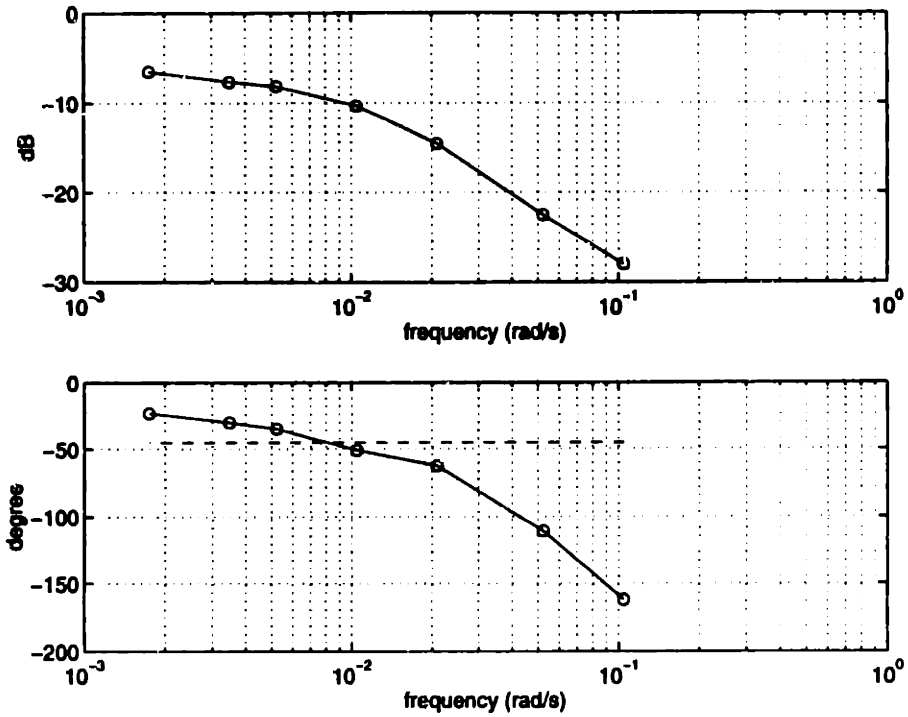

Figure 5.5: Bode plot for system identification at location I

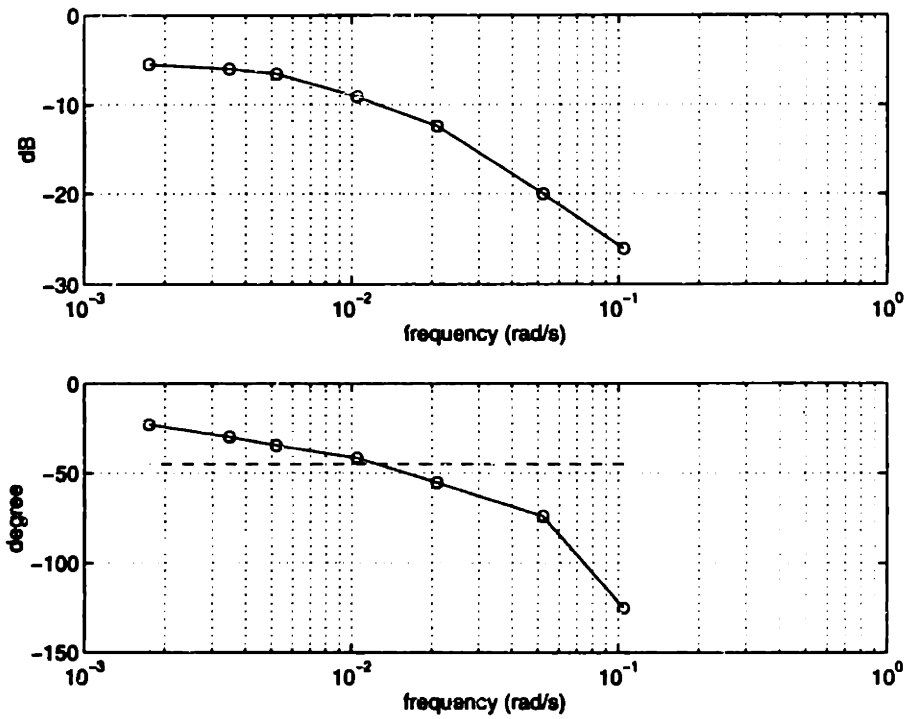

Figure 5.6: Bode plot for system identification at location II

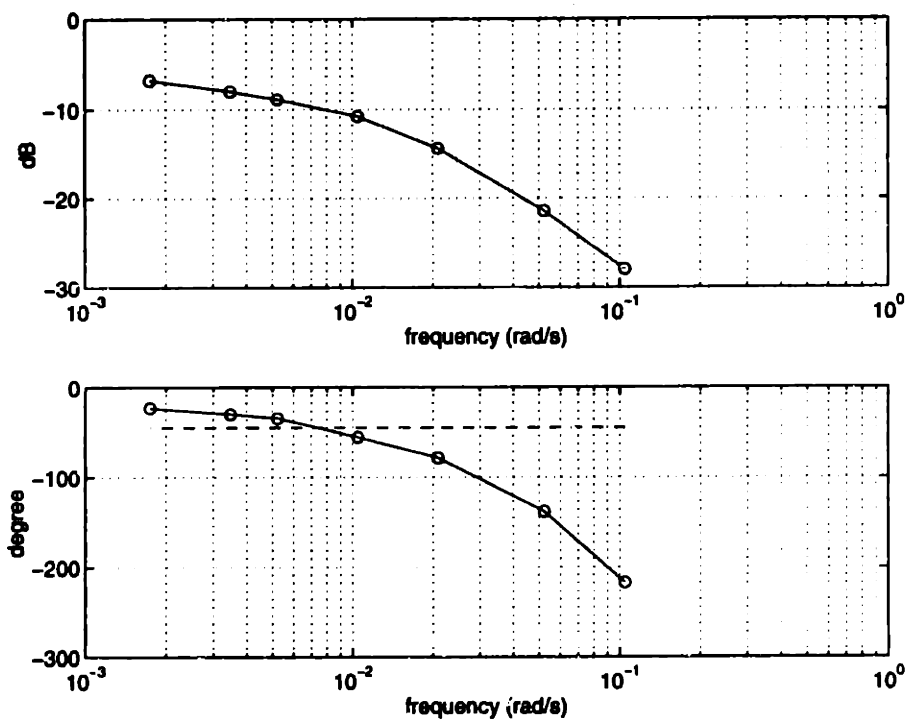

Figure 5.7: Bode plot for system identification at location III

Chapter 6

System Analysis and Control Design

In Chapter 3, it was shown that a simple PI controller is not robust enough to deal with many plant uncertainties. This chapter presents a systematic approach to the design of a stable and robust controller for ZLC. The approach utilizes the model-based linear design techniques. Using the models developed in Chapter 4 and Chapter 5, linear models of the plant are obtained. Controllers are designed using the discrete time pole placement method and the linearized plant models. The selection of design parameters for achieving prescribed stability robustness and system performance is also discussed. Experimental results using the model-based ZLC are presented at the end of this chapter.

6.1 Linear Analysis of the Plant

In the ZLC paradigm, the plant consists of the HVAC system, the thermal environment, the human subject, and the blood flow sensor. Tools from linear systems theory are used to study the plant, and important characteristics of the plant are presented in this section.

6.1.1 Linearized Human Thermoregulation Model

The non-linear human thermoregulation model (equations (4.7),(4.8)) can be linearized at a reference state (T_c^r, T_s^r). To simplify the procedure, two new state variables and a new input variable are introduced:

$$x_1 = T_c - T_c^r \tag{6.1}$$

$$x_2 = T_s - T_s^r \tag{6.2}$$

$$u = T_a - T_a^r \tag{6.3}$$

The linearized thermoregulation model can be written as:

$$\dot{x}_1 = A_{11}x_1 + A_{12}x_2 + v_1 \tag{6.4}$$

$$\dot{x}_2 = A_{21}x_1 + A_{22}x_2 + B_2u + v_2 \tag{6.5}$$

where:

$$A_{11} = -(e_2 \cdot e_4)/\bar{C}_c^r \tag{6.6}$$

$$A_{12} = -(e_1 + e_3 + e_5)/\bar{C}_c^r \tag{6.7}$$

$$A_{21} = (e_2 + e_4)/\bar{C}_s^r \tag{6.8}$$

$$A_{22} = (e_1 + e_3 - e_6 - h_a)/\bar{C}_s^r \tag{6.9}$$

$$B_2 = \bar{h}_a/\bar{C}_s^r \tag{6.10}$$

$$v_1 = (H/A_{Du} - e)/\bar{C}_c^r \tag{6.11}$$

$$v_2 = (e - \bar{h}_a(T_s^r - T_a^r))/\bar{C}_s^r \tag{6.12}$$

and:

$$e = (\bar{h}_K^r + (\rho c_p)_{bl}\,\bar{\Omega}_p^r)\cdot(T_c^r - T_s^r) \tag{6.13}$$

$$e_1 = \frac{\partial \bar{h}_K^r}{\partial T_s}(T_c^r - T_s^r) - \bar{h}_k^r \tag{6.14}$$

$$e_2 = \bar{h}_k^r \tag{6.15}$$

$$e_3 = (\rho c_p)_{bl}\frac{\partial \bar{\Omega}_p^r}{\partial T_s}(T_c^r - T_s^r) - (\rho c_p)_{bl}\,\bar{\Omega}_p^r \tag{6.16}$$

$$e_4 = (\rho c_p)_{bl}\frac{\partial \bar{\Omega}_p^r}{\partial T_c}(T_c^r - T_s^r) + (\rho c_p)_{bl}\,\bar{\Omega}_p^r \tag{6.17}$$

$$e_5 = \frac{H/A_{Du} - e}{C_c^r}\cdot\frac{\partial C_c^r}{\partial T_s} \tag{6.18}$$

$$e_6 = \frac{e - \bar{h}_a(T_s^r - T_a^r)}{C_s^r}\cdot\frac{\partial C_s^r}{\partial T_s} \tag{6.19}$$

Linearized blood flow rate is:

$$\bar{\Omega}_p = \bar{\Omega}_p^r + C_1x_1 + C_2x_2 \tag{6.20}$$

where:

$$C_1 = \frac{\partial \bar{\Omega}_p^r}{\partial T_c} \tag{6.21}$$

$$C_2 = \frac{\partial \bar{\Omega}_p^r}{\partial T_s} \tag{6.22}$$

Let $x = [x_1, x_2]^T$, and $y = (\bar{\Omega}_p - \bar{\Omega}_p^r)$, we can rewrite the system equations as:

$$\dot{x} = Ax + Bu + v \tag{6.23}$$

$$y = Cx \tag{6.24}$$

where:

$$A = \begin{bmatrix} A_{11} & A_{12} \\ A_{21} & A_{22} \end{bmatrix}, \quad B = \begin{bmatrix} 0 \\ B_2 \end{bmatrix}, \quad v = \begin{bmatrix} v_1 \\ v_2 \end{bmatrix}, \quad C = [C_1, C_2] \tag{6.25}$$

Using the linear system equations (6.23-6.24), the transfer function from input u (i.e. T_a) to output y (i.e. $\bar{\Omega}_p$) can be derived:

$$G_m(s) = \frac{B_2(C_2\, s + A_{12}C_1 - A_{11}C_2)}{s^2 - (A_{11} + A_{22})s + A_{11}A_{22} - A_{12}A_{21}} \tag{6.26}$$

To account for the non-linear effect of the original model, three linear transfer functions linearized at different thermal states of the body are considered. In the following calculations, the data for subject F is used. For $T_c^r = 36.6°C$ and $T_s^r = 34.1°C$, the body is at a thermally neutral state. The linear transfer function can be evaluated as:

$$G_m^{(n)}(s) = \frac{0.001464s + 4.478 \cdot 10^{-6}}{s^2 + 0.004202s + 9.299 \cdot 10^{-7}} \tag{6.27}$$

The blood flow rate at this state is $\bar{\Omega}_p = 6.3\ liter/hr\, m^2$. At a cold state: $T_c^r = 36.3°C$ and $T_s^r = 25°C$, the transfer function is:

$$G_m^{(c)}(s) = \frac{0.00001325s + 7.123 \cdot 10^{-10}}{s^2 + 0.0001803s + 6.965 \cdot 10^{-9}} \tag{6.28}$$

Blood flow rate at this state is $\bar{\Omega}_p = 1.1\ liter/hr\, m^2$. For the warm state of $T_c^r = 36.9°C$ and $T_s^r = 36°C$, the transfer function is:

$$G_m^{(w)}(s) = \frac{0.00004614}{s^2 + 0.01765s + 1.37 \cdot 10^{-6}} \tag{6.29}$$

The corresponding blood flow rate is $\bar{\Omega}_p = 28.8\ liter/hr\, m^2$.

The pole and zero locations of the above transfer functions are shown in Figure 6.1. These plots show that the zero of the system move from a location close to the imaginary axis to negative infinity when the state of the body changes from cold to warm.

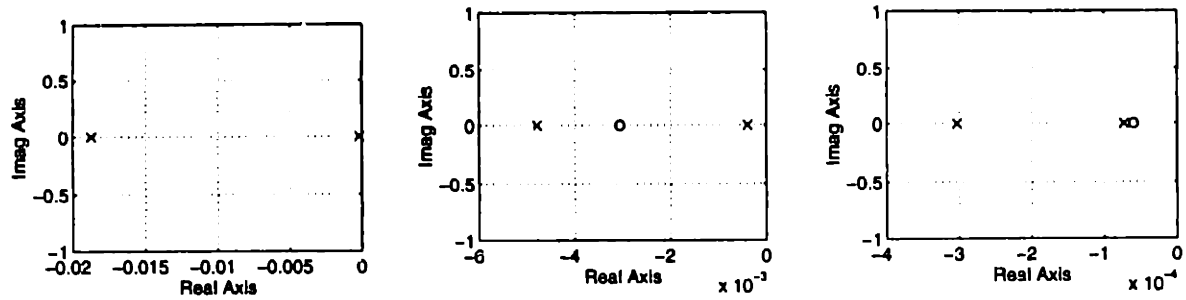

(a) warm state (b) neutral state (c) cold state

Figure 6.1: Pole-zero maps for different thermal states of Subject F: (a), $T_c = 36.9°C$, $T_s = 36°C$; (b), $T_c = 36.6°C$, $T_s = 34.1°C$; (c), $T_c = 36.3°C$, $T_s = 25°C$.

6.1.2 Plant Model

The plant and the closed-loop control system are shown in Figure 6.2. The model of the plant dynamics consists of three transfer functions, namely $G_e(s)$ for the thermal environment, $G_m(s)$ for the human thermoregulation, and $G_f(s)$ for the sensor.

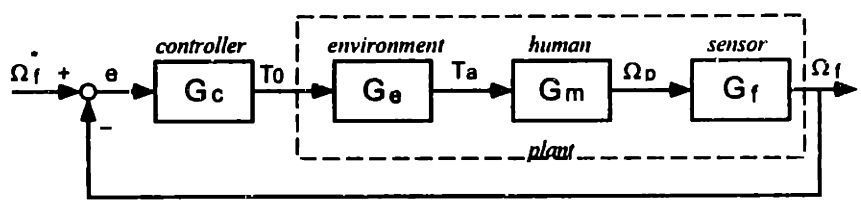

Figure 6.2: The plant of ZLC

The thermal environment transfer function is:

$$G_e(s) = e^{-\tau_d^e s} \frac{K_e}{1 + \tau_e s} \tag{6.30}$$

The transfer function for the human thermoregulation is given in equation(6.26). If the penetration time through clothing as well as body tissue is considered, the transfer function $G_m(s)$ given in equation (6.26) can be modified by adding a pure time delay as:

$$G'_m(s) = e^{-\tau_d^m s} G_m(s) \tag{6.31}$$

The sensor dynamics consists of two parts: the photoelectric circuit and the filter. The dynamics of the circuit is much faster than the rest of the dynamics involved in

the plant, therefore it can be neglected in the plant model. The sensor dynamics is determined mainly by the dynamics of the filter. The following approximation is used for the filter dynamics:

$$G_f(s) = K_f e^{-\tau_d^f s} \tag{6.32}$$

By merging the time delay terms into a single term, the plant transfer function can be written as:

$$G_{plant}(s) = e^{-\tau_d s} G_p(s) = \frac{e^{-\tau_d s} B(s)}{A(s)} \tag{6.33}$$

where $A(s)$ and $B(s)$ are polynomials of s.

6.1.3 Stability of the PI Controller

Using the linear human thermoregulation model and the models for the air temperature in the test chamber (equations (5.18), (5.18)), the stability of the PI controller used earlier can be analyzed.

Figure 6.3 and Figure 6.4 are the discrete time Bode plots for the loop transfer functions of the closed-loop system with the PI controller used in Chapter 3 for a warm state and a cold state of the body respectively. The stability margins are tremendously different at the two different states. At the warm state, the system has a gain margin less than 1.2 or 1.6 dB, while the gain margin for the system at the cold body state is greater than 500. These values indicate that the control gains are close to the maximal allowable values for the warm state, and much larger gains can be used when the body is cold.

The small gain margin at the warm state explains the unstable behavior shown in Figure 3.11. When the subject moved to a more drafty location, the heat transfer coefficient $\bar{h}_a$ increased. From equations (6.10) and (6.26), it can be shown that one consequence of such a change is the increase of the open loop gain. If the gain margin is not big enough, this gain increase can drive the closed-loop system unstable.

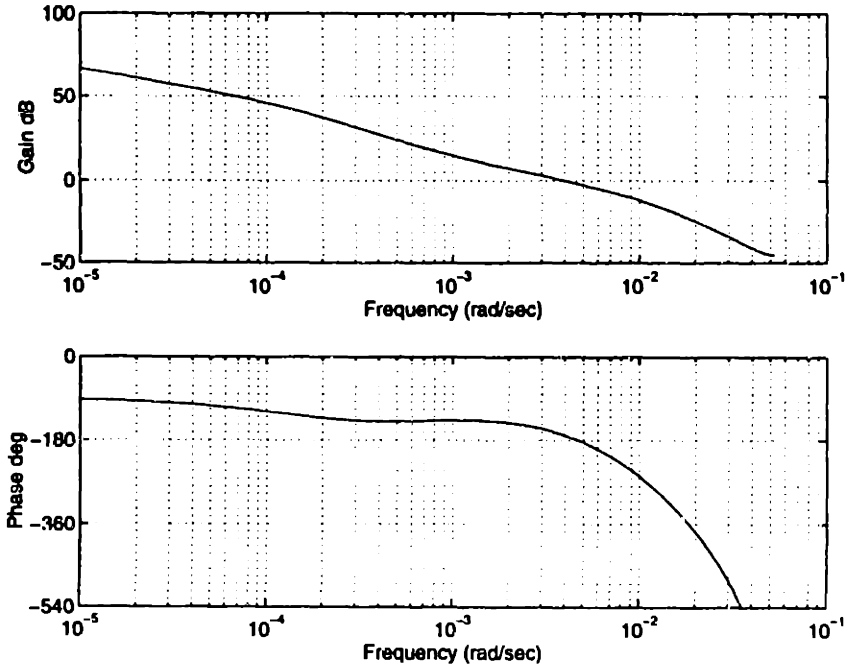

Figure 6.3: Bode plot for the system with a PI controller and $G_m(s)$ evaluated at $T_c = 36.9°C$ and $T_s = 36°C$

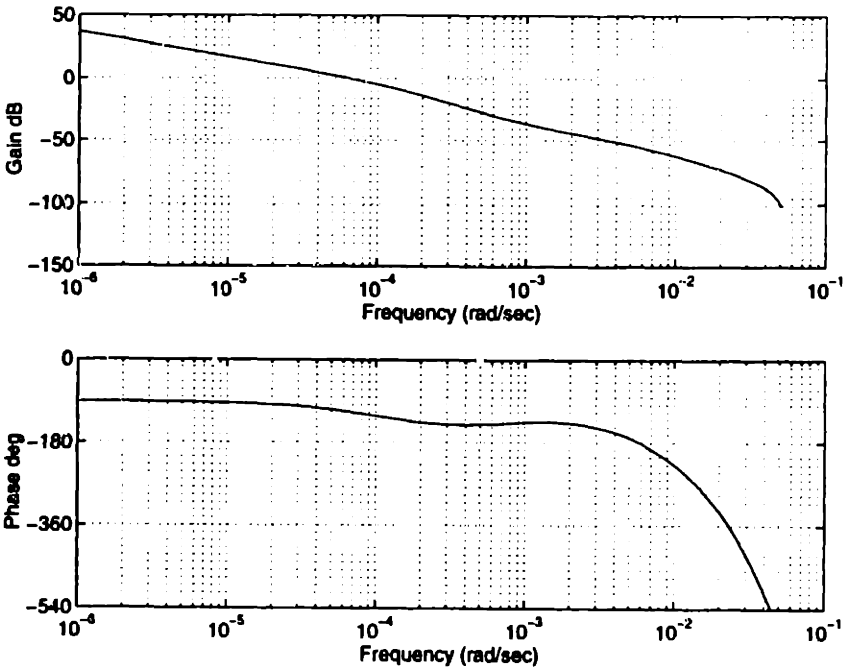

Figure 6.4: Bode plot for the system with a PI controller and $G_m(s)$ evaluated at $T_c = 36.3°C$ and $T_s = 25°C$

6.2 Model-Based Control Design

With the knowledge of the dynamics of human thermoregulation and the thermal environment, sophisticated controllers can be designed systematically based on the models. There are many model-based control design methods, and the one used here is the pole placement method for discrete time systems. The discrete time pole placement method is applicable to systems of any order, and most importantly, it is suitable for systems with any pure time delay.

6.2.1 Pole Placement Method

The pole placement method is summarized as follows. For any given plant, the pulse transfer function can be expressed as:

$$G_p(q^{-1}) = \frac{q^{-d}B(q^{-1})}{A(q^{-1})} \tag{6.34}$$

where:

$$A(q^{-1}) = 1 + a_1 q^{-1} + a_2 q^{-2} + ... + a_n q^{-n} \tag{6.35}$$

$$B(q^{-1}) = b_1 q^{-1} + b_2 q^{-2} + ... + b_m q^{-m} \tag{6.36}$$

and q^{-1} is the delay or backward shift operator.

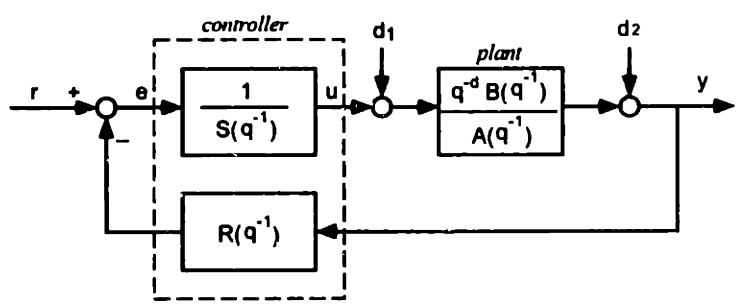

Figure 6.5: Poles placement controller

The structure of the digital controller is shown in Figure 6.5. The controller is represented by two polynomials $R(q^{-1})$ and $S(q^{-1})$. For a given controller (R, S), the closed-loop transfer function is:

$$G_d(q^{-1}) = \frac{q^{-d}B(q^{-1})}{A(q^{-1})S(q^{-1}) + q^{-d}B(q^{-1})R(q^{-1})} \tag{6.37}$$

The pole placement method determines the polynomials $R(q^{-1})$ and $S(q^{-1})$ by locating the poles of the closed system at pre-selected locations. Usually, these pre-selected pole locations are those of a reference model. Polynomials $R(q^{-1})$ and $S(q^{-1})$ can be determined based on the plant model as well as a reference model that defines the desired pole locations of the closed-loop system. The selection of the reference model will be discussed later in this section. Let $P(q^{-1})$ be the characteristic polynomial of the reference model, then the following equation can be used to determine $R(q^{-1})$ and $S(q^{-1})$:

$$A(q^{-1})S(q^{-1}) + q^{-d}B(q^{-1})R(q^{-1}) = P(q^{-1}) \tag{6.38}$$

This equation, known as the *Bezout identity*, has a unique solution for $R(q^{-1})$ and $S(q^{-1})$ if the following conditions are satisfied:

- $A(q^{-1})$ and $B(q^{-1})$ do not have common factors;
- $\deg P(q^{-1}) \leq 2r - 1$, and $\deg S(q^{-1}) = \deg R(q^{-1}) = r - 1$, where:

$$r = \max \deg(n, m + d) \tag{6.39}$$

The solution of equation (6.38) has the form of:

$$S(q^{-1}) = 1 + s_1 q^{-1} + ... + s_{r-1} q^{-(r-1)} \tag{6.40}$$

$$R(q^{-1}) = r_0 + r_1 q^{-1} + ... + r_{r-1} q^{-(r-1)} \tag{6.41}$$

The pole placement method presented above can be used for both stable and unstable systems. There is no restriction on the time delay or the order of the system. The selection of reference model and the treatment for steady state error are discussed in the following sections.

6.2.2 Steady-State Error

To have a zero steady-state error in the closed-loop response to a step input or in the presence of disturbance, the feed-forward channel must contain a digital integrator [39]. So the polynomial $S(q^{-1})$ must be augmented as:

$$S'(q^{-1}) = S(q^{-1})\,(1 - q^{-1}) = S(q^{-1})\,H_2(q^{-1}) \tag{6.42}$$

Furthermore, for digital robustness reasons[39], a filter is used in cascade with $R(q^{-1})$:

$$R'(q^{-1}) = R(q^{-1}) \left(\frac{1}{1-\alpha} - \frac{\alpha}{1-\alpha} q^{-1} \right) = R(q^{-1})\, H_1(q^{-1}) \tag{6.43}$$

where $0 < \alpha \ll 1$. The closed-loop transfer function becomes:

$$G_{cl}(q^{-1}) = \frac{q^{-d} B(q^{-1})}{A(q^{-1})S(q^{-1})H_2(q^{-1}) + q^{-d}B(q^{-1})R(q^{-1})H_1(q^{-1})} \tag{6.44}$$

and equation (6.38) becomes:

$$A(q^{-1})S(q^{-1})H_2(q^{-1}) + q^{-d}B(q^{-1})R(q^{-1})H_1(q^{-1}) = P(q^{-1}) \tag{6.45}$$

The digital filter $H_1(q^{-1})$ and $A(q^{-1})$ must not have common factors in order to have an unique solution for R and S.

The steady-state gain of this closed-loop function is:

$$G_{cl}(1) = \frac{B(1)}{A(1)S(1)H_2(1) + B(1)R(1)H_1(1)} = \frac{1}{R(1)} \tag{6.46}$$

A gain $K = R(1)$ is added before the feedback loop as shown in Figure 6.6. As a result, the steady-state gain becomes unitary, and therefore the steady-state error for a step input is zero. Notice that the gain is only a function of R, it does not explicitly depend on A or B. So once a controller (S, R) is chosen, the steady-state gain is always 1, and uncertain model parameters do not cause a steady-state error for a step input.

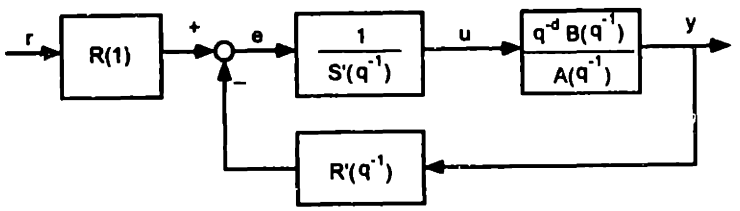

Figure 6.6: Poles placement controller with zero steady-state error

The transfer function from disturbances d_1 and d_2 to the output are:

$$G_{d1}(q^{-1}) = \frac{q^{-d}B(q^{-1})S(q^{-1})H_2(q^{-1})}{A(q^{-1})S(q^{-1})H_2(q^{-1}) + q^{-d}B(q^{-1})R(q^{-1})H_1(q^{-1})} \tag{6.47}$$

$$G_{d2}(q^{-1}) = \frac{q^{-d}A(q^{-1})S(q^{-1})H_2(q^{-1})}{A(q^{-1})S(q^{-1})H_2(q^{-1}) + q^{-d}B(q^{-1})R(q^{-1})H_1(q^{-1})} \tag{6.48}$$

The steady-state gains of both transfer functions are zero.

6.2.3 Selection of the Reference Model

One important step in the pole placement control design is defining the closed-loop poles, or selecting the polynomial $P(q^{-1})$. Usually, $P(q^{-1})$ is specified as the characteristic polynomial of a second-order system which can be obtained by discretizing the continuous time system:

$$G(s) = \frac{\omega_0^2}{s^2 + 2\zeta\omega_0 s + \omega_0^2} \tag{6.49}$$

The damping coefficient ζ is generally chosen between 0.7 to 1.0. The value of ω_0, which determines the bandwidth of the closed-loop system, and is the central parameter to be specified in the design procedure. Several issues must be taken into account when specifying ω_0:

- Response speed. The bandwidth is directly related to the response speed of the system. A higher bandwidth means a faster response speed. One important performance requirement for the ZLC is to improve the responding speed over the traditional control, so that the HVAC system can relieve the stress on the human occupant as soon as possible.

- Actuator saturation. The fast response of the closed-loop system can only be achieved by intense outputs from the actuators. For example, to cool an occupant quickly, a very low supply air temperature is required when the flow rate is fixed. Because all actuators have their limited operation ranges, the saturation problem will arise if too much effort is demanded. So the saturation of actuators places an upper bound on the bandwidth of the closed-loop system.

- Sampling time. For discrete time systems, the closed-loop bandwidth is also constrained by the sampling time. The following criterion is usually used[39]:

  $$0.25 < \omega_0 T_s \leq 1.5 \tag{6.50}$$

  where T_s is the sampling time in seconds.

- Stability robustness. When the model used for control design is not accurate, the modeling error will place another upper bound on the bandwidth of the closed-loop system. Because of the potentially large error in the human thermoregulation

model shown in Chapter 4, this constraint becomes dominant. More about the stability robustness and its relation to the bandwidth selection will be presented in future sections.

Once ζ and ω_0 are selected, the polynomial $P(q^{-1})$ can be obtained by taking the z-transform of the system (6.49) with zero-order hold.

6.3 Model-Based ZLC

The pole placement method presented in the previous section is used to design the controller for ZLC. The thermoregulation model of Subject F is used in all analysis and design procedures. We will begin with the selection of closed-loop bandwidth based on the modeling errors.

6.3.1 Closed-Loop Bandwidth Based on Modeling Errors

The human thermoregulation model developed in Chapter 4 is only an approximation of the human thermoregulatory system. If the difference between the model and the actual system is large, then the digital controller designed based on the approximate model may not guarantee the stability of the closed-loop system. The stability robustness in the presence of model uncertainties can be analyzed using the Nyquist criterion and the Small Gain theory[40].

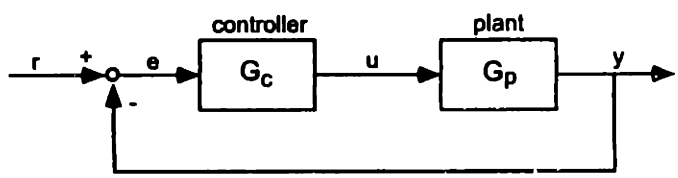

Figure 6.7: The standard form of a feedback system

For the standard feedback configuration shown in Figure 6.7, the model uncertainty can be expressed in a multiplicative form:

$$G_p'(j\omega) = [1 + L(j\omega)]G_p(j\omega) \tag{6.51}$$

with:

$$|L(j\omega)| < E(\omega) \qquad \forall\omega \geq 0 \tag{6.52}$$

where G_p is the nominal model of the plant, G'_p is the actual plant model, and E is a positive scalar function. Using the Nyquist criterion, it can be derived that for the actual closed-loop system to be stable with controller G_c, the following condition must be satisfied:

$$|G_{cl}(j\omega)| = \left| \frac{G_c(j\omega)G_p(j\omega)}{1 + G_c(j\omega)G_p(j\omega)} \right| < 1/E(\omega) \tag{6.53}$$

Clearly, equation (6.53) indicates that to ensure stability, the closed-loop gain must be small when the modeling error is large.

To apply the above result to our problem, it is necessary to find the error bound function $E(\omega)$. Since only very limited knowledge about the actual plant G'_p is known, we can only estimate this bound using the experimental data obtained in Chapter 4. For example, using the first order time constants, one can obtain an estimation of $E(\omega)$ as follows. If we approximate both the actual plant and the model by a first order system, then:

$$G_p = \frac{1}{\tau_{model}s + 1}, \qquad G'_p = \frac{1}{\tau_{exp}s + 1} \tag{6.54}$$

The error can be obtained by rewriting the function G'_p as:

$$G'_p = \frac{1}{\tau_{exp}s + 1} = G_p \frac{\tau_{model}s + 1}{\tau_{exp}s + 1} = G_p \left[1 + \frac{(\tau_{model} - \tau_{exp})s}{\tau_{exp}s + 1} \right] \tag{6.55}$$

which gives:

$$E(\omega) = \left| \frac{(\tau_{model} - \tau_{exp})j\omega}{\tau_{exp}j\omega + 1} \right| \tag{6.56}$$

For $\tau_{exp}\omega \gg 1$, we have:

$$E(\omega) \approx \left| \frac{(\tau_{model} - \tau_{exp})j\omega}{\tau_{exp}j\omega} \right| = \frac{|\tau_{model} - \tau_{exp}|}{\tau_{exp}} = e_\tau \tag{6.57}$$

The graphical meaning of condition (6.53) is that the magnitude plot of the closed-loop system based on the nominal plant model shall be under the curve of $1/E(\omega)$. If the magnitude plot crosses the $1/E(\omega)$ curve, then there exists a perturbation L which satisfies (6.51) and could cause the closed-loop system to be unstable. The minimal distance between the two curve represents the stability margin of the system.

Using the values in Table 4.6, we have the following values for Subject F: $\tau_{exp} \approx 700$, $\max|\tau_{model} - \tau_{exp}| = 480$, and $e_\tau \approx 69\%$. The error bound based on this first order analysis becomes:

$$E(\omega) = \left| \frac{480j\omega}{700j\omega + 1} \right| \tag{6.58}$$

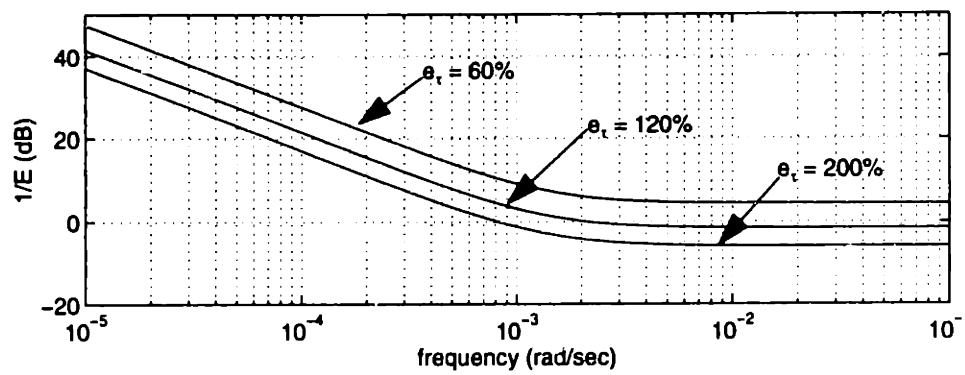

Figure 6.8: Multiplicative error bounds based on time constants ($\tau_{exp} = 700$).

Figure 6.8 plots three different functions of $E(\omega)$ corresponding to different modeling errors e_τ. These curves indicate that if the modeling error e_τ is 200%. the maximal closed-loop bandwidth is $8 \cdot 10^{-4}$ (rad/s). If the error is reduced to 120%. then the allowable bandwidth increases to $2.5 \cdot 10^{-3}$ (rad/s). The curve of the 60% error implies that if the reference model is not under-damped ($\zeta > 0.7$) and both the plant and the model are first order linear system, then the closed-loop bandwidth can be very high. Since our actual plant is not linear, the bandwidth should be limited even for $e_\tau = 60\%$. To specify a sufficient stability margin of the closed-loop system, $\omega_0 = 2.5 \cdot 10^{-3}$ (rad/s) is used for the reference model.

6.3.2 Nonlinear Properties

Because the plant is non-linear and the pole placement method is based on the linearized model, multiple digital controllers are required for a wide range of human thermal states. The number of controllers required for the full operating range depends on several criteria, such as the tracking accuracy, response speed, and stability robustness, etc.. Since tracking a transient trajectory is not the objective of current research

work and stability is our major concern, we will not divide the overall range of states into a lot of intervals and design a controller for each of them. Instead, three digital controllers are designed based on the linearized models at a warm state, a neutral state, and a cold state as shown in Table 6.1.

controller	T_c^r (^oC)	T_s^r (^oC)
$(R,S)^{(w)}$	36.9	36
$(R,S)^{(n)}$	36.6	34.1
$(R,S)^{(c)}$	36.3	25

Table 6.1: Three different controllers

At any state of the body, one of the three controllers is used. It is important to study the stability of closed-loop system when a controller is used for a body state which is different from the body state based on which the controller is designed. One simple method is to check the closed-loop pole locations of the system when the controller applied to all three states of the body. Table 6.2 provides the results of such an analysis.

controller	warm state	neutral state	cold state
$(R,S)^{(w)}$	stable	stable	stable
$(R,S)^{(n)}$	unstable	stable	stable
$(R,S)^{(c)}$	unstable	unstable	stable

Table 6.2: Stability of the controllers at different body states

The above analysis shows that the system is stable as long as the state of the body is on the cooler side of the reference state of the controller. This conclusion suggests that two controllers will suffice for ZLC, i.e. $(R,S)^{(w)}$ for a cooling task, which bring the state of the body from warm to neutral, and $(R,S)^{(n)}$ for a heating task, which changes the body from cool to neutral. A more conservative approach is to use a single controller, $(R,S)^{(w)}$, for both tasks. In the latter case, the performance of the closed-loop system may not be satisfactory because of the slow reaction during a warming process.

Another way to study this issue is to use the Nyquist criterion (6.53). For each controller, we can check the magnitude Bode plot with different plant models, and

verify if the small gain condition is violated. For example, the magnitude Bode plots for the systems with controller $(R,S)^{(w)}$ applied to the three reference body states are shown in Figure 6.9. All the resulting systems are guaranteed to be stable even with a modeling error $e_r = 60\%$. The stability margin increases as the state of the body becomes cooler.

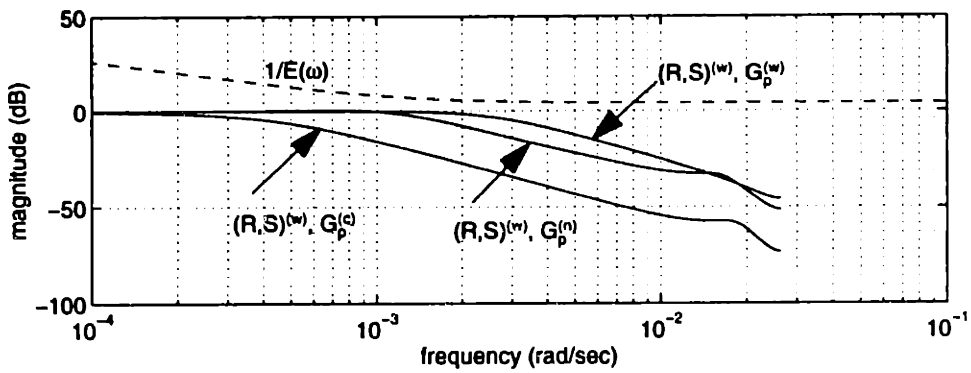

Figure 6.9: Stability robustness analysis of the controller $(R,S)^{(w)}$ applied to the different states of the body (the model of Subject F is used).

Similar analysis is performed for the controller $(R,S)^{(n)}$, and the result is shown in Figure 6.10. The stability condition (6.53) is clearly violated when the controller $(R,S)^{(n)}$ is used for the warm state of the body. The conclusions of the stability robustness analysis agree with those in Table 6.2.

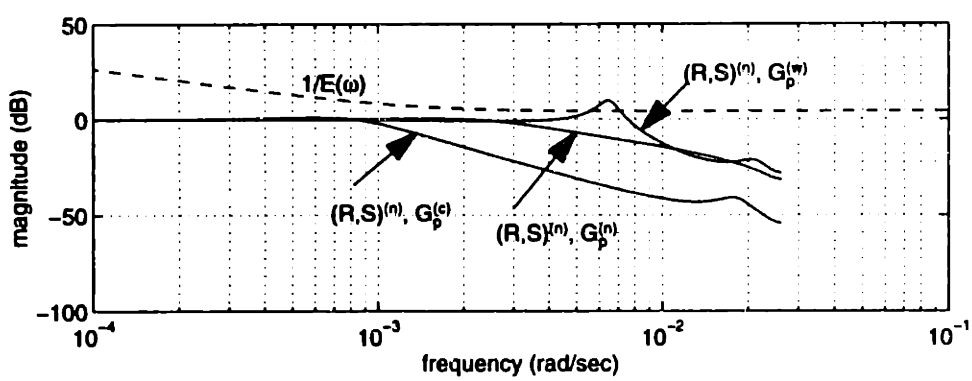

Figure 6.10: Robustness analysis of the controller $(R,S)^{(n)}$ applied to the different states of the body (the model of Subject F is used).

6.3.3 Uncertain Model Parameters

In Section 6.3.1, the stability robustness with regard to unstructured model uncertainties was addressed. To gain more insights into the influence of uncertainties in specific model parameters, in this section we will study the stability robustness issue for the case of parametric uncertainty.

Both environmental model and the human thermoregulation model have some uncertain parameters, such as body fatness, heat transfer coefficient, etc.. The digital controllers are designed based on nominal values of these parameters. In practice, the actual values of these parameters are different from the nominal values, and some of them are time-varying. To guarantee the stability of the closed-loop system, it is necessary to know the allowable varying ranges of the parameters for a given controller.

The uncertain model parameters studied here are:

1. Body conductance h_K, which is a function of body fatness.

2. Heat transfer coefficient h_a, which depends on local air velocity, mean radiant temperature, clothing insulation, etc..

3. Pure time delay τ_d, which depends on the flow field, location in the space, and clothing insulation.

Table 6.3 shows the stable ranges of these important parameters for controller $(R,S)^{(w)}$. The results indicate that the controller can tolerate quite large variations of the parameters. For example, the heat transfer coefficient $\bar{h}_a$ is a function of clothing insulation. The nominal value used for designing $(R,S)^{(w)}$ is $I_{cl} = 0.6\ clo$. The condition $\frac{\bar{h}_a - \bar{h}_a^r}{\bar{h}_a^r} < 140\%$ implies that the system is stable even if the clothing insulation is $I_{cl} = 0.2\ clo$. In physical sense, the values of I_{cl} suggest that even though the controller is designed for Subject F wearing shirt and trousers, the system is stable when the subject is actually wearing shorts. If the uncertainty of $\bar{h}_a$ is due to the local air velocity, then $\frac{\bar{h}_a - \bar{h}_a^r}{\bar{h}_a^r} < 140\%$ means that the system is stable for a velocity as high as 1.0 m/s. even though the nominal air velocity used in the model is 0.15 m/s.

The above analysis gives the allowable ranges of certain model parameters for a given controller. The reverse problem is more important for control design. If we know the

parameter	stable range
h_K (body conductance)	$0 < \frac{h_K - h_K^r}{h_K^r} \leq 200\%$
$\bar{h}_a$ (heat transfer coefficient)	$0 < \frac{\bar{h}_a - \bar{h}_a^r}{\bar{h}_a^r} < 140\%$
τ_d (total time delay)	$\lvert\tau_d - \tau_d^r\rvert \leq t_s$

Table 6.3: stability margins of some model parameters

possible ranges of the parameters, how should we utilize the information in designing the controller? Or more specifically, how should we relate the ranges of uncertain model parameters to the selection of the closed-loop bandwidth?

Again, the problem can be solved by using the Nyquist criterion (6.53). Substituting different values of a parameter into the linear plant model, we can obtain a multiplicative error bound of the model caused by the uncertain model parameter. For example, if everything else is fixed and only $\bar{h}_a$ varies within a given range, we can plot the corresponding error bounds for different sizes of the range. Figure 6.11 shows the results of three different ranges of $\bar{h}_a$. If the parameter range is $\frac{|\bar{h}_a - \bar{h}_a^r|}{\bar{h}_a^r} < 200\%$, then the plot indicates the maximal bandwidth is $3.5 \cdot 10^{-4}$ (rad/s). For the range of $\frac{|\bar{h}_a - \bar{h}_a^r|}{\bar{h}_a^r} < 140\%$, the maximal bandwidth is $2.5 \cdot 10^{-3}$ (rad/s), which was used for our control design. The same procedure can be repeated for other model parameters as well.

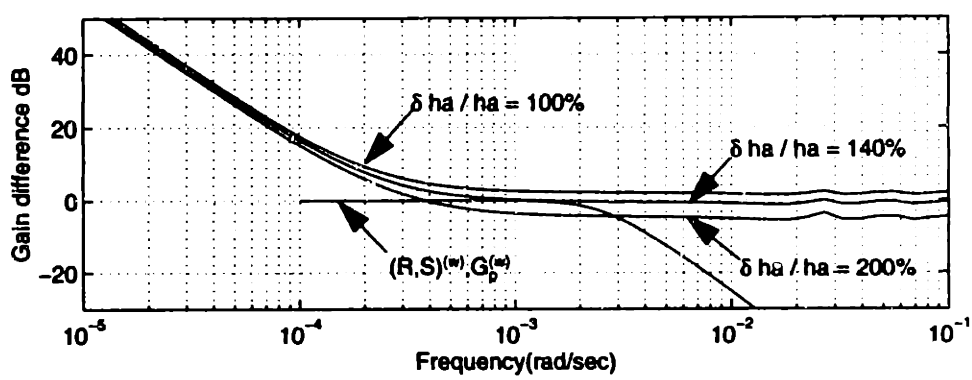

Figure 6.11: Bandwidth selection based on uncertain $\bar{h}_a$ (based on the model of Subject F).

6.4 Experimental Results

So far, we have developed digital controllers for Subject F. These controllers were used for the following experiments on Subject F. The first experiment was a cooling test, and the controller $(R, S)^{(w)}$ was used for the entire process. Figure 6.12 shows the result of this experiment. The subject was first warmed for two hours with 31^oC air temperature in the test chamber. Then the controller was activated and the subject was seated at location I. At the time as marked in the figure, the subject moved to location II. The plots show clearly the effect of body movement, which is treated as a disturbance in our analysis. The model-based controller maintained the closed-loop stability under these circumstances.

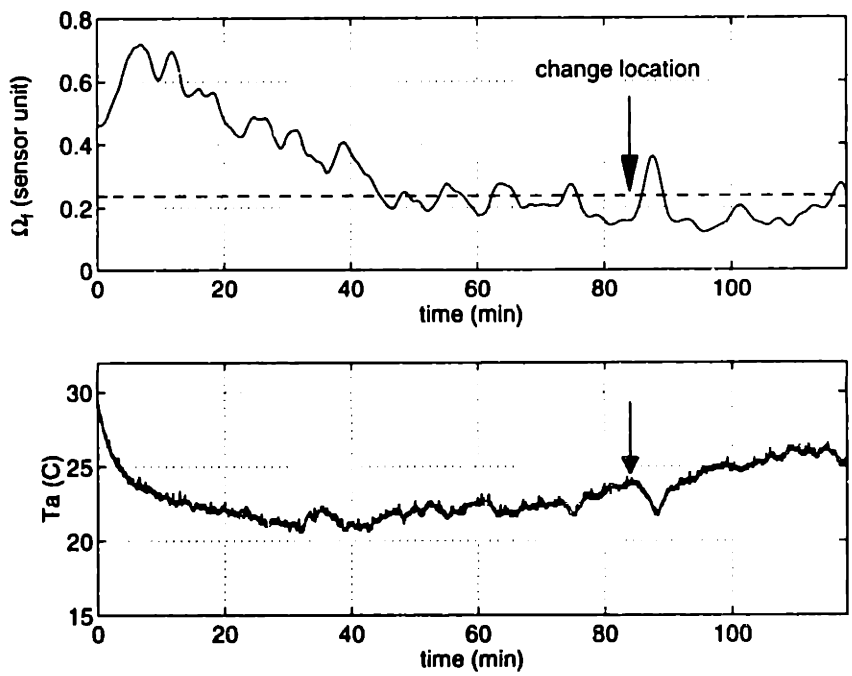

Figure 6.12: Model-based ZLC: starting from a warm state

This test was similar to the cases of Figure 3.10 and 3.11, in which the PI controller was used. Unlike the PI controller, which yielded a unstable closed-loop system when the subject moved from location I to Location II, the model-based controller maintained the stability of the system with such a movement.

Figure 6.13 shows the result of another test using controller $(R, S)^{(n)}$. The subject was pre-cooled at air temperature 18^oC for an hour. The controller was then turned on

and the subject was located at position I.

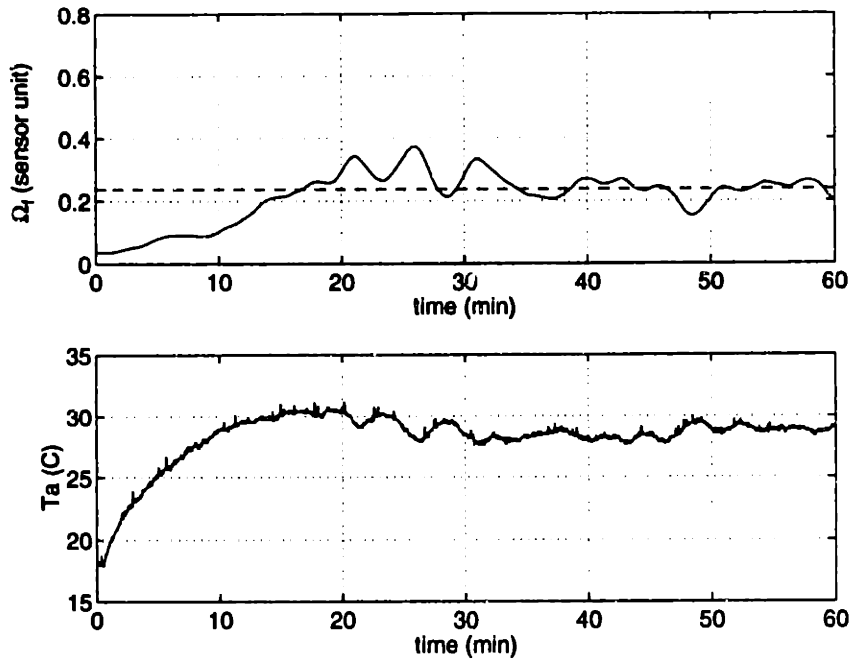

Figure 6.13: Model-based ZLC: starting from a cool state

The above experimental results show that model-based controllers result in stable, robust closed-loop systems. Also note that the control inputs, i.e. the supply air temperatures, are smoother than those of the PI controller in all cases.

This chapter described a systematic way to design stable and robust zero-load controllers for any given human occupant. The controllers can be designed by pole placement method based on the plant models and a reference closed-loop model. The bandwidth of the reference model are selected according to model uncertainties, either unstructured uncertainties or parametric uncertainties. Important nonlinear properties of the system are also addressed in this chapter.

Chapter 7

Conclusions

7.1 Summary of Zero-Load Control

A new methodology for thermal environment control, zero-load control, is presented in this thesis. Unlike traditional environment control approaches which regulate one or a group of environmental variables, ZLC regulates the thermal states of the human occupants. As a result, the human body reaches a physiologically neutral state. The instrumentation for ZLC is simple, requiring only one real time measurement: finger blood flow rate. A micro-size optical blood flow rate sensor embedded in a finger ring makes ZLC acceptable to most human occupants.

To guarantee the stability of the closed-loop system, the model-based control design method is adopted. The basic steps for model-based ZLC are:

Step1 **Model the thermal environment.** The air temperature dynamics of most indoor thermal environments can be modeled as a first order system. The constant and the DC gain of the first order dynamics should be identified. Methods provided in Chapter 5 can be used for this purpose.

Step2 **Identify the human occupant.** From basic human factors, such as weight and height, the linear thermoregulation models at the warm state and the cold state can be established. Clothing insulation, local air velocity, and mean radiant temperature are also required to evaluate the heat transfer coefficient used in the model.

Step3 **Estimate uncertainties.** For any uncertain parameters used in the first two steps, estimate the bounds of the uncertainties.

Step4 **Calibrate the sensor.** For each human subject, a simple thermal transient test similar to those in Chapter 4 is performed. A model simulation of the same process

is also performed using the non-linear human thermoregulation model. From both the test and simulation results, the values of r_Ω and Ω_f^* can be obtained.

Step5 **Determine a reference model.** Using the parameter bounds obtained in Step 3, estimate the maximal bandwidth of the closed-loop system. Other criteria for selecting the bandwidth should also be verified. A second order reference model can be obtained based on the specified bandwidth and a damping coefficient of 0.7.

Step6 **Design the controllers.** Using the linear models from Step 1 and 2, and the calibration results from Step 4, digital controllers for the warm state and the neutral state are computed using the pole placement method. The controller obtained from the warm state model is used for the cooling task, and the other controller is used for the heating task.

7.2 Major Contributions of the Thesis

The contributions of this thesis are summarized as follows.

A new environment control algorithm

Zero-load control is the first environment control algorithm that utilizes real-time human physiological signal in the feedback loop. Because the human body is used as the environment sensor and the body reaction to the thermal environment is measured by a single sensor, the instrumentation required by ZLC is much simpler than other comfort control methods. The real time feedback of the human signal makes it possible to compensate for the dynamics of the body, and thus the uncomfortable transient period can be significantly reduced. This control algorithm can be applied to both uniform and non-uniform thermal environments.

A practical instrumentation scheme

In ZLC, the human thermal load is estimated based on a reflex-controlled physiological variable, the peripheral blood flow rate. Therefore, only a single point measurement is needed for the feedback, and the implementation of the closed-loop control is highly

feasible. By embedding a small optical blood flow sensor in a ordinary finger ring, the ZLC paradigm can be accepted by most occupants.

A low-order human thermoregulation model

A second order nonlinear model of the human thermoregulatory system is developed for both system analysis and control design purposes. The model is capable of predicting the different dynamics at different states of the body. As shown by experimental data, the modeling errors are within reasonable ranges for most people.

A systematic design method for ZLC

This thesis presents a systematic approach to designing zero-load controllers, with the objective of achieving a desirable performance while maintaining a specified level of stability robustness. This approach utilizes both the human thermoregulation model and the environment model to design digital controllers. Modeling errors as well as uncertainties of model parameters are directly linked to the control design parameters, and the maximal bandwidth of the closed-loop system is determined based on the amount of uncertainties that may present. The study of the nonlinear properties of the system leads to a simple control strategy: one controller for the cooling task, and one controller for the heating task. Both analysis and experiments show that the resulting controllers provide better closed-loop properties than a PI controller.

7.3 Future Directions

This thesis developed a new and promising environment control algorithm: zero-load control. This algorithm was implemented for a special configuration, i.e. a single actuator and a single human occupant, to demonstrate the concept. The concept of ZLC can certainly be applied to more complex configurations, and certain aspects of the six steps of the ZLC design can be modified or improved. The following are a few valuable extensions to the current work that are worth of further pursuit.

- Multi-input, multi-output (MIMO) control design. The concept of ZLC can be readily applied to the multi-actuator and multi-occupant situations. In control theory, this is a typical MIMO control design problem. The MIMO version of

ZLC can be immediately applied to the climate control in automobiles, air plane cabins, and some office spaces.

- Improvement of sensor design. Because photoelectric plethysmography provides only a relative blood flow rate, the blood flow sensor requires an experimental procedure for its calibration. The calibration procedure can be simplified or eliminated if more sophisticated blood flow sensors can be designed. A possible solution is to use electrical impedance plethysmography, which is capable of absolute blood flow measurement.

- Adaptable vasomotor control model. Even though the human thermoregulation model is capable of adapting to the different physical characteristics of the human body, it cannot account for the differences of vasomotor control caused by aging. To guarantee the performances of ZLC when it is applied to different age populations, an age-adaptable vasomotor control model is needed.

- Other advanced control techniques. Current design of ZLC is based on a single sensor measurement and the standard pole placement technique. We can certainly improve the system performance by using additional measurements, such as skin temperature, or by applying other advanced control techniques, such as adaptive or learning control.

Appendix A

Test Chamber Design

A HVAC test chamber was constructed in the d'Arbeloff Laboratory at MIT as part of this thesis work. This test chamber is equipped with two separate climate control systems: an air handling system and a radiant heating/cooling system. Direct digital controller is used to control each device, and high level control algorithms are implemented on a PC, which communicates with the device controller. The chamber structure as well as the control system is presented in details in this chapter.

A.1 Chamber Structure

The chamber has a 12'x10' floor area and a height of 8' as shown in Figure A.1. The room has one door and one window, both of which are off the shelf products. There are two different walls installed in the chamber. One is an ordinary insulated wall (Figure A.3) and the other is a radiant wall (Figure A.4). The insulation of all walls is R19. The floor of the chamber is also activated by radiant circuits. The radiant floor has a similar structure to the radiant walls, as shown in Figure A.4.

There are two hydraulic circuits in each radiant wall or floor. The four circuits in the two radiant walls share one manifold, and the two circuits in the floor use another manifold. Hot water is supplied to the manifolds from an electrical heater and chilled water can be supplied from the central chill water supply in the lab.

There are three air supplies and one air return in the chamber as shown in Figure A.1. Two of the air supplies are wall diffusers, while the other is a ceiling diffuser. The dimensions of the diffusers are tabulated in Table A.1.

The air is supplied from a central air handling unit, which consists of a fan and a cooling coil. The air is first cooled to a low temperature, and then reheated to the desired temperature by the local electrical heater at each branch of the supply. The supply flow rate of each outlet is controlled by a VAV box, which is located at the

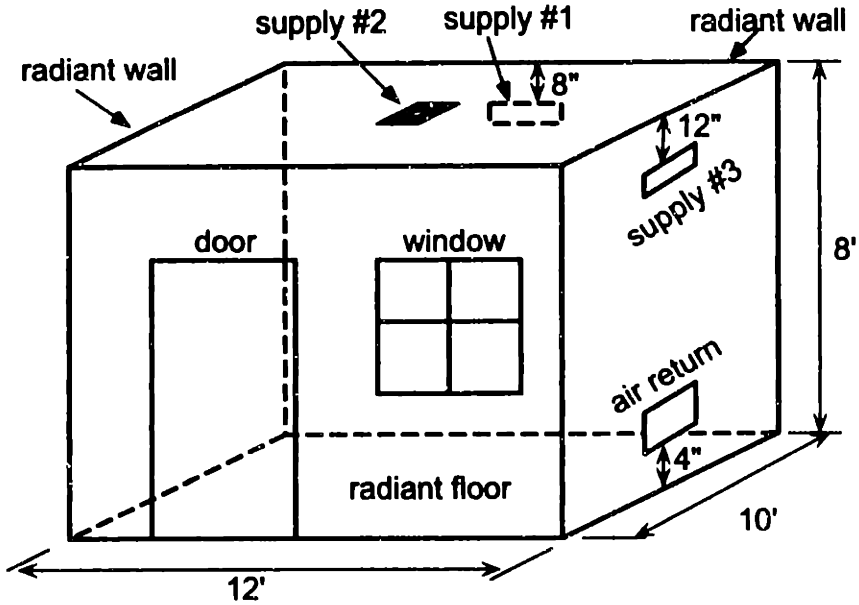

Figure A.1: Dimensions of the HVAC test chamber. The dimensions of the air diffusers are listed in Table A.1.

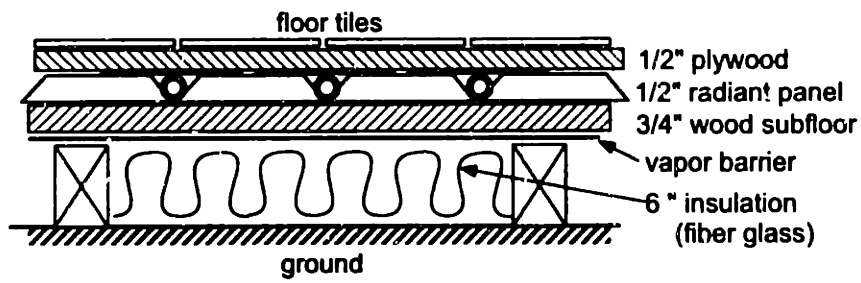

Figure A.2: Floor structure

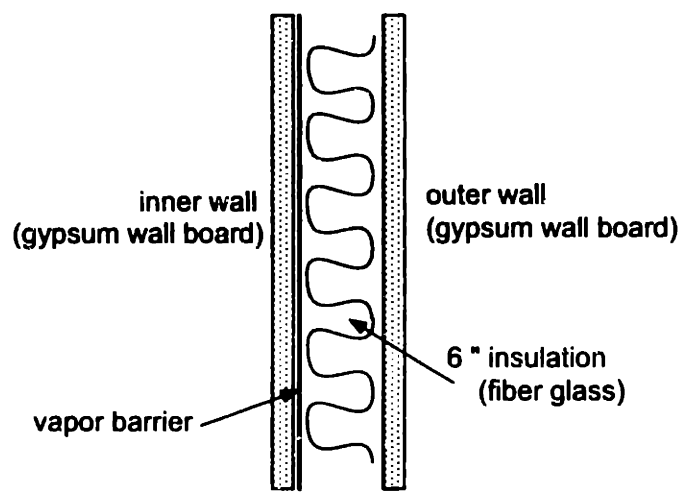

Figure A.3: Structure of insulation walls

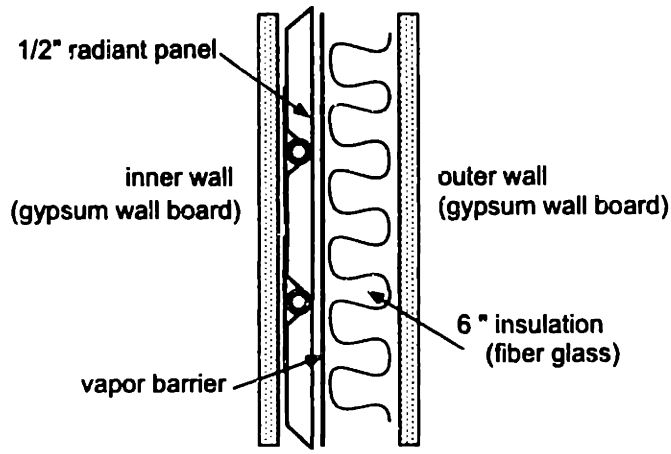

Figure A.4: Structure of radiant walls

object	dimension
wall diffuser	16" x 4"
ceiling diffuser	8" x 8"
air return	8" x 8"

Table A.1: Dimensions of various openings

immediate downstream of the local electrical heater. This hardware design allows us to control the air temperature as well as the air flow rate at each outlet independently. A VAV box is also installed in the air return to control the pressure difference between the indoor and outdoor air. Part of the air handling system and the radiant system are shown in Figure A.5.

A.2 Control System

Figure A.6 shows the overall control system of the test chamber. All actuators, such as mixing valves on the manifolds, electrical heaters, VAV damper etc., are controlled by two device controllers (SCX 900, Andover Controls). Each channel on these device controllers can be independently programmed. A PID controller is used to control each device, and the gains are turned to best performance separately. The complete code for all device controls are attached at the end of this appendix.

Table A.3 and Table A.5 list the actuators controlled the two device controllers: M01_CondoFan and M01_CondoLab, respectively. The sensor information used by the

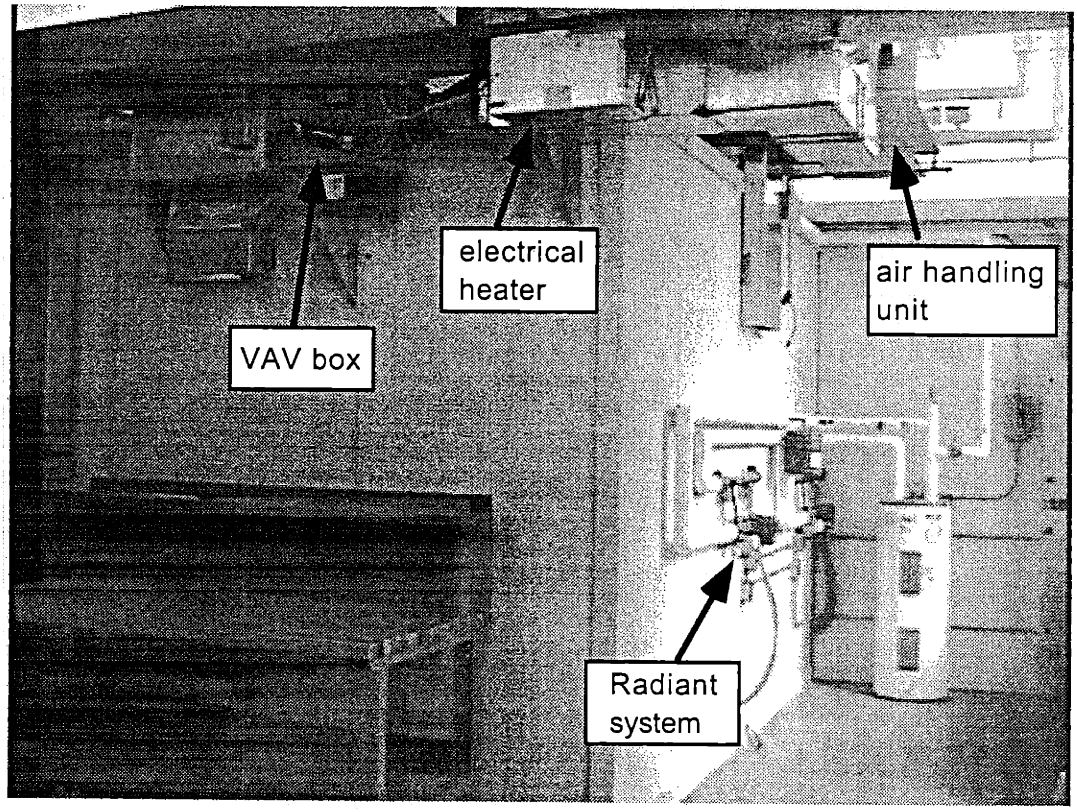

Figure A.5: The rear view of the test chamber

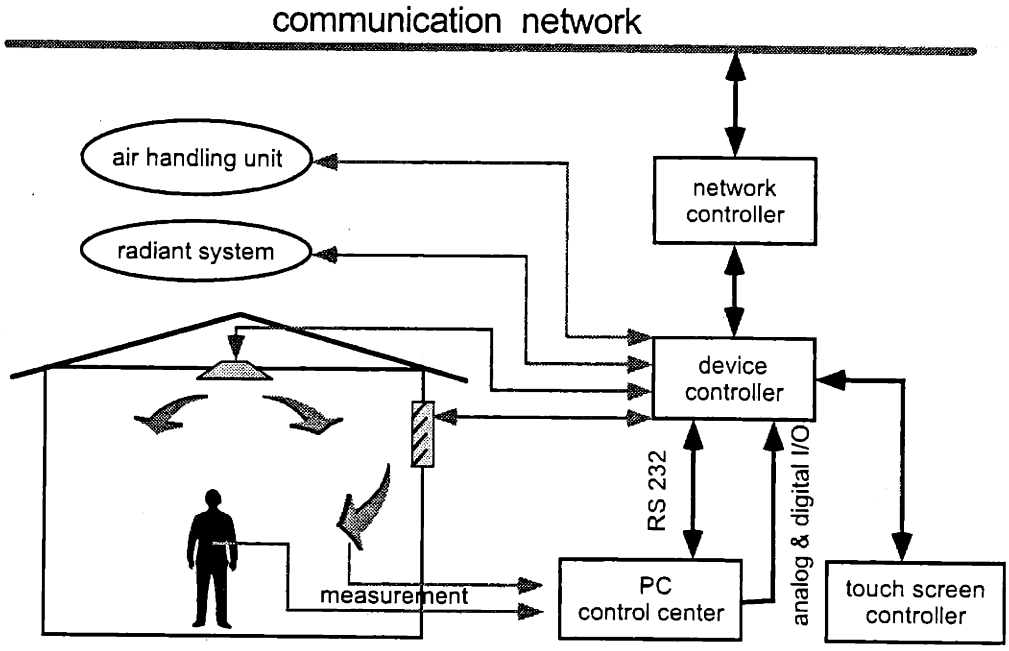

Figure A.6: Control system of the test chamber

controllers are provided in Table A.2 and Table A.4. These device controllers regulate the states of the corresponding actuators to the specified set points. These set points are provided by high level control algorithms, such as ZLC. The high level controller is implemented on a PC, which is connected to the device controllers through a serial connection and direct digital and analog I/O. Through the serial connection, an operator can monitor the state of each device, change the set points manually, modify and download/upload device control programs by using a serial communication program, such as *CrossTalk*. The analog and digital I/O channels are used for real time communication between the PC and the device controllers. For example, the set points are provided to the device controllers through analog channels.

Table A.2: Input channels of device controller M01_CondoFan (SCX 900)

channel No.	variable	description
1	FloorHW_Te	mixing water temperature of the floor manifold (^oF)
2	WallHW_Te	mixing water temperature of the wall manifold (^oF)
3	Floor_Te	floor surface temperature (^oF)
4	Wall_Te	radiant wall surface temperature (^oF)
5	Room_Te	room temperature (thermostat) (^oF)
6	analog1	analog output Channel 1 of DDA-06 board (V)
7	analog1	analog output Channel 2 of DDA-06 board (V)
8	analog1	analog output Channel 3 of DDA-06 board (V)
9	analog1	analog output Channel 4 of DDA-06 board (V)
10	analog1	analog output Channel 5 of DDA-06 board (V)
11	analog1	analog output Channel 6 of DDA-06 board (V)
12	PA0	digital output channel PA0 of DDA-06 board
13	PA1	digital output channel PA1 of DDA-06 board
14	PA2	digital output channel PA2 of DDA-06 board
15	PA3	digital output channel PA3 of DDA-06 board

The PC and the device controllers are installed outside the test chamber, so are some other electronic devices such as signal processing boards. Figure A.7 shows the actual setup configuration. A touch screen controller (DCX 250, Andover Controls) is installed inside the test chamber. Users can monitor the current room status and change set points through this graphic user interface. The functions available on the touch screen controller can also be programmed. The current functions of the touch

Table A.3: Output channels of device controller M01_CondoFan (SCX 900)

channel No.	variable	description
1	ClngVlv	opening of the chilled water supply valve
2	AHFan	fan of the air handling unit
3	HwPmp	power to the circulation pumps on the manifold
4	FloorHwVlvOpen	opening of the mixing valve on the floor manifold
5	FloorHwVlvClose	closing of the mixing valve on the floor manifold
6	WallHwVlvOpen	opening of the mixing valve on the wall manifold
7	WallHwVlvClose	closing of the mixing valve on the wall manifold

Table A.4: Input channels of device controller M01_CondoLab (SCX 900)

channel No.	variable	description
1	SupAir1_VP	dynamic pressure at supply No. 1 (*in water*)
2	SupAir2_VP	dynamic pressure at supply No. 2 (*in water*)
3	SupAir3_VP	dynamic pressure at supply No. 3 (*in water*)
4	ExhAir_VP	dynamic pressure at air return (*in water*)
5	Room_SP	pressure difference between indoor and outdoor air (*in water*)
7	SupAir1_Te	air temperature of supply No. 1 (^oF)
8	SupAir2_Te	air temperature of supply No. 2 (^oF)
9	SupAir3_Te	air temperature of supply No. 3 (^oF)
10	ExhAir_Te	air temperature at the return (^oF)

Table A.5: Output channels of device controller M01_CondoLab (SCX 900)

channel No.	variable	description
1	SupAirDmp1	damper position of the VAV box for supply No. 1
2	SupAirDmp2	damper position of the VAV box for supply No. 2
3	SupAirDmp3	damper position of the VAV box for supply No. 3
4	ExhAirDmp	damper position of the VAV box for the air return
5	ElecReHt1	electrical heater for supply No. 1
6	ElecReHt2	electrical heater for supply No. 2
7	ElecReHt3	electrical heater for supply No. 3

screen controller are provided in the program attached. The activities of the device controllers as well as the touch screen controller can be supervised by a workstation on the Internet through a network controller (CX 9200, Andover Controls).

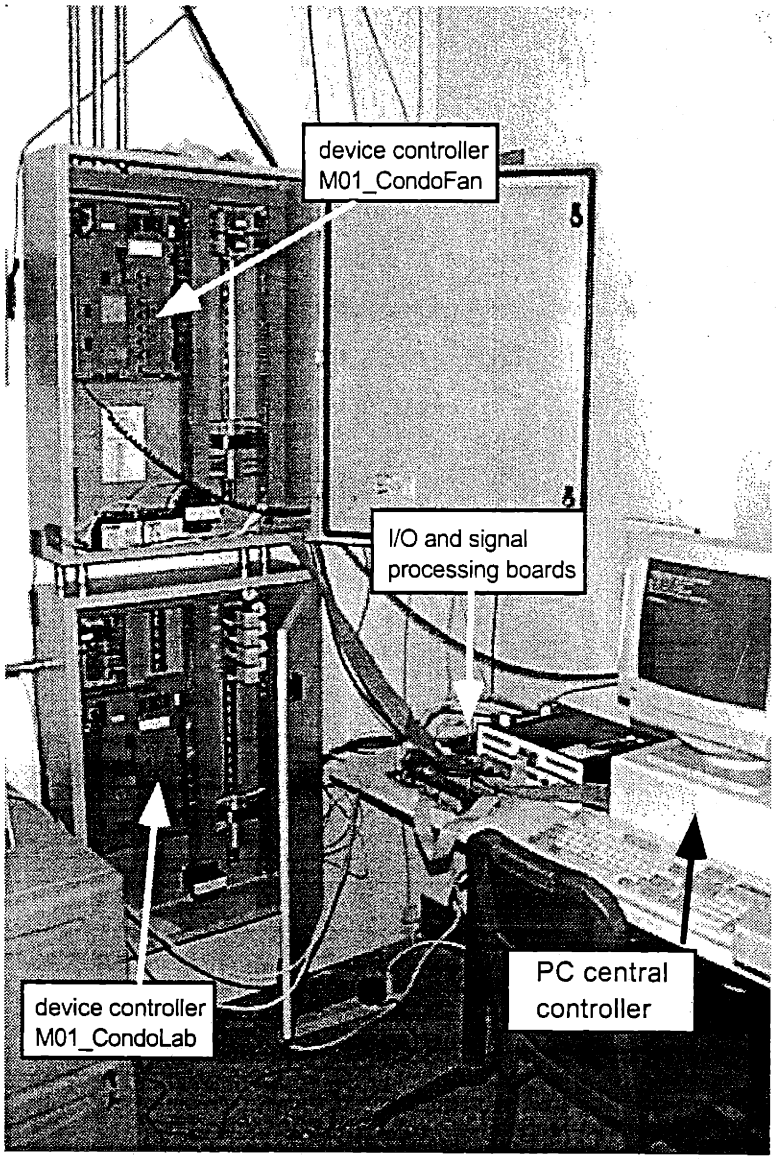

Figure A.7: Device controllers and the PC control center of the test chamber

Programs for the Device Controllers and the Touch Screen Controller [1]

[1]Each program begins with the keyword **Object**, and ends with the keyword **EndObject**. For more about the programing language and the built-in functions, please refer to "*Plain English Language Refenrence*" by Andover Controls.

```
--------------------------------------------------------------------------------
Device Controller:  M01_CondoFan
--------------------------------------------------------------------------------
CONDOFAN PROGRAMS:

 Program          : ClngVlv.Pr       : 0
 Program          : HWPmp.Pr         : 0
 Program          : AHFan.Pr         : 0
 Program          : AHMisc.Pr        : 0
 Program          : FloorHWVlv.Pr    : 0
 Program          : WallHWVlv.Pr     : 0

Object : ClngVlv.Pr
 Type : Program
 LastChange : 7-29-1997 11:20:55 AM
 Description : Cooling Valve Control
 State : Enabled
 Status : Active
 AutoStart : True
 FlowType : Looping
 Debug : Disabled
 ExecTimeOut : 0
 CommandLine : False
 ShareFlag : False
 Code :

Numeric SupAir_Te
Numeric SupAirTe_Se

CNTRL:
  If (Occupancy = OFF) then Goto OFF_LINE
  SupAirTePID[1] = 0.02
  SupAirTePID[2] = 0.001
  SupAirTePID[3] = 0.1
'  SupAir_Te = avg(M01_CondoLab SupAir1_Te, M01_CondoLab SupAir2_Te,
                   M01_CondoLab SupAir3_Te)
  SupAirTe_Se = avg(M01_CondoLab SupAir1Te_Se, M01_CondoLab SupAir2Te_Se,
                    M01_CondoLab SupAir3Te_Se)
'  SupAirTe_Se = avg(M01_CondoLab SupAir1Te_Se, M01_CondoLab SupAir3Te_Se)
'  SupAir_Te = M01_CondoLab SupAir2_Te
  If (SupAirTe_Se > 90) then
'    SupAirTe_Se = 85
    ClngVlv = 0
  Else
'    SupAirTe_Se = 50
    ClngVlv = 1
  Endif
'  ClngVlv = PID.Fn(SupAir_Te, SupAirTe_Se, SupAirTePID[1], SupAirTePID[2],
                    SupAirTePID[3], 0.5, 1, SupAirTePID[4], SupAirTePID[5])

OFF_LINE:
```

```
  ClngVlv = 0
  SupAirTePID[4] = 0
  SupAirTePID[5] = 0
  If (Occupancy = ON) then Goto CNTRL
 EndCode
EndObject

Object : HWPmp.Pr
 Type : Program
 LastChange : 7-29-1997 11:20:58 AM
 Description : HW Pump Control
 State : Enabled
 Status : Active
 AutoStart : True
 FlowType : Looping
 Debug : Disabled
 ExecTimeOut : 0
 CommandLine : False
 ShareFlag : False
 Code :

CNTRL:
  If (Occupancy = OFF) then Goto OFF_LINE
  HWPmp = ON

OFF_LINE:
  HWPmp = OFF
  If (Occupancy = ON) then Goto CNTRL
 EndCode
EndObject

Object : AHFan.Pr
 Type : Program
 LastChange : 7-29-1997 11:20:59 AM
 Description : Supply Fan Control
 State : Enabled
 Status : Active
 AutoStart : True
 FlowType : Looping
 Debug : Disabled
 ExecTimeOut : 0
 CommandLine : False
 ShareFlag : False
 Code :

CNTRL:
  If (Occupancy = OFF) then Goto OFF_LINE
  AHFan = ON

OFF_LINE:
  AHFan = OFF
```

```
  If (Occupancy = ON) then Goto CNTRL
 EndCode
EndObject

Object : AHMisc.Pr
 Type : Program
 LastChange : 7-29-1997 11:21:01 AM
 Description : AH Miscellaneous Setup
 State : Enabled
 Status : Active
 AutoStart : True
 FlowType : Looping
 Debug : Disabled
 ExecTimeOut : 0
 CommandLine : False
 ShareFlag : False
 Code :

CALCULATE:
  Goto CALCULATE
'  SupAirFlow = Filter.Fn((SupAir_Ve * 90), SupAirFlow, 4)
 EndCode
EndObject

Object : FloorHWVlv.Pr
 Type : Program
 LastChange : 7-29-1997 11:21:02 AM
 Description : Floor HW Valve Control
 State : Enabled
 Status : Active
 AutoStart : True
 FlowType : Looping
 Debug : Disabled
 ExecTimeOut : 0
 CommandLine : False
 ShareFlag : False
 Code :

Numeric Fdbk
Numeric Rntm
Numeric Sync
Numeric LastHour
DateTime Timer

CNTRL:
  If (Occupancy = OFF) then Goto OFF_LINE
  If (LastHour <> Hour) then
    Sync = ON
    LastHour = Hour
  Endif
  Rntm = 180
```

```
  FloorHWPID[1] = 0.035
  FloorHWPID[2] = 0.0005
  FloorHWPID[3] = 0.01
  FloorHWVlvPct = PID.Fn(FloorHW_Te, Floor_Se, FloorHWPID[1], FloorHWPID[2],
                         FloorHWPID[3], 0, 0, FloorHWPID[4], FloorHWPID[5])
  FloorHWVlvOpen = Pulse.Fn(FloorHWVlvPct, Rntm, Fdbk, Timer, Sync,
                            FloorHWVlvOpen, FloorHWVlvClose)

OFF_LINE:
  Fdbk = 0
  FloorHWVlvPct = 0
  FloorHWVlvOpen = OFF
  FloorHWPID[4] = 0
  FloorHWPID[5] = 0
  FloorHWVlvClose = Rntm
  If ((Occupancy = ON) & (TS > Rntm)) then Goto CNTRL
 EndCode
EndObject

Object : WallHWVlv.Pr
 Type : Program
 LastChange : 7-29-1997 11:21:04 AM
 Description : Wall HW Valve Control
 State : Enabled
 Status : Active
 AutoStart : True
 FlowType : Looping
 Debug : Disabled
 ExecTimeOut : 0
 CommandLine : False
 ShareFlag : False
 Code :

Numeric Fdbk
Numeric Rntm
Numeric Sync
Numeric LastHour
DateTime Timer

CNTRL:
  If (Occupancy = OFF) then Goto OFF_LINE
  If (LastHour <> Hour) then
    Sync = ON
    LastHour = Hour
  Endif
  Rntm = 180
  WallHWPID[1] = 0.018
  WallHWPID[2] = 0.00015
  WallHWPID[3] = 0.1
  WallHWVlvPct = PID.Fn(WallHW_Te, Wall_Se, WallHWPID[1], WallHWPID[2],
                        WallHWPID[3], 0, 0, WallHWPID[4], WallHWPID[5])
```

```
  WallHWVlvOpen = Pulse.Fn(WallHWVlvPct, Rntm, Fdbk, Timer, Sync, WallHWVlvOpen,
                           WallHWVlvClose)

OFF_LINE:
  Fdbk = 0
  WallHWVlvPct = 0
  WallHWVlvOpen = OFF
  WallHWPID[4] = 0
  WallHWPID[5] = 0
  WallHWVlvClose = Rntm
  If ((Occupancy = ON) & (TS > Rntm)) then Goto CNTRL
 EndCode
EndObject
-------------------------------------------------------------------------------



-------------------------------------------------------------------------------
Device Controller:  M01_CondoLab
-------------------------------------------------------------------------------
CONDOLAB PROGRAMS:

 Program          : SupAirDmp1.Pr    : 0
 Program          : SupAirDmp2.Pr    : 0
 Program          : SupAirDmp3.Pr    : 0
 Program          : ExhAirDmp.Pr     : 0
 Program          : ElecReHt1.Pr     : 0
 Program          : ElecReHt2.Pr     : 0
 Program          : ElecReHt3.Pr     : 0
 Program          : setpoints.pr     : 0
 Program          : RoomMisc.Pr      : 0

Object : SupAirDmp1.Pr
 Type : Program
 LastChange : 7-29-1997 11:23:30 AM
 Description : Supply Air Damper Control
 State : Enabled
 Status : Active
 AutoStart : True
 FlowType : Looping
 Debug : Enabled
 ExecTimeOut : 0
 CommandLine : True
 ShareFlag : False
 Code :
Numeric TotalFlow1

CNTRL:
  If (Occupancy = OFF) then Goto OFF_LINE
  SupAirFlowPID[1] = 0.03
  SupAirFlowPID[2] = 3.5e-005
```

```
  SupAirFlowPID[3] = 0.0001

  SupAirDmp1 = PID.Fn(InFlow1,SupAirFlow1_Se,SupAirFlowPID[1],SupAirFlowPID[2],
                      SupAirFlowPID[3],0,0,SupAirFlowPID[4],SupAirFlowPID[5])

OFF_LINE:
  SupAirDmp1 = 0
  SupAirFlowPID[4] = 0
  SupAirFlowPID[5] = 0
  If (Occupancy = ON) then Goto CNTRL
 EndCode
EndObject

Object : SupAirDmp2.Pr
 Type : Program
 LastChange : 7-29-1997 11:23:42 AM
 Description : Supply Air Damper Control
 State : Enabled
 Status : Active
 AutoStart : True
 FlowType : Looping
 Debug : Enabled
 ExecTimeOut : 0
 CommandLine : True
 ShareFlag : False
 Code :

CNTRL:
  If (Occupancy = OFF) then Goto OFF_LINE
  SupAirFlowPID[1] = 0.01
  SupAirFlowPID[2] = 3.5e-005
  SupAirFlowPID[3] = 0.0001
  SupAirDmp2 = PID.Fn(InFlow2,SupAirFlow2_Se,SupAirFlowPID[1],SupAirFlowPID[2],
                      SupAirFlowPID[3],0,0,SupAirFlowPID[6],SupAirFlowPID[7])

OFF_LINE:
  SupAirDmp2 = 0
  SupAirFlowPID[6] = 0
  SupAirFlowPID[7] = 0
  If (Occupancy = ON) then Goto CNTRL
 EndCode
EndObject

Object : SupAirDmp3.Pr
 Type : Program
 LastChange : 7-29-1997 11:23:43 AM
 Description : Supply Air Damper Control
 State : Enabled
 Status : Active
 AutoStart : True
 FlowType : Looping
```

```
 Debug : Enabled
 ExecTimeOut : 0
 CommandLine : True
 ShareFlag : False
 Code :

CNTRL:
  If (Occupancy = OFF) then Goto OFF_LINE
  SupAirFlowPID[1] = 0.003
  SupAirFlowPID[2] = 3.5e-005
  SupAirFlowPID[3] = 0.0005

  SupAirDmp3 = PID.Fn(InFlow3,SupAirFlow3_Se,SupAirFlowPID[1],SupAirFlowPID[2],
                      SupAirFlowPID[3],0,0,SupAirFlowPID[8],SupAirFlowPID[9])

OFF_LINE:
  SupAirDmp3 = 0
  SupAirFlowPID[8] = 0
  SupAirFlowPID[9] = 0
  If (Occupancy = ON) then Goto CNTRL
 EndCode
EndObject

Object : ExhAirDmp.Pr
 Type : Program
 LastChange : 7-29-1997 11:23:44 AM
 Description : Exhaust Air Damper Control
 State : Enabled
 Status : Active
 AutoStart : True
 FlowType : Looping
 Debug : Enabled
 ExecTimeOut : 0
 CommandLine : True
 ShareFlag : False
 Code :

CNTRL:
  If (Occupancy = OFF) then Goto OFF_LINE
  ExhAirFlowPID[1] = 0.001042
  ExhAirFlowPID[2] = 3.5e-005
  ExhAirFlowPID[3] = 0.001953

  ExhAirDmp = PID.Fn(ExhAirFlow,ExhAirFlow_Se,ExhAirFlowPID[1],ExhAirFlowPID[2],
                     ExhAirFlowPID[3],0,0,ExhAirFlowPID[4],ExhAirFlowPID[5])

OFF_LINE:
  ExhAirDmp = 0
  ExhAirFlowPID[4] = 0
  ExhAirFlowPID[5] = 0
  If (Occupancy = ON) then Goto CNTRL
```

```
 EndCode
EndObject

Object : ElecReHt1.Pr
 Type : Program
 LastChange : 7-29-1997 11:23:46 AM
 Description : Electric Reheat Control
 State : Enabled
 Status : Active
 AutoStart : True
 FlowType : Looping
 Debug : Enabled
 ExecTimeOut : 0
 CommandLine : True
 ShareFlag : False
 Code :

CNTRL:
  If (Occupancy = OFF) then Goto OFF_LINE
  SupAirTePID[1] = 0.08
  SupAirTePID[2] = 0.002
  SupAirTePID[3] = 0.8
  ElecReHt1 = PID.Fn(SupAir1_Te, SupAir1Te_Se, SupAirTePID[1], SupAirTePID[2],
                     SupAirTePID[3], 0.5, 0, SupAirTePID[4], SupAirTePID[5])

OFF_LINE:
  ElecReHt1 = 0
  SupAirTePID[4] = 0
  SupAirTePID[5] = 0
  If (Occupancy = ON) then Goto CNTRL
 EndCode
EndObject

Object : ElecReHt2.Pr
 Type : Program
 LastChange : 7-29-1997 11:23:47 AM
 Description : Electric Reheat Control
 State : Enabled
 Status : Active
 AutoStart : True
 FlowType : Looping
 Debug : Enabled
 ExecTimeOut : 0
 CommandLine : True
 ShareFlag : False
 Code :

CNTRL:
  If (Occupancy = OFF) then Goto OFF_LINE
  SupAirTePID[1] = 0.1
  SupAirTePID[2] = 0.002
```

```
  SupAirTePID[3] = 1
  ElecReHt2 = PID.Fn(SupAir2_Te, SupAir2Te_Se, SupAirTePID[1], SupAirTePID[2],
              SupAirTePID[3], 0.5, 0, SupAirTePID[6], SupAirTePID[7])

OFF_LINE:
  ElecReHt2 = 0
  SupAirTePID[6] = 0
  SupAirTePID[7] = 0
  If (Occupancy = ON) then Goto CNTRL
 EndCode
EndObject

Object : ElecReHt3.Pr
 Type : Program
 LastChange : 7-29-1997 11:23:48 AM
 Description : Electric Reheat Control
 State : Enabled
 Status : Active
 AutoStart : True
 FlowType : Looping
 Debug : Enabled
 ExecTimeOut : 0
 CommandLine : True
 ShareFlag : False
 Code :

CNTRL:
  If (Occupancy = OFF) then Goto OFF_LINE
  SupAirTePID[1] = 0.1
  SupAirTePID[2] = 0.002
  SupAirTePID[3] = 1
  ElecReHt3 = PID.Fn(SupAir3_Te, SupAir3Te_Se, SupAirTePID[1], SupAirTePID[2],
              SupAirTePID[3], 0.5, 0, SupAirTePID[8], SupAirTePID[9])

OFF_LINE:
  ElecReHt3 = 0
  SupAirTePID[8] = 0
  SupAirTePID[9] = 0
  If (Occupancy = ON) then Goto CNTRL
 EndCode
EndObject

Object : setpoints.pr
 Type : Program
 LastChange : 7-29-1997 11:23:49 AM
 Description : change setpoints of each supply
 State : Enabled
 Status : Active
 AutoStart : True
 FlowType : Looping
 Debug : Disabled
```

```
 ExecTimeOut : 0
 CommandLine : True
 ShareFlag : False
 Code :
Numeric BaseTe
Numeric DeltaTe
Numeric BaseFlow
Numeric DeltaFlow

COMPUTER_CONTROL:
  If (M01_CondoFan PA0 < 0.5) then Goto NO_SETPT
  BaseTe = 41
  DeltaTe = 60
  BaseFlow = 0
  DeltaFlow = 150
  SupAir1Te_Se = BaseTe + DeltaTe * M01_CondoFan analog1
  SupAir3Te_Se = BaseTe + DeltaTe * M01_CondoFan analog1
  SupAir2Te_Se = BaseTe + DeltaTe * M01_CondoFan analog1
'  SupAirFlow2_Se = BaseFlow + DeltaFlow * M01_CondoFan analog2

NO_SETPT:
  If (M01_CondoFan PA0 > 0.5) then Goto COMPUTER_CONTROL
 EndCode
EndObject

Object : RoomMisc.Pr
 Type : Program
 LastChange : 7-29-1997 11:23:51 AM
 Description : Room Miscellaneous Setup
 State : Enabled
 Status : Active
 AutoStart : True
 FlowType : Looping
 Debug : Disabled
 ExecTimeOut : 0
 CommandLine : False
 ShareFlag : False
 Code :

Numeric VAVCalibrator1
Numeric VAVCalibrator2
Numeric VAVCalibrator3
Numeric VAVCalibrator4
Numeric TotalFlow1
Numeric TotalFlow2
Numeric TotalFlow3

CALCULATE:
  VAVCalibrator1 = 1
  VAVCalibrator2 = 1
  VAVCalibrator3 = 1
```

```
  VAVCalibrator4 = 1
  TotalFlow1 = 170
  TotalFlow2 = 190
  TotalFlow3 = 170
  ExhAirFlow = Filter.Fn((sqrt(ExhAir_VP) * 700 * VAVCalibrator4),
                         ExhAirFlow, 4)
  SupAirFlow1 = Filter.Fn((sqrt(SupAir1_VP) * 700 * VAVCalibrator1),
                          SupAirFlow1, 4)
  SupAirFlow2 = Filter.Fn((sqrt(SupAir2_VP) * 700 * VAVCalibrator2),
                          SupAirFlow2, 4)
  SupAirFlow3 = Filter.Fn((sqrt(SupAir3_VP) * 700 * VAVCalibrator3),
                          SupAirFlow3, 4)
  InFlow1 = TotalFlow1 - SupAirFlow1
  InFlow2 = TotalFlow2 - SupAirFlow2
  InFlow3 = TotalFlow3 - SupAirFlow3

 EndCode
EndObject
-------------------------------------------------------------------------------



-------------------------------------------------------------------------------
Device Controller:  M01_CondoDisplay
-------------------------------------------------------------------------------
CONDODISPLAY PROGRAMS:

 Program          : Floorplan.Pr     : 0
 Program          : Backlight.Pr     : 0
 Program          : MainMenu.Pr      : 0
 Program          : Security.Pr      : 0
 Program          : Setpoints.Pr     : 0
 Program          : SetSup1.pr       : 0
 Program          : setsup2.pr       : 0
 Program          : setsup3.pr       : 0
 Program          : SetFloor.Pr      : 0
 Program          : SetWall.Pr       : 0
 Program          : RoomStatus.Pr    : 0

Object : Floorplan.Pr
 Type : Program
 LastChange : 7-29-1997 11:18:00 AM
 Description : Floorplan Drawing Control
 State : Enabled
 Status : Active
 AutoStart : True
 FlowType : Looping
 Debug : Disabled
 ExecTimeOut : 0
 CommandLine : True
 ShareFlag : False
```

```
 Code :
DRAWSTRUCTURE:
  ClearScreen
  Stop MainMenu.Pr
  Stop Security.Pr
  Stop Setpoints.Pr
  Locate 50, 190
  Print "ROOM STRUCTURE OF THE TEST-BED"

' make the drawing and labels
  drawroom.fn
  Locate 118, 52
  Print "SUPPLY#1"
  Locate 3, 127
  Print "SUPPLY#3"
  Locate 118, 127
  Print "SUPPLY#2"
  Locate 90, 80
  Print "RADIANT    FLOOR"
  Locate 190, 163
  Print "DOOR"
  Locate 80, 163
  Print "WINDOW"
  Locate 60, 40
  Print "RADIANT"
  Locate 170, 40
  Print "WALL#1"
  Locate 242, 110
  Print "RW#2"
  control 1, 250, 1, 319, 31, True, MainMenu.Pr Status, "MENU", , 0, 1
  Goto UP_DATE

UP_DATE:
'  SetDisplay Blue, Nofill
  Locate 20, 10
  Print Wkd, Time
  Goto WAIT

WAIT:
  If (TS > 0) then Goto UP_DATE

 EndCode
EndObject

Object : Backlight.Pr
 Type : Program
 LastChange : 7-29-1997 11:18:02 AM
 Description : Backlight Control
 State : Enabled
 Status : Active
 AutoStart : True
```

```
 FlowType : Looping
 Debug : Disabled
 ExecTimeOut : 0
 CommandLine : True
 ShareFlag : False
 Code :

CHECK:
  If (Touchedcell) then Goto TURN_ON

TURN_ON:
  Start MainMenu.Pr
  Backlight = 300
  Goto WAIT

WAIT:
  If (Touchedcell) then Backlight = 300
  If (Backlight = 0) then Goto TURN_OFF

TURN_OFF:
  ClearScreen
  Stop Floorplan.Pr
  Stop MainMenu.Pr
  Stop Security.Pr
  Stop Setpoints.Pr
  Goto CHECK
 EndCode
EndObject

Object : MainMenu.Pr
 Type : Program
 LastChange : 7-29-1997 11:18:03 AM
 Description : Main Menu Control
 State : Enabled
 Status : Active
 AutoStart : True
 FlowType : Looping
 Debug : Disabled
 ExecTimeOut : 0
 CommandLine : True
 ShareFlag : False
 Code :

SETUP:
  ClearScreen
  Stop Floorplan.Pr
  Stop Security.Pr
  Stop Setpoints.Pr
  Stop RoomStatus.Pr
  Stop SetSup1.pr
  Stop setsup2.pr
```

```
  Stop setsup3.pr
  Stop SetFloor.Pr
  Stop SetWall.Pr
  SetDisplay Fill, White
  DrawRectangle 1, 1, 320, 200
  SetDisplay Nofill, blue
  DrawRectangle 3, 3, 318, 198
  Frame.Fn(5, 5, 316, 196, "HVAC TEST-BED MAIN MENU", blue)
  SetDisplay Nofill, blue
  control 1, 80, 125, 240, 160, True, Floorplan.Pr Status, "ROOM STRUCTURE", ,
          0, 1
  control 1, 80, 75, 240, 110, True, RoomStatus.Pr Status, "CURRENT STATUS", ,
          0, 1
  control 1, 80, 25, 240, 60, True, Security.Pr Status, "CHANGE SETPOINTS", ,
          0, 1
'  control 1, 15, 75, 105, 110, True, DSP.SECURITY Status, "4", , 0, 1
'  control 1, 115, 75, 205, 110, True, DSP.SECURITY Status, "5", , 0, 1
'  control 1, 215, 75, 305, 110, True, DSP.SECURITY Status, "6", , 0, 1
'  control 1, 15, 25, 105, 60, True, DSP.SECURITY Status, "7", , 0, 1
'  control 1, 115, 25, 205, 60, True, DSP.SECURITY Status, "8", , 0, 1
'  control 1, 215, 25, 305, 60, True, DSP.SECURITY Status, "9", , 0, 1
  Locate 27, 10
  Print "Touch a Button to View your Selection"
  Goto UP_DATE

UP_DATE:
  SetDisplay blue, Nofill
  Locate 55, 169
  Print Wkd, Time
  Goto WAIT

WAIT:
  If (TS > 0) then Goto UP_DATE
 EndCode
EndObject

Object : Security.Pr
 Type : Program
 LastChange : 7-29-1997 11:18:06 AM
 Description : User Security Control
 State : Enabled
 Status : Active
 AutoStart : True
 FlowType : Looping
 Debug : Disabled
 ExecTimeOut : 0
 CommandLine : True
 ShareFlag : False
 Code :

Numeric PASSWORD
```

```
Numeric A
Numeric B
Numeric C
Numeric Try

SETUP:
  Stop Floorplan.Pr
  Stop MainMenu.Pr
  Stop Setpoints.Pr
  ClearScreen
  PASSWORD = 117
  Try = 0
  A, B and C = -1
  SetDisplay Fill, White
  DrawRectangle 1, 1, 320, 200
  SetDisplay Nofill, blue
  DrawRectangle 7, 5, 313, 195
  Locate 50, 180
  Print "Please Enter Your Security Code"
  Locate 110, 165
  Print "And Press OK"
  Button.Fn(40, 125, 80, 150, Nofill)
  Button.Fn(40, 100, 80, 125, Nofill)
  Button.Fn(40, 75, 80, 100, Nofill)
  Button.Fn(80, 125, 120, 150, Nofill)
  Button.Fn(80, 100, 120, 125, Nofill)
  Button.Fn(80, 75, 120, 100, Nofill)
  Button.Fn(120, 125, 160, 150, Nofill)
  Button.Fn(120, 100, 160, 125, Nofill)
  Button.Fn(120, 75, 160, 100, Nofill)
  Button.Fn(80, 50, 120, 75, Nofill)
  Button.Fn(200, 110, 280, 150, Nofill)
  control 1, 200, 50, 280, 75, True, MainMenu.Pr Status, "MENU", , 0, 1
  DrawRectangle 40, 15, 280, 40
  Locate 57, 135
  Print "1"
  Locate 57, 110
  Print "4"
  Locate 57, 85
  Print "7"
  Locate 97, 135
  Print "2"
  Locate 97, 110
  Print "5"
  Locate 97, 85
  Print "8"
  Locate 137, 135
  Print "3"
  Locate 137, 110
  Print "6"
  Locate 137, 85
```

```
  Print "9"
  Locate 97, 60
  Print "0"
  Locate 232, 125
  Print "OK"
  Goto CHECK

CHECK:
  If (Touchedcell is 18) then
    If (C = -1) then
      C = 1
      Goto UP_DATE
    Endif
    If (B = -1) then
      B = C
      C = 1
      Goto UP_DATE
    Endif
    If (A = -1) then
      A = B
      B = C
      C = 1
      Goto UP_DATE
    Endif
  Endif
  If (Touchedcell is 19) then
    If (C = -1) then
      C = 2
      Goto UP_DATE
    Endif
    If (B = -1) then
      B = C
      C = 2
      Goto UP_DATE
    Endif
    If (A = -1) then
      A = B
      B = C
      C = 2
      Goto UP_DATE
    Endif
  Endif
  If (Touchedcell is 20) then
    If (C = -1) then
      C = 3
      Goto UP_DATE
    Endif
    If (B = -1) then
      B = C
      C = 3
      Goto UP_DATE
```

```
  Endif
  If (A = -1) then
    A = B
    B = C
    C = 3
    Goto UP_DATE
  Endif
Endif
If (Touchedcell is 26) then
  If (C = -1) then
    C = 4
    Goto UP_DATE
  Endif
  If (B = -1) then
    B = C
    C = 4
    Goto UP_DATE
  Endif
  If (A = -1) then
    A = B
    B = C
    C = 4
    Goto UP_DATE
  Endif
Endif
If (Touchedcell is 27) then
  If (C = -1) then
    C = 5
    Goto UP_DATE
  Endif
  If (B = -1) then
    B = C
    C = 5
    Goto UP_DATE
  Endif
  If (A = -1) then
    A = B
    B = C
    C = 5
    Goto UP_DATE
  Endif
Endif
If (Touchedcell is 28) then
  If (C = -1) then
    C = 6
    Goto UP_DATE
  Endif
  If (B = -1) then
    B = C
    C = 6
    Goto UP_DATE
```

```
  Endif
  If (A = -1) then
    A = B
    B = C
    C = 6
    Goto UP_DATE
  Endif
Endif
If (Touchedcell is 34) then
  If (C = -1) then
    C = 7
    Goto UP_DATE
  Endif
  If (B = -1) then
    B = C
    C = 7
    Goto UP_DATE
  Endif
  If (A = -1) then
    A = B
    B = C
    C = 7
    Goto UP_DATE
  Endif
Endif
If (Touchedcell is 35) then
  If (C = -1) then
    C = 8
    Goto UP_DATE
  Endif
  If (B = -1) then
    B = C
    C = 8
    Goto UP_DATE
  Endif
  If (A = -1) then
    A = B
    B = C
    C = 8
    Goto UP_DATE
  Endif
Endif
If (Touchedcell is 36) then
  If (C = -1) then
    C = 9
    Goto UP_DATE
  Endif
  If (B = -1) then
    B = C
    C = 9
    Goto UP_DATE
```

```
    Endif
    If (A = -1) then
      A = B
      B = C
      C = 9
      Goto UP_DATE
    Endif
  Endif
  If (Touchedcell is 43) then
    If (C = -1) then
      C = 0
      Goto UP_DATE
    Endif
    If (B = -1) then
      B = C
      C = 0
      Goto UP_DATE
    Endif
    If (A = -1) then
      A = B
      B = C
      C = 0
      Goto UP_DATE
    Endif
  Endif
  If (Touchedcell is either 22, 23, 30 or 31) then
    Try = (A * 100 + B * 10 + C)
    If Try = PASSWORD then
      Locate 80, 25
      Print "Logon Attempt Successful"
      Goto WAIT
    Else
      Locate 80, 25
      Print "Invalid Code. Try Again"
      Try = 0
      A, B and C = -1
      Goto RESET
    Endif
  Endif
  If (TS > 10) then
    Try = 0
    A, B and C = -1
    Goto RESET
  Endif

UP_DATE:
  Locate 80, 25
  If (C = -1) then
    Print "                          "
    Goto CHECK
  Endif
```

```
  If (B = -1) then
    Print "       #                "
    Goto CHECK
  Endif
  If (A = -1) then
    Print "       #   #            "
    Goto CHECK
  Endif
  Print "       #   #   #        "
  Goto CHECK

WAIT:
  If (TS > 1) then
    Start Setpoints.Pr
    Stop
  Endif

RESET:
  If (TS > 1) then
    Locate 80, 25
    Print "                              "
    Goto CHECK
  Endif
 EndCode
EndObject

Object : Setpoints.Pr
 Type : Program
 LastChange : 7-29-1997 11:18:09 AM
 Description : Setpoint Control
 State : Enabled
 Status : Active
 AutoStart : True
 FlowType : Looping
 Debug : Disabled
 ExecTimeOut : 0
 CommandLine : True
 ShareFlag : False
 Code :

SETUP:
  ClearScreen
  Stop Floorplan.Pr
  Stop MainMenu.Pr
  Stop Security.Pr
  Stop SetSup1.pr
  Stop setsup2.pr
  Stop setsup3.pr
  Stop SetFloor.Pr
  Stop SetWall.Pr
  SetDisplay Fill, White
```

```
  DrawRectangle 1, 1, 320, 200
  SetDisplay Nofill, blue
  DrawRectangle 2, 2, 319, 199
  Frame.Fn(4, 4, 317, 197, "CONDO PROJECT SETPOINTS", blue)
  SetDisplay blue 'Nofill
  control 1, 40, 130, 100, 160, True, SetSup1.pr Status, "Sup#1", , 0, 1
  control 1, 130, 130, 190, 160, True, setsup2.pr Status, "Sup#2", , 0, 1
  control 1, 220, 130, 280, 160, True, setsup3.pr Status, "Sup#3", , 0, 1
  control 1, 40, 75, 140, 105, True, SetFloor.Pr Status, "Radiant Floor", , 0, 1
  control 1, 180, 75, 280, 105, True, SetWall.Pr Status, "Radiant Wall", , 0, 1
  control 1, 120, 10, 200, 40, True, MainMenu.Pr Status, "MENU", , 0, 1
  Goto UP_DATE

UP_DATE:
  Locate 80, 50
  Print "Select a Device to Change"
  Goto WAIT

WAIT:
  If (TS > 0) then Goto UP_DATE
 EndCode
EndObject

Object : SetSup1.pr
 Type : Program
 LastChange : 7-29-1997 11:18:11 AM
 Description : Change the setpoint of supply#1
 State : Enabled
 Status : Active
 AutoStart : True
 FlowType : Looping
 Debug : Disabled
 ExecTimeOut : 0
 CommandLine : True
 ShareFlag : False
 Code :
'SetSup1.Pr

SETUP:
  ClearScreen
  Stop Setpoints.Pr
  SetDisplay Fill, White
  DrawRectangle 1, 1, 320, 200
  SetDisplay Nofill, blue
  DrawRectangle 2, 2, 319, 199
  Frame.Fn(4, 4, 317, 197, "AIR SUPPLY #1 SETPOINTS", blue)
  SetDisplay blue 'Nofill
  control 9, 20, 75, 140, 170, True, M01_CondoLab SupAir1Te_Se, "SupTemp", 4, ,
          55, 105, , 50
  control 9, 180, 75, 300, 170, True, M01_CondoLab SupAirFlow1_Se, "AirFlow", 4,
          , 0, 180, , 18
```

```
  control 1, 40, 5, 120, 35, True, Setpoints.Pr Status, "BACK", , 0, 1
  control 1, 200, 5, 280, 35, True, MainMenu.Pr Status, "EXIT", , 0, 1
  Goto UP_DATE

UP_DATE:
  Locate 20, 60
  Print "Current: |###.# F", M01_CondoLab SupAir1_Te
  Locate 180, 60
  Print "Current: |### CFM", M01_CondoLab InFlow1
  Goto WAIT

WAIT:
  If (TS > 0) then Goto UP_DATE

 EndCode
EndObject

Object : setsup2.pr
 Type : Program
 LastChange : 7-29-1997 11:18:14 AM
 Description : Change the setpoint of supply#2
 State : Enabled
 Status : Active
 AutoStart : True
 FlowType : Looping
 Debug : Disabled
 ExecTimeOut : 0
 CommandLine : True
 ShareFlag : False
 Code :
'SetSup2.Pr

SETUP:
  ClearScreen
  Stop Setpoints.Pr
  SetDisplay Fill, White
  DrawRectangle 1, 1, 320, 200
  SetDisplay Nofill, blue
  DrawRectangle 2, 2, 319, 199
  Frame.Fn(4, 4, 317, 197, "AIR SUPPLY #2 SETPOINTS", blue)
  SetDisplay blue 'Nofill
  control 9, 20, 75, 140, 170, True, M01_CondoLab SupAir2Te_Se, "SupTemp", 4, ,
          55, 105, , 50
  control 9, 180, 75, 300, 170, True, M01_CondoLab SupAirFlow2_Se, "AirFlow", 4,
          , 0, 180, , 18
  control 1, 40, 5, 120, 35, True, Setpoints.Pr Status, "BACK", , 0, 1
  control 1, 200, 5, 280, 35, True, MainMenu.Pr Status, "EXIT", , 0, 1
  Goto UP_DATE

UP_DATE:
  Locate 20, 60
```

```
  Print "Current: |###.# F", M01_CondoLab SupAir2_Te
  Locate 180, 60
  Print "Current: |### CFM", M01_CondoLab InFlow2
  Goto WAIT

WAIT:
  If (TS > 0) then Goto UP_DATE

 EndCode
EndObject

Object : setsup3.pr
 Type : Program
 LastChange : 7-29-1997 11:18:17 AM
 Description : Change the setpoint of supply#3
 State : Enabled
 Status : Active
 AutoStart : True
 FlowType : Looping
 Debug : Disabled
 ExecTimeOut : 0
 CommandLine : True
 ShareFlag : False
 Code :
'SetSup3.Pr

SETUP:
  ClearScreen
  Stop Setpoints.Pr
  SetDisplay Fill, White
  DrawRectangle 1, 1, 320, 200
  SetDisplay Nofill, blue
  DrawRectangle 2, 2, 319, 199
  Frame.Fn(4, 4, 317, 197, "AIR SUPPLY #3 SETPOINTS", blue)
  SetDisplay blue 'Nofill
  control 9, 20, 75, 140, 170, True, M01_CondoLab SupAir3Te_Se, "SupTemp", 4, ,
          55, 105, , 50
  control 9, 180, 75, 300, 170, True, M01_CondoLab SupAirFlow3_Se, "AirFlow", 4,
          , 0, 180, , 18
  control 1, 40, 5, 120, 35, True, Setpoints.Pr Status, "BACK", , 0, 1
  control 1, 200, 5, 280, 35, True, MainMenu.Pr Status, "EXIT", , 0, 1
  Goto UP_DATE

UP_DATE:
  Locate 20, 60
  Print "Current: |###.# F", M01_CondoLab SupAir3_Te
  Locate 180, 60
  Print "Current: |### CFM", M01_CondoLab InFlow3
  Goto WAIT

WAIT:
```

```
  If (TS > 0) then Goto UP_DATE

 EndCode
EndObject

Object : SetFloor.Pr
 Type : Program
 LastChange : 7-29-1997 11:18:19 AM
 Description : Change setpoint of radiant floor
 State : Enabled
 Status : Active
 AutoStart : True
 FlowType : Looping
 Debug : Disabled
 ExecTimeOut : 0
 CommandLine : True
 ShareFlag : False
 Code :
'SetFloor.Pr

SETUP:
  ClearScreen
  Stop Setpoints.Pr
  SetDisplay Fill, White
  DrawRectangle 1, 1, 320, 200
  SetDisplay Nofill, blue
  DrawRectangle 2, 2, 319, 199
  Frame.Fn(4, 4, 317, 197, "RADIANT FLOOR SETPOINTS", blue)
  SetDisplay blue 'Nofill
  control 9, 80, 70, 240, 170, True, M01_CondoFan Floor_Se, "FloorTemp", 4, ,
          55, 105, , 50
  control 1, 40, 5, 120, 35, True, Setpoints.Pr Status, "BACK", , 0, 1
  control 1, 200, 5, 280, 35, True, MainMenu.Pr Status, "EXIT", , 0, 1
  Goto UP_DATE

UP_DATE:
  Locate 80, 60
  Print "CURRENT TEMP: |###.# F", M01_CondoFan Floor_Te
  Goto WAIT

WAIT:
  If (TS > 0) then Goto UP_DATE

 EndCode
EndObject

Object : SetWall.Pr
 Type : Program
 LastChange : 7-29-1997 11:18:21 AM
 Description : Change setpoint of radiant wall
 State : Enabled
```

```
 Status : Active
 AutoStart : True
 FlowType : Looping
 Debug : Disabled
 ExecTimeOut : 0
 CommandLine : True
 ShareFlag : False
 Code :
'SetWall.Pr

SETUP:
  ClearScreen
  Stop Setpoints.Pr
  SetDisplay Fill, White
  DrawRectangle 1, 1, 320, 200
  SetDisplay Nofill, blue
  DrawRectangle 2, 2, 319, 199
  Frame.Fn(4, 4, 317, 197, "RADIANT WALL SETPOINTS", blue)
  SetDisplay blue 'Nofill
  control 9, 80, 70, 240, 170, True, M01_CondoFan Wall_Se, "RW_Temp", 4, , 55,
          105, , 50
  control 1, 40, 5, 120, 35, True, Setpoints.Pr Status, "BACK", , 0, 1
  control 1, 200, 5, 280, 35, True, MainMenu.Pr Status, "EXIT", , 0, 1
  Goto UP_DATE

UP_DATE:
  Locate 80, 60
  Print "CURRENT TEMP: !###.# F", M01_CondoFan Wall_Te
  Goto WAIT

WAIT:
  If (TS > 0) then Goto UP_DATE

 EndCode
EndObject

Object : RoomStatus.Pr
 Type : Program
 LastChange : 7-29-1997 11:18:23 AM
 Description : Show current room status
 State : Enabled
 Status : Active
 AutoStart : True
 FlowType : Looping
 Debug : Disabled
 ExecTimeOut : 0
 CommandLine : True
 ShareFlag : False
 Code :
DRAWSTRUCTURE:
  ClearScreen
```

```
  Stop MainMenu.Pr
  Stop Security.Pr
  Stop Setpoints.Pr

  Locate 50, 190
  Print "CURRENT STATUS OF THE TEST-BED"

' make the drawing and labels
  drawroom.fn
  control 1, 250, 1, 319, 31, True, MainMenu.Pr Status, "MENU", , 0, 1
  Goto UP_DATE

UP_DATE:
'  SetDisplay Blue, Nofill
  Locate 110, 52
  Print "TO_1=|### F", M01_CondoLab SupAir1_Te
  Locate 110, 15
  Print "FO_1=|### CFM", M01_CondoLab InFlow1
  Locate 110, 127
  Print "TO_2=|### F", M01_CondoLab SupAir2_Te
  Locate 110, 90
  Print "FO_2=|### CFM", M01_CondoLab InFlow2
  Locate 1, 127
  Print "TO_3=|### F", M01_CondoLab SupAir3_Te
  Locate 1, 90
  Print "FO_3=|### CFM", M01_CondoLab InFlow3
  Locate 90, 160
  Print "T_room=|### F", M01_CondoFan Room_Te
  Locate 90, 150
  Print "T_floor=|### F", M01_CondoFan Floor_Te
  Locate 165, 40
  Print "T_RW1=|### F", M01_CondoFan Wall_Te
  Locate 241, 115
  Print "T_RW2=|### F", M01_CondoFan Wall_Te
  Goto WAIT

WAIT:
  If (TS > 0) then Goto UP_DATE

 EndCode
EndObject
-------------------------------------------------------------------------
```

Appendix B

Notation

α	thermal expansion coefficient, $[1/K]$
β	jet spreading coefficient
ϵ	emissivity
κ	the coefficient of body conductance at thermal neutrality
κ_0, κ_1	parameters of the convective heat transfer coefficient
Ω_f	finger blood flow rate, in sensor unit
Ω_f^*	finger blood flow rate at thermal neutrality, in sensor unit
Ω_p	total peripheral blood flow rate, $[liter/hr]$
Ω_p^*	total peripheral blood flow rate at thermal neutrality, $[liter/hr]$
$\bar{\Omega}_p$	peripheral blood flow rate per unit skin surface area, $[liter/(hr\ m^2)]$
ω	frequency, $[rad/s]$
ρ	density, $[kg/m^3]$
Σ_{warm}	physiological warmth signal
Σ_{cold}	physiological cold signal
σ	Stefan-Boltzmann constant: $5.67 \cdot 10^{-8}\ W/m^2K^4$.
τ	time constant of a first order system. $[s]$
τ_d	pure time delay, $[s]$
τ_{exp}	time constant estimated from experimental data, $[s]$
τ_{model}	time constant calculated from the model, $[s]$
θ_0	initial jet angle, $[rad]$
ζ	damping coefficient
A_0	area of the jet opening, $[m^2]$
A_B	cross section area of the buffer zone, $[m^2]$
A_{Du}	DuBois area (surface area of nude body), $[m^2]$
A_j	cross section area of the jet, $[m^2]$

Ar	Archimedes number, Equation (5.6)
C	thermal mass, $[J/K]$
c_p	specific heat, $[J/(kgK)]$
D_c	minimal distance below which a jet will attach to the surface, $[m]$
$E(\omega)$	the multiplicative bound of the modeling error
E_d	the heat loss due to vapor diffusion through skin, $[W]$
E_{res}	total respiration heat loss, $[W]$
E_{sw}	the heat loss through sweat evaporation, $[W]$
e	difference between the reference signal and the real time signal
e_τ	relative error in time constant
F_0	initial jet flow rate, $[m^3/s]$
F_J	air flow rate of the jet, $[m^3/s]$
F_i	fraction of F_0 which affects location i, $[m^3/s]$
f_c	impulse frequency of the vasoconstrictor efferent signal, $[impulse/s]$
f_{tone}	impulse frequency of the vasomotor tone, $[impulse/s]$
G_c	transfer function of the controller
G_e	transfer function of the environment
G_f	transfer function of the sensor
G_m	transfer function of the human thermoregulatory system
G_p	nominal transfer function of the plant
G'_p	actual transfer function of the plant
g	gravitational acceleration: 9.8 m/s^2
H	internal heat dissipated through skin, $[W]$
h_a	total heat transfer coefficient between skin and thermal environment, $[W/K]$
h_{cond}	total conduction heat transfer coefficient, $[W/K]$
h_{conv}	total convection heat transfer coefficient, $[W/K]$
h_{rad}	total radiation heat transfer coefficient, $[W/K]$
h_K	tissue conductance, $[W/K]$
I_{cl}	thermal resistance of the clothing, $[clo]$
j	$\sqrt{-1}$
K_I	integral control gain

K_P	proportional control gain
K_{ts}	tissue conductivity, $[W/m\ K]$
L_f	human thermal load in terms of impulse frequency
L_Ω	human thermal load in terms of blood flow rate
M	human metabolic rate, $[W]$
m	mass, $[kg]$
N	total number of sampling points
p_{exp}	dominant pole of the experimental result
p_{model}	dominant pole of the model
Q_T	total thermal load applied to the environment, $[W]$
Q_i	part of Q_T that affects location i, $[W]$
Q_{ts}	total heat conducted from core to shell, $[W]$
Q_{bl}	total heat delivered by blood stream from core to skin, $[W]$
Q_{int}	total heat transferred from body core to body shell, $[W]$
Q_{env}	total heat dissipated to the environment from skin surface, $[W]$
Q_{cond}	total heat conducted through clothing, $[W]$
Q_{conv}	total convective heat dissipated at clothing surface, $[W]$
Q_{rad}	total radiative heat dissipated at the clothing surface, $[w]$
q^{-1}	shift (delay) operator
r	reference input variable
r_Ω	sensor calibration ratio $(\Omega_f/\bar{\Omega}_p)$, $[sensor\_unit \cdot m^2 \cdot hr/liter]$
s	Laplace variable
T	temperature, $[^oC]$
T_{mrt}	mean radiant temperature, $[^oC]$
T_c^Σ	threshold core temperature: 36.6^oC
T_s^Σ	threshold skin temperature: 34.1^oC
t	time, $[s]$
U_0	discharge velocity of teh jet, $[m/s]$
v	air velocity, $[m/s]$
v_B	air velocity in the buffer zone, $[m/s]$
W	external mechanical work done by the human body, $[W]$

x	distance in the jet direction, $[m]$
y	system output variable or the vertical coordinate, depends on the context.

Subscripts:

0	air supply
a	local air
b	whole body
bl	blood
c	body core
cl	clothing
s	body shell
ts	tissue

Others:

$\bar{}$ (top bar)	the value of the corresponding variable per unit skin area (e.g. $\bar{\Omega}_p = \Omega_p / A_{Du}$).

Bibliography

[1] ANSI/ASHRAE Standard 55-1992, "Thermal Environmental Conditions for Human Occupancy", Atlanta, Georgia, 1992

[2] Gagge, A.P., Stolwijk, J.A., Nishi, Y., "An Effective Temperature Scale Based on a Simple Model of Human Physiological Regulatory Response", ASHRAE Transactions, 77, Part 1: 247-262, 1971

[3] Fanger, P.O., "Thermal Comfort", McGraw-Hill, 1970

[4] MacArthur, J.W., Grald, E.W., "Optimal Comfort Control for Variable-Speed Heat Pumps", ASHRAE Transactions, 1283-1296, 1988

[5] Liu, S., He, X., "A Distributed-Parameter-Model Approach to Optimal Comfort Control in Air Conditioning Systems", American Control Conference, 1994.

[6] Niu, J., Kooi, J.V., "Two dimensional Simulation of Airflow and Thermal Comfort in a Room with Open-window and Indoor Cooling System", Energy and Buildings, 18, 65-75, 1992

[7] Dounis, A.I., Santamouris, M.J., Lefas, C.C., "Implementation of Arteficial Intelligence Techniques in Thermal Comfort Control for Passive Solar Buildings", Energy Convers. Mgmt., Vol. 33, No.3, 175-182, 1992.

[8] Federspiel, C.C., "User-Adaptable and Minimum-Power Thermal Control", PhD thesis, MIT, 1992.

[9] Folk, G.E., "Introduction to Environmental Physiology", Lea & Febiger, 1966.

[10] Clark, R.P., Edholm, O.G., "Man and His Thermal Environment", Edward Arnold, 1985.

[11] Schmidt, R.F., Thews, G., "Human Physiology", 2nd Ed., Springer-Verlag, 1989.

[12] Mitchell, D., Wyndham, C.H., "Comparison of Weighting Formulas for Calculating Mean Skin Temperature", Journal of Applied Physiology, 26, 616-622, 1969.

[13] Hensel, H., "Thermoreception and Temperature Regulation" Academic Press, 1981.

[14] Guyton, A.C., "Textbook of Medical Physiology", 6th edition, W.B. Saunders Company, Philadelphia, 1981.

[15] Zhou, M., Liu, S., Asada, H., "Zero-Load Control of Indoor Thermal Environment", ASHRAE Transactions, 104, Pt.1, 1998.

[16] Greenfield, A.D.M., "The Circulation Through the Skin", Handbook of Physiology, Vol. II, Section 2, American Physiology Society, Washinton, D.C., 1965.

[17] Folkow, B., "Nervous Control of the Blood Vessels", Physiological Review, 35, 629-663, 1955.

[18] Hales, J.R.S., Fawcett, A.A., Bennett, J.W., "Differential Influences of CNS and Superficial Body Temperatures on the Partition of Cutaneous Blood Flow Between Capillaries and Arteriovenous Anastomoses", Pfluger Arch., 361, 105-106. 1975.

[19] Hales, J.R.S., Jessen, C., Fawcett, A.A., King,R.B., "Skin AVA and Capillary Dilation and Constriction Induced by Local Skin Heating", Pflugers Arch., 404, 203-207, 1985.

[20] Wenger, C.B., Roberts, M.F., "Thermoregulatory Control of Finger Blood Flow", Journal of Applied Physiology, 38, 1078-1082, 1975.

[21] Nagasaka, T., Cabanac, M., Hirata, K., Nunomura, T., "Control of Local Heat Gain by Vasomotor Response of the Hand", Journal of Applied Physiology, 63, 1335-1338, 1987.

[22] Kramer, K., Lochner, W., Wetterer, E., "Methods of Measuring Blood Flow", Handbook of Physiology, Vol. II, Section 2, American Physiology Society, Washinton, D.C., 1965.

[23] Wissler, E.H., "A Review of Human Thermal Models", Mekjavic, I.B. *et al* (ed.), Environmental Ergonomics, Taylor & Franics, London, 267-285, 1988.

[24] Werner, J., "Thermoregulatory Models", Scand. Journal Work Environment Health, 15, Suppl. 1, 34-46, 1989.

[25] DuBois, D., DuBois, E.F., "The Measurement of the Surface Area of Man", Archives of Internal Medicine, 15, 868-881, 1915.

[26] Shitzer, A., Stroschein, L.A., Gonzalez, R.R., "Application of a Lumped-Parameter Heat Exchange Model to Cold-Induced Temperature and Blood Flow Measurements in the Finger-Tip", J. Therm. Biol., Vol. 21, No. 4, 213-222, 1996.

[27] Thauer, R., "Circulation Adjustments to Climatic Requirements", in *Handbook of Physiology, A Critical, comprehensive presentation of physiological knowledge and concept*, Section 2, Vol. III, American Physiological Society, 1965.

[28] Jones, B.W., "Transient Model of the Human Body and Clothing Systems". Technical Report 91-01, Institute for Environmental Research, Kansas State University, 1991.

[29] Stolwijk, J.A.J., Hardy, J.D., "Temperature Regulation in Man - A Theoretical Study", Pfugers Archiv., 291, 129-162, 1966

[30] Braune, W., Fischer, O., "Determination of Moments of Inertia of the Human Body and Its Limbs", Springer-Verlag, 1988.

[31] IER, "IER Clothing and Fabric Data Base", Institute for Environmental Research, Kansas State University, Manhattan, Kansas, 1992.

[32] Colin, J., Houdas, Y., "Experimental Determination of Coefficient of Heat Exchanges by Convection of Human Body", Journal of Applied Physiology, 22, 31-38, 1967.

[33] Abramovich, "The Theory of Turbulent Jets", The M.I.T Press, 1963.

[34] Rajaratnam, N., "Turbulent Jets", Elserier Scientific Publishing Company, 1976.

[35] Awbi, H., B., "Ventilation of Buildings", E & FN SPON, London. 1991.

[36] Koestel, A., "Paths of Horizontally Projected Heated and Chilled Air Jets", Trans. ASHAE, 61, 213-232, 1955.

[37] Frean, D. H., Billington, N.S., "The Ventilation Jet", JIHVE, 23, 313-333, 1955.

[38] Baturin, V.V., "Fundamentals of Industrial Ventilation", Pergamon, Oxford, 1972.

[39] Landau, I.D., "System Identification and Control Design", Prentice Hall, Englewood Cliffs, 1990.

[40] Doyle J.D., Stein, G., "Multivariable Feedback Design: Concepts for a Classical/Modern Synthesis", IEEE Trans. Automatic Control, Vol.AC-26, 4-16, 1981.